The use of computer simulation as a design tool for thermal hydraulic systems

Sidders, John Anthony

Award date:
1999

Awarding institution:
University of Bath

THE USE OF COMPUTER SIMULATION AS A DESIGN TOOL FOR THERMAL HYDRAULIC SYSTEMS

submitted by

John Anthony Sidders

for the degree of PhD

of the University of Bath

1999

COPYRIGHT

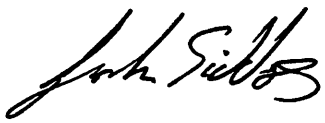

ProQuest LLC
789 East Eisenhower Parkway
P.O. Box 1346
Ann Arbor, MI 48106-1346

SUMMARY

This thesis describes a modelling philosophy aimed at improving the design and analysis of thermal hydraulic systems. A set of lumped parameter differential equations representing conservation of mass and energy is developed for this purpose. These have been applied using computer simulation for the determination of the steady state and dynamic performance of three systems. These systems comprise power generating plant, hydraulic fluid power, and vehicle cooling systems.

The modelling approach is shown to be generically applicable to all three systems. The representation of the conservation equations in terms of pressure and temperature is described. This allows a variety of thermal hydraulic systems to be investigated. This is due to the availability of data for properties such as bulk modulus, and the coefficient of cubical expansion, for many fluids. The relationship between these properties and the conservation equations is discussed. It is shown that fluid pressure and temperature are coupled dynamically.

The development of a nuclear power plant low pressure feed system model is described. The behaviour of vessels containing two phase water is assessed and the model is compared with plant data representing a transient fault situation. It is shown that the vessel models require a two phase drains flow representation to maintain system stability.

A hydraulic fluid power system is assessed. It is shown that the component hydraulic characteristics are viscosity dependent, and must be included in models, if a close correspondence with experimental data is required. It is shown that the thermal response of the system is dominated by the heat capacity of the reservoir.

A description of a vehicle cooling system model is presented. The flexibility of the modelling approach is demonstrated. The basis of a theoretical wax pellet thermostat model is presented that incorporates many nonlinear physical effects.

ACKNOWLEDGEMENTS

The author wishes to express his gratitude to Dr D G Tilley for the guidance and many technical discussions throughout the course of this work..

The author also wishes to thank Nuclear Electric Ltd for permission to include the research and development of the LP Feed System model in this thesis. Particular thanks are due to Mr G P Merriman of Nuclear Electric Ltd for many discussions on two phase thermodynamics.

Thanks are also due to the Ford Motor Company for permission to publish work contained in this thesis.

CONTENTS

NOTATION

Chapter 2

Cp	Specific heat capacity at constant pressure
h	Specific enthalpy
M	Mass
p	Pressure
q_h	Rate of heat transfer
t	Time
T	Temperature
U	Internal energy (extensive property)
u	Specific internal energy
V	Volume
w	Mass flow rate
Ws	Rate of work done by the fluid
x_T	Isothermal compressibility
β	Coefficient of cubical expansion
ρ	Density
Bm	Fluid isothermal bulk modulus

Subscripts

ave	Average
e	Exit
l	Leaving

Chapters 3 & 4

A	Area
Ac	Averaging coefficient

A_c Area of tubing exposed to steam

A_w Area of tubing exposed to water

A_d Orifice throat area

BFPT Boiler Feed Pump Turbine

Cp Specific heat capacity at constant pressure

Cv Specific heat capacity at constant volume

d tube diameter

DA Deaerator

FW Feed Water

g Gravitational acceleration coefficient

h Specific enthalpy

hcon condensate enthalpy

hfg The change in enthalpy between saturated liquid and vapour for a given pressure/temperature

htc Heat Transfer Coefficient

htc_c Condensing Heat Transfer Coefficient

IP/LP Intermediate Pressure / Low Pressure

k_m Function of orifice to pipe diameter, eqn (3.30)

k_T Turbine resistance coefficient

k_{th} Thermal conductivity

k Function of pressure ratio, eqn (3.30)

LMTD Log mean temperature difference

LP Low pressure

m Polytropic exponent

M Mass

Mw Water mass

N	number of tubes
p	Pressure
PMSP	Plant Modelling System Programme
PS	Power Station
PWR	Pressurised Water Reactor
q	Rate of heat transfer
q_h	Rate of heat transfer
Q	Temperature ratio, dimensionless
R	gas constant
t	Time
T	Temperature
Tcon	Condensate temperature
TMEC	Turbine Moisture Extraction Condenser
ΔT_m	LMTD
U	Overall heat transfer coefficient
U	Internal energy (extensive property)
u	Specific internal energy
V	Volume
w	Mass flow rate
w_c	Condensing mass flow rate
w_{gi}	Drains cooler inlet mass flow rate dry steam component
w_T	Turbine mass flow rate per stage
W_{sw}	Mass flow rate of dry steam condensing across drains cooler tube bundle
wcon	condensate mass flow rate
x	Dryness fraction (quality of water / steam mixture)
z	Height

υ	Specific volume
ρ	Density
Δ	Difference
η_s	Isentropic efficiency
γ	Ratio of specific heat at constant pressure to that at constant volume
μ	Viscosity

Subscripts

ave	Average
d	Drain
dh1	Heater 1 drain
df1	Flash vessel 1 drain
e	Exit
f	Saturated water conditions
g	Dry saturated steam conditions
gi	Drains Cooler dry steam conditions at inlet
i	Inlet
l	Leaving
o	Outlet
p	Primary
s	Steam
s	Secondary
t	Tube
tot	Total
w	Water

x	Mixture

Chapters 5 & 6

A	Area
Cmin	minimum heat capacity
Cp	Specific heat capacity at constant pressure
Cr	Orifice flow coefficient (product of valve area and valve discharge coefficient)
D	Pump displacement
h	Heat Transfer Coefficient
M	Fluid mass within control volume
p	Pressure
q_h	Rate of heat transfer
Q_d	Pump discharge volumetric flow rate
Q_l	Pump flow loss
t	Time
T	Temperature
Tq_l	Pump torque loss
U	Overall Heat Transfer Coefficient
V	Control volume
w	Mass flow rate
Ws	Rate of shaft work
x_T	Isothermal compressibility
β	Coefficient of cubical expansion
Δp	Valve pressure drop
ϵ	Cooler effectiveness
η_o	Pump efficiency

θ	Temperature difference
ρ	Density
υ	Specific volume
Bm	Fluid isothermal bulk modulus
μ	Dynamic viscosity

Subscripts

ave	Average
e	Exit
l	Leaving
ref	Reference value

Chapter 7

A	Area
Bm	Bulk modulus
Cmin	Minimum heat capacity
Cr	Bypass restriction coefficient
Cp	Specific heat capacity
d	hose diameter
f	Friction factor
Fw	Viscous friction force
g	Gravitational acceleration
h	Deaeration tank coolant height
h_{ws}	Heat transfer coefficient - hose wall to surroundings
h_{fw}	Heat transfer coefficient - fluid to hose wall
H	Head

k	Thermal conductivity
k_f	Head loss coefficient - hose additional losses (bends etc)
k_r	Port restriction coefficient (hose models)
l	Length
M	Mass
N	Speed
Nus	Nusselt number
p	Pressure
Δp	Pressure drop
Pr	Prandtl number
q_h	Rate of heat transfer
Q	Volumetric flow rate
R	Specific gas constant
Re	Reynolds number
Re_{crit}	Critical Reynolds number (laminar - turbulent transition)
rr	Relative roughness (hose)
T	Temperature
Tr	Torque
u	Velocity
V	Volume
w	Mass flow rate
x	position
Δz	Gravitational head difference
β	Coefficient of cubical expansion
ϵ	Effectiveness
ρ	Density

υ	Specific volume
υ_{kin}	Kinematic viscosity
θ	Temperature difference
μ	Dynamic viscosity

Subscripts

a	Air
c	Coolant
i	Inlet / internal
fw	Fluid - wall
ws	Wall - surroundings
m	Material
o	Outside
s	Surroundings

CHAPTER 1

INTRODUCTION

In recent years the advances made in computer hardware have led to vastly increased computational engine speeds. This has allowed the engineer and scientist alike to develop increasingly more realistic and usually more complex mathematical models of physical systems. It is the aim of this research to extend the range and sophistication of such modelling techniques that will allow the engineer greater flexibility in design and analysis of thermal hydraulic systems.

Mathematical models of thermal hydraulic systems exist in many forms, and have been developed to provide insight into the behaviour of equipment and systems alike. The work presented here will concentrate on the development of lumped parameter models. These models are generally configured to work in the Bath*fp* simulation environment, Richards and Tilley[1991], which has been made available to the author for the period of this work. It should be recognised that this does not detract from the generic applicability of the research, as the modelling techniques developed are applicable to many commonly used engineering processes. This is demonstrated in research work and case studies where the modelling techniques developed have been applied to the study of power generation plant, fluid power systems and vehicle cooling systems.

The emphasis on lumped parameter modelling provides not only individual component descriptions, but complete systems may be analyzed without large computational cost. In this respect, the operational performance of the complete design may be assessed in a reasonable period of time. Lumped parameter modelling techniques provide the engineer with a tool to find an optimal solution to the system performance in the non-linear domain. This has traditionally

been achieved by adjusting model system parameters heuristically, until an acceptable performance has been obtained. Occasionally this process can be enhanced by techniques such as linearizing the system model about a steady state operating point, to gain a greater theoretical insight into stability margins, and often this will increase the engineers understanding of the system dynamics. The key point is that the lump parameter system simulation provides the engineer with a means to study the operational performance of the 'system' in question at the design stage.

Chapter 2 develops the theoretical background necessary to study the steady state and dynamic performance of thermal hydraulic systems. This concentrates on a formal development of the conservation equations for mass and energy, which is a prerequisite to predicting the dynamic performance of systems of this kind. It will be shown in later chapters that the conservation equations (Chapter 2) may be used, with suitable assumptions applied, to represent all of the systems studied in this thesis.

The following sections provide an introduction to the aims of the research in this thesis and reviews previous work in each area of study. The first section (1.1) is concerned with power generating plant, which is a natural starting point as the author has previously studied systems of this type, during his career with the Electricity Supply Industry, Sidders[1987]. It should be appreciated that the study of thermal effects is a necessary part of operating complex nuclear power generating plant. It is therefore natural that the conservation equations have been applied in many forms to aid in the understanding of the dynamic performance of these systems. The analysis of thermal effects in fluid power systems has not been explored to such an extent, when compared with power generating plant. Section 1.2 addresses the area of fluid power systems, and in particular highlights some of the deficiencies that have been found in predicting the thermal hydraulic performance of these systems. Section 1.3 explores the thermal hydraulic

performance of vehicle cooling systems, again using lumped parameter modelling techniques. Although a wide variety of steady state predictive modelling tools exist for prediction of cooling system performance, there is little available for determining the dynamic performance of the complete cooling system.

By using the conservation equations derived in Chapter 2 to predict the performance of the three types of thermal hydraulic system described above, the aim is to show that the approach is generically applicable from a lumped parameter modelling perspective. In this respect it should be possible to use the techniques developed to examine a much wider range of systems which possess the characteristics of transferring energy between a fluid and its surroundings in the form of heat or mechanical work.

1.1 INTRODUCTION TO POWER GENERATING PLANT

The study of thermal effects in power generating plant is to some degree implicit, due to the nature of systems of this kind. They are thermal systems which convert a proportion of thermal energy to electrical energy. The examination of nuclear power generating plant performance has in the main been achieved in the UK by a suite of purpose built codes, Whitmarsh-Everiss[1993]. In particular, the dynamic performance of these systems has been studied using the Plant Modelling System Programme (PMSP). This modelling environment was established within the Electricity Supply Industry specifically to study both the steady state and dynamic aspects of the total plant system, Whitmarsh-Everiss[1993]. In this respect, modules are developed, which may be linked together to provide a mathematical description of the whole plant.

One deficiency of PMSP total plant lumped parameter modelling codes used by Nuclear Electric is that most have little or no low pressure (LP) feed representation (excluding Sizewell B nuclear

power station). Therefore studies involving perturbations to the LP feed system must be undertaken in a qualitative manner, unless precise information regarding the nature of the boundary conditions is known. The lack of LP feed representation in general does not preclude a vast amount of transient analysis to be performed confidently, since the codes previously mentioned have detailed representations of the boiler/turbine units, nuclear reactor and control systems. One of the current problems that is addressed in this thesis involves the understanding of the thermal hydraulics associated with processing vast quantities of high quality steam into the main condensers of the nuclear plant. To understand this process and the subsequent disturbances to the nuclear island, requires accurate LP feed system models. In principle, the LP feed system components comprise turbines, condensers, heaters and two phase vessels of various description. It should be noted that many of the model components have well established pedigrees, NNC Ltd[1994], and do not require detailed examination for the purposes of this research. However, research and development of indirect contact feed heater models, and their interaction when coupled together in a cascaded system, is required in this particular study. This involves studying the behaviour of vessels containing condensing two phase mixtures with heat transfer to a single phase fluid. A variety of ways to solve the mass and energy conservation equations are explored for the feed heater model. Integral to the study of feed heaters is heat exchanger performance. The study of heat exchangers is vast, and performance prediction is typified in texts such as Holman[1992]. Generally, heat exchanger performance is undertaken using methods such as the Log Mean Temperature Difference (LMTD) or the Number of Transfer Units (NTU). These cater for many different types of heater arrangements but are generally used for steady state situations. NNC Ltd[1994] employs a subtle variation to the LMTD approach which allows the stored energy in the heater tube material to be taken into account dynamically. In principle, this involves introducing a tube material temperature into the equation set. Rates of heat transfer can then be deduced on both sides of the tube wall from which a tube temperature derivative may be calculated. This technique is expanded in Chapter

3. The underlying problem with the heater representation of NNC Ltd[1994] is that on the condensing side (heater shell), the effect of transient variation in heater water level is ignored. All heater exit drain flows are assumed to equal the condensing steam flows to the heater. In this respect, the shell side conserves mass from a steady state considerations only. In principle, it would seem a relatively simple task to implement a dynamic continuity equation and specify the boundary flows independently. However, if the water level enters the drain pipe, some steam entrainment occurs which effectively means that the drains orifice is passing two phase flow. Chapter 3 examines the effect of two phase drains flow, and its stabilising influence on the heater system.

1.2 INTRODUCTION TO HYDRAULIC FLUID POWER SYSTEMS

Many researchers have contributed to the study of thermal effects in hydraulic systems including Harris[1990], Yang[1987], Kjolle[1978], Tomlinson[1987] and Buckingham [1986]. It is the author's opinion however that Harris[1990] has given the most thorough exposition of thermal effects relating to lumped parameter modelling of hydraulic systems that is generally available at present. The major contribution Harris made was to consider the working fluid from a thermodynamic view point. In this respect, previous researchers had paid little attention to energy conservation. For example consideration of fundamental relationships related to the energy equation have been overlooked, Yang[1987]. The approach of Yang[1987] considered the change in enthalpy of the working fluid as a constant pressure process, since he assumed that the effect of pressure to be small, e.g.

$$h = Cp\ T \tag{1.1}$$

Yang then chose to define the work term in the energy equation for items such as pressure loss through a valve which strictly speaking should have been incorporated within the definition of enthalpy, clearly there will be no work transfer between the fluid and valve. Extending the valve

example, it can be inferred from Yang that in the steady state, the following relationship should hold, neglecting heat transfer to the surroundings:

$$0 = \upsilon \, \Delta p + Cp \, \Delta T \tag{1.2}$$

In the absence of external work and heat transfer the change in enthalpy of the fluid should be zero. As this is a flow process being described, this defines the fluid enthalpy as being constant for this condition, i.e dh = 0. The above equation then should describe the change in fluid enthalpy across the valve. This is in fact an oversight by Yang brought about by an incomplete analysis of the thermodynamic process. Harris realised this and approached the development of an equation for conservation of energy from a sound theoretical background. Harris[1990] arrived at an expression for the change in enthalpy in terms of pressure and temperature as follows:

$$\Delta h = (\upsilon - \upsilon \beta T)\Delta p + Cp\Delta T \tag{1.3}$$

The above relationship can be verified in many thermodynamic texts where the thermodynamic properties are in differential form. However Harris chose to ignore the error in assuming that the partial coefficients remain constant between the limits of the analytical integration. It can be shown that this error is very small, Kjolle[1978], and has been subsequently justified by the very good correspondence achieved between model and experimental results. Harris however had to make certain limiting assumptions about the terms in the differential energy equation in order to eliminate unwanted parameters which were a consequence of the derivation. Effectively Harris was left with expressions for enthalpy and internal energy entering and leaving the control volume which included reference values evaluated from integration. Consider the origin of equation (1.3) that Harris considered as follows:

$$dh = \frac{\partial h}{\partial p}\Big|_T dp + \frac{\partial h}{\partial T}\Big|_p dT \tag{1.4}$$

From which Harris arrived at:

$$h = h_o + (\upsilon - \upsilon\beta T)(p - p_o) + Cp(T - T_o) \tag{1.5}$$

Where the subscript 'o' refers to the reference state from integration. A similar expression can also be deduced for the change in internal energy. Harris decided to substitute these expressions directly into the following rate dependent energy equation:

$$M\frac{du}{dt} + u\frac{dM}{dt} = w_{in}h_{in} - w_{out}h_{out} + W - q_h \tag{1.6}$$

One can appreciate that the reference values ($h_\infty u_\infty p_o$ etc) will be retained once this equation is modified and re-arranged to find a temperature derivative, the preferred choice to represent the rate of change of energy in the control volume using hydraulic fluids. Harris found that the only way to eliminate these terms was to assume that the inlet mass flow rate was equal to the outlet mass flow rate so that these reference values cancelled out. However, making this assumption effectively precluded the use of the pressure derivative term within the energy equation. Clearly if the inlet and outlet mass flow rates are identical, then in the absence of heat transfer the pressure will remain fixed with respect to time. This to some extent is contradictory, as Harris used the standard dynamic continuity equation to determine pressure separately, which is based on the pressure derivative being proportional to the difference in inlet/outlet mass flow rates. If Harris has firstly re-arranged equation (1.6) such that terms involving enthalpy and internal energy entering and leaving the control volume could be added or subtracted directly, then these reference values would cancel out. This approach is expanded on in Chapter 2.

All previously published research found by the author in the area of hydraulics, including that of Harris, has ignored the cross coupling between the continuity and energy equations. This was

brought about by considering that pressure was only a function of density. This is quite acceptable when performing calculations with the assumption that the temperature is constant. It is shown in Chapter 2 that there is an implicit relationship between conservation of mass and energy.

1.3 INTRODUCTION TO VEHICLE COOLING SYSTEMS

A search on the topic of thermal effects in vehicle cooling systems revealed a wide variety of techniques used to predict thermal performance. Some approaches use techniques which utilise a number of different software tools in combination. Blumcke and Nefischer[1995] are examples of such an approach. They established a technique which centres on a main calculational heat flux code KULI. This code determines heat rates for a number of system components, for example the radiator. Other software tools are primarily used to produce input data for KULI, such as FLOWMASTER and STAR-CD. For example, the FLOWMASTER code determines the pressures and flow rates in the cooling circuit for a given configuration. These data are pre-processed and input to KULI in terms of Reynolds number and alike information necessary for KULI to quantify heat transfer coefficients, and therefore perform heat rate calculations. The STAR-CD code is used to calculate the complex cooling flow within the engine water jacket. This code utilises a finite volume technique solving a 3 - dimensional flow regime. These data are used to predict accurate heat transfer coefficients which KULI uses in heat rate calculations.

The output from the above analysis is steady state information which is an accurate statement of the cooling performance at different operating conditions. Clearly the process is fairly lengthy as several different software tools must be used to give cooling performance predictions. Comparison of this technique with Bath*fp* provides a vivid contrast in approach and the type of information provided. Analysis of vehicle cooling system performance could be completed entirely with Bath*fp* with the additional benefit of transient thermal/hydraulic performance

prediction, once the components models have been developed. The precise determination of steady state operating points will not be quite so accurate as the process described by Blumcke and Nefischer[1995]. However, Bath*fp* offers a flexible total system modelling environment producing both steady state and transient information.

Design of vehicle cooling systems has also been examined by Bauer *et al.*[1995]. The end result is a steady state prediction of cooling performance, similar to Blumcke and Nefischer [1995]. However there is only one software tool KUEBER which performs the main heat transfer calculations, as opposed to the approach taken by Blumcke and Nefischer[1995] which requires several codes as a pre-processor to the main calculation. KUEBER does however require boundary conditions concerning the under bonnet cooling air flow and this is provided by STAR-CD, previously described. In this application, it is performing computational fluid calculations and solving the 3-dimensional Navier-Stokes equations for the cooling air flow under the bonnet. This is in contrast to Blumcke and Nefischer[1995] who use this software tool to calculate the complex flow regime within the engine water jacket. Other inputs to KUEBER include information relating to the driving performance for a given speed and loading condition for example, transmission efficiency and tyre rolling resistance, see Figure (1.1). This is stored in a data base along with engine performance, radiator and air conditioning data.

It should be stated that the techniques described by Blumcke and by Bauer above provide a very accurate performance statement for a range of operational steady states. In this respect, the use of several different software tools can be justified. Here the role of a lumped parameter simulation tool such as Bath*fp* will be more suited to performing calculations where qualitative information is required and in situations where extensive analysis is not justified. Examples of this would be exploring different design configurations with modified components in a limited period of time. Should a particular configuration prove worth investigating further, then more

detailed design calculations could then take place with the techniques described by Blumcke and Bauer. Another very important area which is not addressed by either Blumcke or Bauer, but is one of the fundamental aspects of Bath*fp*, is the ability to predict the transient performance of the system.

Tomlinson and Burrows[1994] have approached the prediction of vehicle cooling system performance using the lumped parameter code Bath*fp*. This work focused on the study into the merits of thermostat position within the cooling circuit, and in particular the effects of mounting the thermostat at either the engine inlet or outlet. Unfortunately the study presented only model prediction without engine rig data, and can therefore only be viewed qualitatively. The study did however highlight the flexibility of using a lumped parameter simulation code for this application albeit using simplified models.

There are a number of areas where the work of Tomlinson and Burrows could be improved. For instance the study used pure water which although suitable for the purposes of the analysis, does not reflect the typical coolant properties normally used. Most internal combustion engine cooling systems use a mix of water and ethylene glycol. This inhibits the change in phase at low temperatures (coolant temperature $\leq$ 0°C). A secondary and beneficial effect is that coolant with the addition of ethylene glycol also reduces the onset of cavitation at the coolant pump inlet. The effect of different coolant mixes results in the change of both the thermodynamic and transport properties of the coolant, and also the partial properties. These properties are required by the simulation in the relationships describing many of the physical phenomena that take place. One way of overcoming this problem is to extract the coolant properties from enhanced data bases such as PPDS which can determine these properties based on the proportion of basic constituents. It is possible to evaluate the required properties by either fitting polynomials to the data, or constructing a property map and interpolating between points.

It is the author's view that one of the main deficiencies of work by Tomlinson and Burrows[1994] is the steady state calculation for coolant outlet temperature for both the engine block and radiator. These components carry a significant proportion of the total coolant in the cooling system and as such, any transient performance prediction will deviate from the actual performance because the coolant heat capacity will be under-estimated. This will tend to speed up the transient response significantly.

One area where research is required is the thermostat thermal performance. Under transient conditions, the thermal characteristics are affected by thermal inertia and internal friction such that the operational performance can exhibit significant delays. The thermostat also exhibits significant hysteresis, Ford Motor Company[1995]. These inherent characteristics mean that matching thermostats to engine cooling systems can be an arduous task. If not matched correctly, the thermostat can oscillate which induces cycling of the coolant mass flow rate such that the engine block is subjected to repeated thermal shock. If the transient performance characteristics of thermostats are adequately represented, then it will be possible to obtain the dynamic characteristics of the cooling system by simulation.

1.4 INVESTIGATIONS UNDERTAKEN

Chapters 3 and 4 explore aspects of thermal hydraulic analysis applied to power generating plant. In particular, a discussion of the philosophy relating to the physical processes involved in modelling vessels containing two phase mixtures is presented. A case study is presented relating to the dynamic behaviour of the LP feed train of Heysham 2 Nuclear Power Station which is an advanced gas cooled reactor design. A suite of lumped parameter component models are developed for the LP feed train which comprise turbines, condensers, indirect contact feed heaters, flashing vessels, condensate pumps and deaerator, along with a number of control systems. The models have been developed in the PMSP simulation environment, Whitmarsh-

Everiss[1993], which was made available to the author throughout the period of this work with Nuclear Electric, a subsidiary of British Energy. Advances in heat exchanger representation have been made as a result of this study which are presented. The LP feed train model is compared with plant data representing a fault situation (boiler quadrant trip).

The LP feed train model was subsequently used by Nuclear Electric to study the feasibility and implications of an automatic grid frequency control mode of operation of Heysham 2 Nuclear Power Station.

Of increasing importance to engineering design is the efficiency of systems, as this will contribute significantly to the lifetime operational cost of a system. By extending the analysis of hydraulic fluid power systems to incorporate thermal effects, it has been possible to examine circuit performance in greater detail. In this respect it is possible to optimise the circuit performance by selecting components for the system which are suitably matched. Maintaining thermal constraints imposed by materials/fluids limitations will also contribute to the longevity of systems.

Chapters 5 and 6 present a study using the theory developed in Chapter 2 for fluid power systems, where an open loop fluid power circuit is analyzed. The circuit comprises a pump, reservoir, heat exchanger and loading valve.The experimental results are compared with model prediction from which a number of observations are made. The key findings of this work were subsequently published, Sidders *et al.*[1996].

Chapters 7 and 8 test the theory and approach developed for a single phase fluid on vehicle cooling systems where the working fluid medium is a mixture of water and ethylene glycol. The research in this area highlighted that fluid temperatures are subject to greater variation than is

the case with normal fluid power systems. If one considers extreme coolant temperatures in the range of -35 to 120°C then the corresponding variation in coolant viscosity amounts to two orders of magnitude. Coupled with this is the small absolute value of viscosity (due to the water content) which was found to cause numerical difficulties with the computation of hose friction factor in the laminar / turbulent flow transition region. As such, various approaches are explored to satisfy this condition. All main cooling system components are studied and their thermal hydraulic performance characterised against experimental data for the system. A complete system model was developed from component models in the Bath*fp* simulation environment and tested against experimental data. Further exploratory model predictions are performed to show the flexibility of this approach and its use as a design and development tool. The key findings of this research work were subsequently published, Sidders and Tilley[1997].

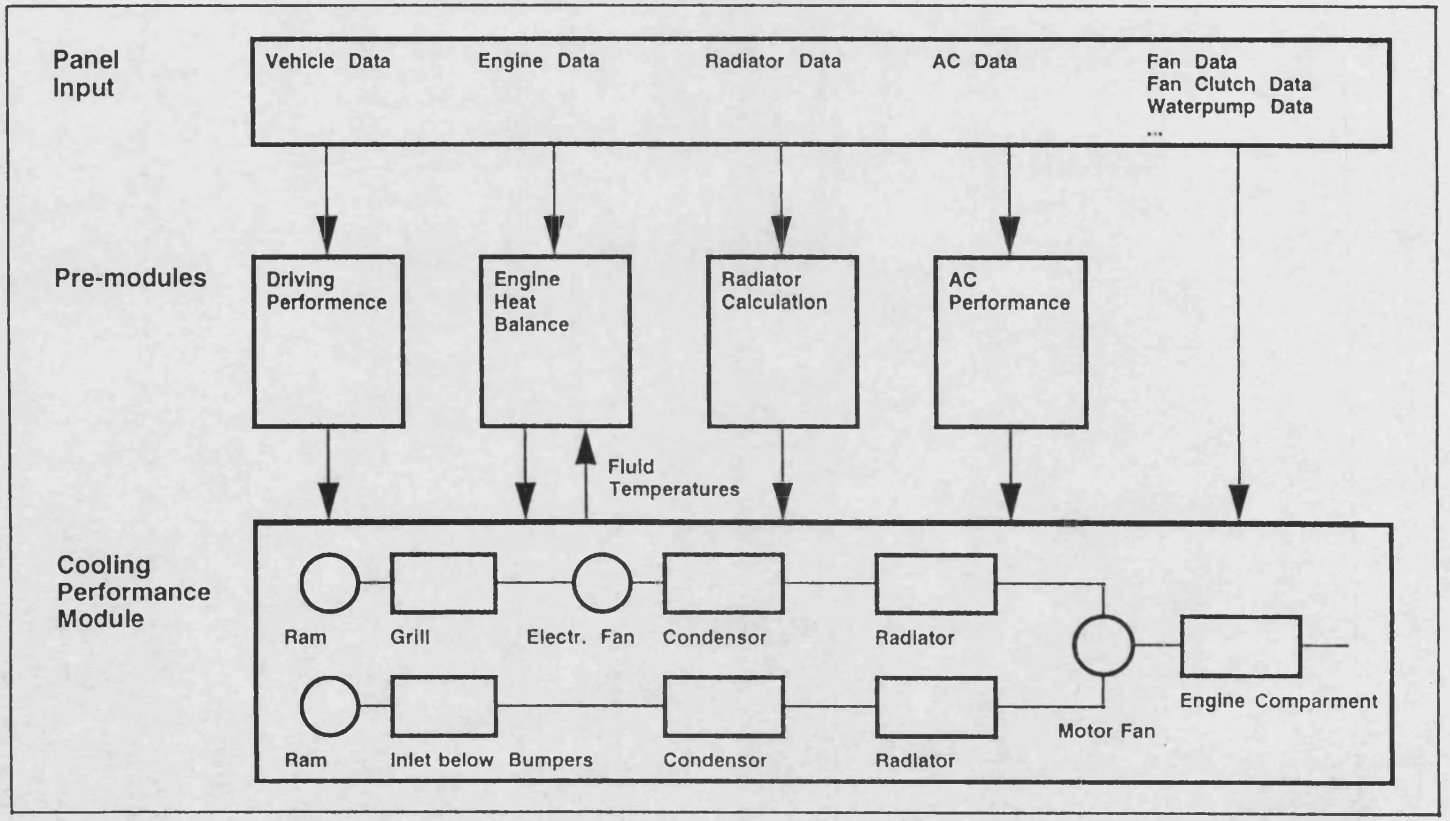

Flow Chart of KUEBER

FIGURE 1.1

CHAPTER 2

THEORETICAL BACKGROUND TO THERMAL HYDRAULIC ANALYSIS USING LUMPED PARAMETER MODELLING TECHNIQUES

2.1 INTRODUCTION

In general the prediction of component or system thermal hydraulic performance requires that the conservation laws of mass, momentum and energy are satisfied. Secondly and of equal importance, parameters such as heat transfer and frictional restriction coefficients need to be established accurately if quantitative model prediction is required. Such parameters can sometimes be established analytically if the fluid flow regime is laminar, but more generally they are determined empirically. The purpose of this Chapter is to address the former requirement in establishing a consistent set of conservation equations for lumped parameter systems. These will subsequently be used as a basis for modelling components and systems with suitable assumptions applied.

The development of a set of conservation equations has been assisted by the author's experience within the Electricity Supply Industry to represent the thermal hydraulics of a number of boiler/turbine units in lumped parameter form, Sidders[1989]. The basic concepts used are in fact the same for the analysis of fluid power systems and vehicle cooling systems, however the working fluids are clearly different. For this reason it is necessary to extend the development of the equations which allows mineral oil and vehicle coolant as the working fluid. It will be appreciated that this is more restricting since a thermodynamic property map for oils and coolants have not been developed, as has been done for water. Even if this were the case, several databases would have to be available to cater for the wide variety of oils and hydraulic fluids in use. For this reason it is sensible to progress the development of the equation set to those which allows both hydraulic fluids and vehicle coolants to be represented.

2.2 CONSERVATION EQUATIONS

A detailed derivation of both mass and energy conservation equations is provided in appendix A which determines two ordinary differential equations to describe the thermodynamic state of a fluid within a control volume. These equations are in extensive form such that they represent the total mass and internal energy of the fluid within the control volume as follows.

$$\frac{dM}{dt} = w_e - w_l \tag{2.1}$$

$$\frac{dU}{dt} = w_e h_e - w_l h_l - p\frac{dV}{dt} + q_h - W_s \tag{2.2}$$

However for the purposes of examining fluid power and vehicle cooling systems it is appropriate to re-arrange these equations in terms of properties that are both readily measurable and consistent with properties that are available for both types of fluid. For this reason, pressure and temperature have been chosen to represent conservation of mass and energy.

Continuity

Firstly to convert the conservation of mass equation (2.1) into intensive form, the following relationship is used: $\rho_{ave} = M/V$. Therefore:

$$\frac{dM}{dt} = \rho\frac{dV}{dt} + V\frac{d\rho}{dt} \therefore \frac{d\rho}{dt} = \frac{\frac{dM}{dt} - \rho\frac{dV}{dt}}{V} \tag{2.3}$$

Re-formulating the continuity equation in terms of pressure, noting that the inclusion of temperature will be made as it is readily derived from the energy equation, gives:

$$\frac{dp}{dt} = \frac{\partial p}{\partial \rho}\Big|_T \frac{d\rho}{dt} + \frac{\partial p}{\partial T}\Big|_\rho \frac{dT}{dt} \tag{2.4}$$

but the isothermal fluid bulk modulus is defined as $B_m = \rho\, \partial p/\partial \rho|_T$. Combining this with equation (2.1) and (2.3), and substituting into (2.4) gives:

$$\frac{dp}{dt} = \frac{B_m \left[(w_e - w_l) - \rho \frac{dV}{dt} \right]}{\rho V} + \frac{\partial p}{\partial T}\Big|_\rho \frac{dT}{dt} \qquad (2.5)$$

Rogers & Mayhew[1980a] site $\partial p/\partial T|_v$ equates to β/x_T where β is the coefficient of cubical expansion and x_T is the isothermal compressibility. It is also acceptable to equate $\partial p/\partial T|_\rho$ with $\partial p/\partial T|_v$ since by definition if the specific volume is constant then so is the density. Substituting this result into equation (2.5) gives:

$$\frac{dp}{dt} = \frac{B_m \left[(w_e - w_l) - \rho \frac{dV}{dt} \right]}{\rho V} + \frac{\beta}{x_T} \frac{dT}{dt} \qquad (2.6)$$

The properties such as bulk modulus, compressibility and cubical expansion will also be required to solve the equation set. Various researchers have contributed to the extrapolation of these quantities, and often they are arrived at by fitting polynomials in pressure and temperature, Harris[1990].

Noting that B_m is the reciprocal of x_T then equation (2.6) can be expressed as :

$$\frac{dp}{dt} = \frac{B_m \left[(w_e - w_l) - \rho \frac{dV}{dt} \right]}{\rho V} + B_m \beta \frac{dT}{dt} \qquad (2.7)$$

Energy

The energy equation (2.2) can now be re-formulated into a temperature derivative that can be simultaneously solved with the continuity equation. The internal energy for the control volume can be converted to specific enthalpy as follows: U = Mu and u = h - p/ρ; M = ρV. Therefore U = ρVh - pV. Substituting this into equation (2.2) gives:

$$\frac{d(\rho Vh - pV)}{dt} = w_e h_e - w_l h_l - p\frac{dV}{dt} + q_h - W_s \qquad (2.8)$$

Expanding the derivative on the left hand side gives:

$$Vh\frac{d\rho}{dt} + V\rho\frac{dh}{dt} + \rho h\frac{dV}{dt} - p\frac{dV}{dt} - V\frac{dp}{dt} = w_e h_e - w_l h_l - p\frac{dV}{dt} + q_h - W_s \qquad (2.9)$$

Re-grouping in terms of the enthalpy derivative gives:

$$\frac{dh}{dt} = \frac{w_e h_e - w_l h_l + q_h - W_s - Vh\frac{d\rho}{dt} - \rho h\frac{dV}{dt} + V\frac{dp}{dt}}{\rho V} \qquad (2.10)$$

Re-grouping in terms of enthalpy has the advantage that Harris[1990] has formulated the partial derivatives of enthalpy with pressure and temperature and also has evaluated an expression for (h_e - h_l) which will be used later in evaluating the temperature derivative. Noting the previous expression for rate of change of density (eqn 2.3) and incorporating with dM/dt, gives:

$$\frac{d\rho}{dt} = \frac{w_e - w_l - \rho\frac{dV}{dt}}{V} \qquad (2.11)$$

Therefore the above term Vh dρ/dt in the energy equation becomes:

$$Vh\frac{d\rho}{dt} = h(w_e - w_l) - \rho h\frac{dV}{dt} \qquad (2.12)$$

It is now necessary to define 'h' the average specific enthalpy in the node and relate it to the entry and leaving properties of the node. This is most commonly done by assuming a flat property

profile within the node (stirred tank approximation), however it is not always desirable to do this. For example where large variations in temperature exist between boundary conditions, implies a temperature gradient across the node which is a desirable assumption for heat transfer calculations. Another problem with the assumption of the flat intensive property profile is that it is not conceptually satisfying when applied to pipes, as the fluid is clearly not well mixed. This assumption can be accommodated with lumped parameter modelling techniques. The concept of intensive property variation across the control volume should not be associated with the individual calculation of distributed effects within a node as clearly the analysis is concerned with lumped parameter models. However, the relationship between inlet and outlet conditions related to a mean property value for a node is necessary in order to solve the equation set. In this respect it is quite acceptable to make assumptions about the variation of an intensive property across a node, e.g. linear, flat etc and relate this to an average value for the node. This assumption allows, a suite of models to be developed for different situations. There is nothing implicit in the development of these equations that dictates that the intensive properties must remain constant parallel to the flow direction throughout the control volume. Therefore the average specific enthalpy 'h' within the control volume can be equated for example to $h = (h_e + h_l)/2$ which assumes a linear variation for the change in enthalpy across the control volume (The 'stirred tank' formulation where $h \rightarrow h_l$ will be dealt with later) . If this is assumed then the development of the equations may continue as follows:

$$h(w_e - w_l) = \frac{w_e h_e}{2} + \frac{w_e h_l}{2} - \frac{w_l h_e}{2} - \frac{w_l h_l}{2} \qquad (2.13)$$

Combining this result with equation (2.12) and substituting into equation (2.10), the energy equation becomes:

$$\frac{dh}{dt} = \frac{1}{\rho V}\left[\frac{w_e h_e}{2} - \frac{w_l h_l}{2} - \frac{w_e h_l}{2} + \frac{w_l h_e}{2} + q_h - W_s + V\frac{dp}{dt}\right] \qquad (2.14)$$

Note that the term ρh dV/dt neatly cancels out on the above substitution. Defining the average mass flow in the control volume to be $w_{ave} = (w_e + w_l)/2$, equation (2.14) becomes:

$$\frac{dh}{dt} = \frac{1}{\rho V}\left[w_{ave}(h_e - h_l) + q_h - W_s + V\frac{dp}{dt} \right] \qquad (2.15)$$

It should be noted that equation (2.15) has been used to represent conservation of energy for water / steam situations, Sidders[1989]. However, the enthalpy derivative, and change of enthalpy will need to be replaced by functions of pressure and temperature for analysing both fluid power and vehicle cooling systems.

To convert the enthalpy derivative to that of temperature, use is made of the following relationship between thermodynamic properties:

$$\frac{dh}{dt} = \frac{\partial h}{\partial p}\Big|_T \frac{dp}{dt} + \frac{\partial h}{\partial T}\Big|_p \frac{dT}{dt} \qquad (2.16)$$

Equating equation (2.15) and (2.16) and re-arranging in terms of the temperature derivative gives:

$$\frac{dT}{dt} = \frac{1}{\frac{\partial h}{\partial T}\Big|_p \rho V}\left[w_{ave}(h_e - h_l) + q_h - W_s + V\frac{dp}{dt} \right] - \frac{1}{\frac{\partial h}{\partial T}\Big|_p}\left[\frac{\partial h}{\partial p}\Big|_T \frac{dp}{dt} \right] \qquad (2.17)$$

This can be simplified with a knowledge of various thermodynamic property relationships, namely: $\partial h/\partial T\,|_p = Cp$ where Cp is the specific heat capacity at constant pressure. From Harris[1990] $\partial h/\partial p\,|_T = v - \beta T v$. The energy equation (2.17) then becomes after the above substitution:

$$\frac{dT}{dt} = \frac{v}{Cp\ V}\left[w_{ave}(h_e - h_l) + q_h - W_s \right] + \frac{v}{Cp}\frac{dp}{dt} - \frac{v - \beta T v}{Cp}\frac{dp}{dt} \qquad (2.18)$$

The last two terms in equation (2.18) can be simplified so that the energy equation becomes:

$$\frac{dT}{dt} = \frac{v}{Cp\ V}\left[\ w_{ave}(h_e - h_l) + q_h - W_s\ \right] + \frac{v}{Cp}\left[\ 1 - (1 - \beta T)\ \right]\frac{dp}{dt} \qquad (2.19)$$

Which becomes:

$$\frac{dT}{dt} = \frac{v}{Cp\ V}\left[\ w_{ave}(h_e - h_l) + q_h - W_s\ \right] + \frac{v\beta T}{Cp}\frac{dp}{dt} \qquad (2.20)$$

Harris[1990] has shown that :

$$h_e - h_l = (v - \beta T v)(p_e - p_l) + Cp\ (T_e - T_l) \qquad (2.21)$$

The above equation has been arrived at by integrating fundamental relationships between enthalpy, pressure and temperature; assuming that the partial properties remain constant between integration limits.

Substituting equation (2.21) into (2.20) gives:

$$\frac{dT}{dt} = \frac{v}{Cp\ V}\left[w_{ave}[(v - \beta T v)(p_e - p_l) + Cp(T_e - T_l)] + q_h - W_s\right] + \frac{v\beta T\,dp}{Cp\ dt} \qquad (2.22)$$

It should be noted that w_{ave} represents the nett mass flow rate entering the control volume where: w ($w_{ave} = (w_e + w_l)/2$) is relative to the control surface and not an inertial reference. Clearly if the control surface is stationary as is generally the case then 'w' represents 'w' with respect to an inertial reference. Both the continuity and energy equation are now in a format that can be used within the Bath*fp* simulation package to solve thermal hydraulic problems, using a wide variety of fluids.

Equation (2.22) has been derived assuming a linear enthalpy profile across the control volume. It is found in the power generation industry that this assumption is useful if complete items of

equipment need to be modelled with one node and if large temperature variations exist between boundaries. For example a heat exchanger will experience a change in temperature or enthalpy along its length unless one or both of the fluids is at its saturation temperature. In order to employ eqn (2.22) which represents the average temperature within the node, one could assume to first approximation that because it has been derived with a linear variation in enthalpy across the node, that also the temperature varies linearly across the node. Therefore, one could equate the leaving temperature as:

$T_l = 2*T_{ave} - T_e$

where T_{ave} is the state variable arrived at by integration of equation (2.22). This, however, causes problems when the upstream temperature (T_e) changes suddenly, creating a 'see saw' effect. This is because the state variable will take time to change in value for a given step change in inlet temperature. As one can appreciate, if the inlet temperature falls rapidly, and the thermal inertia of the node causes the state variable to change slowly, the exit temperature will rise. This is indeed the opposite way to what would happen in practice. Clearly the equations would integrate out to a satisfactory steady state, however, transiently this is un-satisfactory. One way to overcome this effect is to assume that the temperature derivative relates not to the mean value within the node, but either to the entry or exit conditions. This approach has worked well in many power generation applications, Whitmarsh-Everiss[1993], however there will be a small error associated with this assumption.

Another way of overcoming this problem is to assume the average temperature and or specific enthalpy of the node is equal to the exit temperature (flat property profile). In many cases for hydraulic systems only small temperature variations will exist across components so this assumption is well suited. To arrive at the energy equation from a 'flat' intensive property assumption, equation (2.11) requires multiplication by Vh_l instead of Vh assuming now that the leaving enthalpy is equal to the average within the node. When substituting this result into the

energy equation and following the same path to arrive at an equation for temperature derivative, will give:

$$\frac{dT}{dt}=\frac{v}{Cp\ V}\ [w_e[\ (v\ -\ \beta vT)(p_e\ -\ p_l)+\ Cp\ (T_e\ -\ T_l)\ ]\ +\ q_h\ -\ W_s]\ +\ \frac{v\beta T}{Cp}\ \frac{dp}{dt} \quad (2.23)$$

In the above formulation, dT/dt represents the mean temperature derivative of the node (flat profile) and w_e is the entry mass flow rate into the control volume.

Until now nothing has been mentioned concerning the calculation of mass flow rate which is a prerequisite to close the equation set. This can be calculated from either steady state or dynamic momentum considerations. In the development of lumped parameter models, the above equation set can be used with suitable assumptions to represent system components in Bath*fp* as demonstrated in Chapter 6 where a whole circuit simulation is performed.

2.3 CLOSURE

The basic advances in representation compared with the formulation according to Harris[1990] can be summarised as follows:

A The dynamic continuity and energy equation are coupled and form a set of simultaneous differential equations. This means that there is a mode of transient response where pressure and temperature dynamics occur at the same frequency.

B By virtue of condition A above, the continuity equation now includes the effect of temperature.

C Explicit in the formulation is the consideration of moving boundaries.

D The method of derivation caters for a non flat intensive property profile across the control volume since no implicit assumptions have been made about the intensive properties, other than values will change in the direction of the flow path; and that the inlet and outlet conditions are related to a mean value within the control volume. This flexibility is conceptually more satisfying and allows a more representative set of models for application.

The representation of mass and energy in terms of pressure and temperature allows a wide variety of fluids to be investigated. This is primarily due to the availability of data relating to properties such as bulk modulus and the coefficient of cubical expansion, which both happen to be functions of the partial derivatives of the previously defined conservation equations.

Although a similar representation of the conservation equations has been used for analysing power generating plant, this level of detail extends the analysis for both fluid power systems, and vehicle cooling systems.

CHAPTER 3

POWER GENERATING PLANT - LOW PRESSURE FEED TRAIN

3.1 INTRODUCTION

Before embarking on a detailed account of the research and development made in relation to the study of the thermal hydraulic effects of feed systems on nuclear power plant, it is worth explaining the reasons for this work and the development of a low pressure (LP) feed train model.

One important aspect which concerns nuclear safety, is the extent to which the plant has to change power, in order to maintain the equilibrium between supply and demand on the grid system. If the equilibrium is not maintained, then fluctuations in grid frequency ensue, and in the limit, parts of the grid system may be disconnected. Historically, nuclear plant operated by the Central Electricity Generating Board (CEGB), were run at base load, at maximum available output. Provision was made to assist in meeting fluctuations in demand in extreme circumstances by manual operator intervention, however, fossil fired plant carried the responsibility for matching demand with supply requirements, Whitmarsh-Everiss[1990].

One aspect of grid frequency control relates to the need for plant to respond automatically to errors in grid frequency, on a continuous basis. This role was previously adopted by a proportion of fossil fired plant, depending on the merit order (determined by the unit generation cost). However, in an increasing competitive environment, following the privatisation of the electricity supply industry, certain nuclear plants are currently being assessed with respect to providing this role. There are many reasons why nuclear plant have not operated in automatic grid frequency control mode, which have been detailed by Whitmarsh-Everiss[1990]. It is worth looking at some of these aspects, as this bears direct relevance on the operational strategy of nuclear plants

providing this role, and the subsequent research and model development that has taken place in order to study the thermal hydraulic performance.

Integral to the operation of nuclear plant is safety of operation. One of the implications of providing automatic grid frequency response is that the plant must regulate its output power to sustain grid frequency. Changing the power inevitably induces changes in circuit temperatures and pressures which can enhance the onset of fatigue and creep damage. This reduces the lifetime of components and their integrity, and can affect the safety of the plant. In this respect, it is advantageous to maintain the reactor load at a constant output.

Safe operation of nuclear plant is maintained by the operator by constraining various parameters to pre-defined values. If these values are exceeded, then a 'trip' condition will occur which induces part or all of the plant to shut down. For instance, if the reactor neutron flux exceeds a predetermined value, then this automatically initiates a reactor trip with the consequence of lost generation. If the plant is operating in a automatic grid responsive mode, it is likely that occasionally trip margins would be exceeded from time to time thus incurring loss of generation and an inability to provide grid frequency control.

It is well known within the industry that 'once through' boilers of the type used in Advanced Gas Cooled Reactor (AGR) nuclear power plants have little stored energy in comparison to the fossil fired plants. This is primarily due to the large quantity of saturated water that exists in a fossil fired drum boiler, which when subject to a depressurisation (turbine governor valves opening) can flash off vast quantities of steam. In this respect, the ability of an AGR to sustain an increase in demanded power in the short term is reduced. When the turbine governor valves open, there is a fall in pressure with a subsequent release in stored energy. If this stored energy is not replaced quickly enough, then there will be a short fall in the sustained power response from the

plant. Although it might be possible to configure the control systems to improve the power response (this has limited merit as the stored energy is a function of the boiler design), it is highly likely that trip levels could be exceeded if the dynamic excursion to the speed error is large enough.

The above paragraphs have outlined briefly just a few reasons why it is not practical to operate AGR nuclear plant in a grid sensitive mode, with the current plant configuration and control structure.

3.2 PROPOSED PLANT CONFIGURATION

In view of the arguments sited in the introduction to this Chapter, a proposed method of operation known as Automatic Frequency Response Operation (AFRO) for the Heysham 2 nuclear power station was examined. This proposal requires modification to the plant configuration and control systems such that the nuclear island is made relatively insensitive to changes in generated load. Consider Figure 3.1 which presents a simplified schematic of the plant before modification. Not withstanding the range of different control system configurations that could be considered for plant operation, which is not under consideration in this thesis, the traditional way of achieving a primary response to grid frequency has been to take a function of the speed error signal and pass it into the control system which operates the main turbine governor valves. Changes in governor valve position induces change in the steam flow through the turbine train and thus variation in the generated output power to the grid. Transient variations in output power will inevitably feed back through to the boilers and reactor since changes in steam flow will induce variations in circuit pressures and temperatures.

To minimise the effects of changes in generated output on the boilers and reactor, when in an AFRO mode of operation, consider Figure 3.2 which shows the proposed plant modifications.

It has been proposed to implement a bypass line with desuperheating control valves (also referred to as steam dump valves), from the hot reheat steam main to the three main condensers of the plant. This has the affect of bypassing the intermediate (IP) and low pressure (LP) turbine stages. In the AFRO mode of operation, modulation of these control valves in response to errors in grid frequency will provide the means of regulating the generated power in the short term. If the interceptor valve which regulates the steam flow into the intermediate pressure (IP) turbine (Figure 3.2) is used to control steam main pressure to the 100% load condition, then it is anticipated that the boiler / reactor system will not be affected by the AFRO mode of operation. In operation, assuming a near optimal hot reheat steam main pressure control, the steam flow passing through the boiler and HP turbine should remain relatively constant due to the near constant pressure boundary condition.

Near perfect hot reheat steam main pressure control also assumes that the steam dump valve control in response to grid frequency does not interact with the former control system to produce unwanted dynamics or instabilities. The study of this control system interaction is beyond the scope of this thesis but clearly would be addressed within the remit of the overall study.

Assuming that an optimised hot reheat pressure control is viable, which would minimise variations in boiler feed and steam flow, feedwater temperature variations and the subsequent affect on the boiler and reactor thus become relatively more important. To gain an insight into the thermal hydraulic characteristics of the LP feed train (sometimes referred to as the feed system), a programme of model development was undertaken as a precursor to analysing the system as a whole. The first part of the work which is the subject of this thesis, concerns the development of a LP feed train model representative of the Heysham 2 power station (PS), which would be capable of linking in to the whole plant dynamic model when fully developed.

3.3 LP FEED TRAIN PLANT DESCRIPTION

Figure 3.3 shows the plant layout of the LP feed train in more detail. The major plant components are discussed in the following sub-sections.

3.3.1 LP Turbines

The LP turbine cylinders receive steam from the IP/LP crossover which is basically the exhaust from the IP turbine which is augmented by the boiler feed pump turbine (BFPT) exhaust (depending on load level). At 100% load the steam conditions at the LP turbine inlet are as follows, pressure 5 bara (bar absolute), and temperature 265 °C. All three LP turbine cylinders operate in parallel and each one exhausts to individual main condensers. The LP turbine cylinder is split into stages which provide steam bleed points for the a number of feed heaters in the system.

3.3.2 Main Condensers

There are three main condensers whose primary function is to reduce the wet steam from the LP turbine exhaust to saturated water conditions. They achieve this by transferring energy in the form of heat to a secondary fluid (CW), namely sea water, by virtue of a temperature difference. There are two parallel CW paths in each condenser such that in total there are six CW parallel paths. The condensers also receive the drains water from the indirect contact feed heaters in the system. Each condenser is a large construction with a cross section in plan measuring 14m by 6.4m. They are 10m high. The CW tube nest runs the length of the condenser (14m) and the tubes are made of titanium to protect them from the corrosive nature of sea water. There are 29268 CW tubes in total with an OD of 25.4mm and a wall thickness of 0.7mm. It can therefore be appreciated that the total tube mass for all three condensers is very large (100 tonnes). The condensed steam exits the condenser floor and provides the LP feed train with the condensate for the system.

3.3.3 Condensate Feed System

The function of the condensate feed system is to transfer the saturated water (at approximately 30 °C) and deliver it to the deaerator (at approximately 155 °C). It acquires this heat primarily through passing through indirect contact feed heaters in the path to the deaerator. The water transferred to the deaerator must have a low level of chemical impurity, as the boilers are sensitive to the water quality. Although not shown in Figure 3.3, chemical impurities are removed by the condensate polishing plant situated downstream of the condenser level control valves. This plant item has not been shown because early on in the conceptual modelling phase it was decided to ignore the small thermal effects this plant item has on the condensate. The main condenser level control is provided by two valves in parallel which cater for the entire load range. The level error is determined from condenser B.

There are two 100% condensate extraction pumps either of which draw condensate from the common plenum connecting the exits from all three main condensers. In this respect one of the pumps provides a standby facility should the other fail in service. Each pump is of a vertical spindle four stage caisson type which is driven by a constant speed motor, capable of providing 500 $kg.s^{-1}$ with a corresponding discharge pressure of 22 bara. These pumps are situated some 6m below the condensers to provide a margin to cavitation. It should be noted that the water leaving the condensers is in a near saturated condition (at 30 - 40 mbar).

Regenerative feed heating is provided by a number of indirect contact feed heaters in series which utilise bled steam from the LP turbine train. Heating the condensate in this manner improves the cycle efficiency. The physical arrangement of the heaters in relation to the bled steam tapping point pressures is such that each heater operates at a different pressure. The condensate from each heater must constantly be drained away and since they are operating at different pressures it is possible to utilise this heat in the lower pressure heaters. This is achieved by arranging the heaters in a cascaded fashion. LP heater 4 operates at the highest pressure. The

drains flow passes an inlet orifice to a 'flash vessel' (sometimes referred to as flash box) operating very close to the pressure of LP heater 3. This ensures that a proportion of drains flow if flashed to steam within the flash vessel. This steam then augments the bled steam to LP heater 3. This process is repeated in the lower pressure heaters (1 and 2). The heater drains cooler receives the summation of the cascaded drains flows from LP heaters 1 to 4 and this is gravity fed back to the main condensers.

Figure 3.3 shows the TMEC (turbine moisture extraction condenser) which is provided with bled steam from the last stages of all three LP turbines. The TMEC is identical to the LP heaters in function but is independent of the cascaded heater system.

The deaerator (DA) shown if Figure 3.3 provides storage for a large quantity of feed water which supplies the high pressure (HP) feed system to the boilers. Some of the functions of the DA are listed as follows:

1 Reduce the oxygen content of the condensate

2 Provides the boiler feed pumps with adequate suction head

3 Allows transient differences between HP feed flow and condensate feed flow by virtue of retaining a large quantity of stored water.

The thermodynamic conditions that prevail in the DA is provided by the condensate which is augmented by the HP gland, BFPT exhaust or IP/LP crossover steam. The DA is a two phase vessel and as such the condensate exits in a saturated condition in the steady state. At 100% load, the BFPT exhaust elevates the condensate temperature to approximately 155 °C (approx 5 bara).

3.3.4 Condensate Volume Control

The volume of condensate in the system remains relatively constant, however during transient excursions there will be a miss-match between the condensate and steam entering and leaving

both the DA and the main condensers. This manifests itself in variations in water levels within these plant items. The control of water levels has been implemented as follows.

The water level in main condenser B is controlled by two valves in parallel, and these are shown in Figure 3.3 as WC-244 and WC-244Y. These valves are situated in the condensate feed path, down-stream of the condensate extraction pumps. At high load conditions, the main 12 inch valve WC-244 will be controlling level, the smaller valve WC-244Y remains fully open at loads above 45% of maximum due to control action. Both valves operate under proportional plus integral control action with desaturation logic included. The levels in condensers A and C remain approximately at the level of condenser B due to hydrostatic considerations (strictly speaking it is not a hydrostatic situation but the pressure loss due to friction in the condensate drains from each condenser is very low in comparison to the gravitational head).

The DA water level is maintained by adding or removing condensate from the LP feed train. A low level is restored by introducing a make-up flow to main condenser B, supplied from the reserve feed water (RFW) tanks via control valve WC-343. This induces a higher water level in main condenser B and subsequently the condenser level control valves open to restore the water level. In doing so an excess of water is supplied to the DA. A high level is reduced by redirecting a proportion of the condensate down-stream of the condensate polishing plant, back to the RFW tanks via control valve WC-253. Both control valves respond to proportional plus integral control action.

3.4 LP FEED TRAIN MODEL DESCRIPTION

The development of the system component models has been conducted using the Plant Modelling System Program (PMSP) which is an 'in-house' steady state and dynamic simulation code developed by the CEGB and subsequently inherited by Nuclear Electric. The numerical

algorithms and integrators have been designed to cope with the types of problems encountered when simulating power generation plant, although this does not preclude other types of systems being examined. PMSP has its own specific language which provides the user with 'initial', 'dynamic' and 'terminal' sections. Models are written in a procedure oriented way and are called typically from the dynamic section of PMSP. As PMSP is Fortran based, a subset of procedures and Macros may be written using Fortran statements directly.

The LP feed train model encompasses all the components described in section 3.3. The following section details the modelling philosophy that has been used to represent mathematically the LP feed system. Detailed calculations of the coefficients used are shown in appendix B.

3.4.1 LP Turbine Model

The LP turbine model is based on the Sibdym LP turbine (Sizewell B PS) representation, NNC Ltd[1994]. The steam mass flow rate per stage is based on the ellipse law as follows:

$$w_T = k_T \sqrt{p_i \rho_i} \sqrt{1 - \left(\frac{p_o}{p_i}\right)^{\frac{m+1}{m}}} \qquad (3.1)$$

NNC Ltd[1994] state that this is a semi-empirical equation, however it can be derived by considering the pressure loss across the blade row to be proportional to the square of the mass flow and inversely proportion to the steam density. Deacon[a] has suggested that in this respect it is reasonable to assume an equation of the form:

$$k\, w^2 = -\int_{p_i}^{p_o} \frac{dp}{\upsilon} \qquad (3.2)$$

which represents the turbine flow resistance providing the 'k' term is adjusted to reflect the correct distribution in pressure along the turbine stages. Integrating this equation to arrive at

equation (3.1) requires the relationship between the steam specific volume and pressure. The flow of steam through any particular blade row or stage can be considered adiabatic in the sense that it is reasonable to assume that the turbine is insulated from the surroundings. However the process is not reversible due to the affect of friction. Ideally, the steam would expand isentropically to the down-stream pressure thus imparting the maximum amount of energy to the turbine. In practice the frictional effect raises the temperature of the steam and increases the entropy. The expansion is polytropic in form which may be deduced from a few fundamental thermodynamic relationships, and the assumption that the isentropic efficiency is constant for the stage considered. This is not unrealistic since the turbine is to all intents and purposes a constant speed machine over the entire load range. Because the steam velocity is proportional to the blade velocity, Lewitt[1953], the frictional effect will remain practically constant. For an isentropic process the change in enthalpy is related to the specific volume and change of pressure as follows:

$$dh|_s = \upsilon dp \tag{3.3}$$

This is the maximum theoretical enthalpy change from the steam passing through an incremental section of the turbine. To deduce the actual enthalpy change it is common to introduce an efficiency term for the process such that the actual enthalpy change can be represented as:

$$dh = \eta_s \upsilon dp \tag{3.4}$$

If the actual enthalpy change is also expressed in terms of other thermodynamic properties, the 'dh' term can be eliminated to yield the relationship between pressure and specific volume as follows:

$$dh = du + pd\upsilon + \upsilon dp \tag{3.5}$$

Note that the incremental change in internal energy can be expressed as:

$$du = \frac{\partial u}{\partial p}\Big|_{\upsilon} dp + \frac{\partial u}{\partial \upsilon}\Big|_{p} d\upsilon \tag{3.6}$$

Substituting equation (3.6) into (3.5) and equating to (3.4), the following relationship may be found:

$$\frac{dp}{p} = - m \frac{d\upsilon}{\upsilon} \tag{3.7}$$

where

$$m = \frac{1 + \frac{1}{p} \frac{\partial u}{\partial \upsilon}\Big|_{p}}{1 + \frac{1}{\upsilon} \frac{\partial u}{\partial p}\Big|_{\upsilon} - \eta_s} \tag{3.8}$$

It can be seen that integration of equation (3.7) would give

$$p\upsilon^m = constant \tag{3.9}$$

providing m is constant. This may be established as follows, assuming the isentropic efficiency is constant for the stage considered. Assume the steam to behave as a perfect gas. In this respect the internal energy is a function of temperature only, and the relationship between pressure, volume and temperature is characterised by the standard equation of state. The following can then be deduced to arrive at a function for 'm' involving the isentropic efficiency and the ratio of specific heats. If

$$du = Cv\, dT, \quad p\upsilon = RT, \quad Cp - Cv = R, \quad \frac{Cp}{Cv} = \gamma$$

Then

$$\frac{\partial u}{\partial \upsilon}\Big|_{p} = Cv \frac{\partial T}{\partial \upsilon}\Big|_{p} = Cv \frac{p}{R}, \qquad \frac{\partial u}{\partial p}\Big|_{\upsilon} = Cv \frac{\partial T}{\partial p}\Big|_{\upsilon} = Cv \frac{\upsilon}{R}$$

Substituting these relationships into (3.8) gives 'm' as:

$$m = \frac{1 + \dfrac{Cv}{Cp - Cv}}{1 + \dfrac{Cv}{Cp - Cv} - \eta_s} \tag{3.10}$$

which leads to:

$$m = \frac{1}{1 - \dfrac{\eta_s(\gamma - 1)}{\gamma}} \tag{3.11}$$

Therefore providing the stage isentropic efficiency is constant equation (3.9) may be used in (3.2) to arrive at equation (3.1).

The enthalpy drop per stage is based on the isentropic efficiency and is determined from steady state considerations:

$$h_o = h_i - \eta_s (h_i - h_o|_s)$$

Where $h_o|_s$ is the exit enthalpy from the stage assuming the steam has been expanded isentropically. This can be determined from a knowledge of the stage inlet entropy, and one of the exit steam properties. In this instance pressure is used to solve the dynamic continuity equation at the stage exit due to the LP heater bled steam flows, and so this is used.

Each LP turbine is spit into four stages, with a heater bled steam tapping point separating each stage. The last stage from each turbine exits to one of the three main condenser representations. Table 3.1 details the heater bled steam divisions for each turbine stage.

Table 3.1 Relationship between LP turbine stages and bled steam to heaters

LP Turbine	Stage Exit	Bled steam to heater
1	1	2
1	2	1

1	3	TMEC
2	1	3
2	2	1
2	3	TMEC
3	1	4
3	2	1
3	3	TMEC

3.4.2 LP Heater Model

The LP heaters in the condensate feed system are identical in design. They are two phase vessels which receive bled steam from the LP turbine, which in general is augmented by flash steam from the flash vessels. This steam (primary side) is condensed across a two pass tube bundle which imparts energy to the condensate (secondary side) on route to the DA, thus raising its temperature and improving the cycle efficiency. As previously mentioned in Chapter 1 of this thesis, one of the deficiencies of the PMSP total plant modelling codes is that only one code has an LP feed train representation which is based on the Sizewell B PWR PS. This model uses a Log Mean Temperature Difference (LMTD) approach which is modified to account for the stored energy in the tube material. The LMTD approach is well established, and used in its original form, the rate of heat transfer between hot and cold fluids is defined as:

$$q = U A \Delta T_m \tag{3.12}$$

where ΔT_m is a function of the inlet and exit fluid temperatures and represents the LMTD. Introducing the material temperature and therefore describing individual rates of heat transfer from both hot and cold fluids has been achieved by defining an averaging coefficient (Ac) which relates the cold fluid (secondary side) temperatures to the hot fluid (primary side) temperature and the LMTD. This allows a dynamic calculation to be performed which takes account of the tube material stored energy, from what was a steady state technique (LMTD) for determining heat rates. This process has been made easier by the fact that the primary side water/steam

temperature (T_p) within the shell of the heater is uniform across the whole tube bundle, since the steam is condensing within the vessel to saturated water. One can say then that the average condensate temperature passing through the heater, is equal to the primary side temperature minus the LMTD.

$$Tcon_{ave} = T_p - \Delta T_m \tag{3.13}$$

The average condensate temperature can also be defined as:

$$Tcon_{ave} = Tcon_l - Ac\ (\ Tcon_l - Tcon_e) \tag{3.14}$$

The LMTD may be defined as :

$$\Delta T_m = \frac{(\ T_p - Tcon_l\ ) - (\ T_p - Tcon_e)}{\ln Q} \quad where \quad Q = \frac{T_p - Tcon_l}{T_p - Tcon_e}$$

Equating equations (3.13) and (3.14), yields an expression for the averaging coefficient as follows:

$$Ac = \frac{Q}{Q - 1} - \frac{1}{\ln Q} \tag{3.15}$$

In the NNC Ltd[1994] representation, this is defined as an integrator because both the inlet and exit condensate temperatures are algebraic expressions based on the coolant enthalpy and therefore creating an implicit loop. The average condensate enthalpy is a state variable determined from an energy balance as follows:

$$\frac{d(hcon_{ave})}{dt} = \frac{A_s\ htc_s(T_t - Tcon_{ave}) - wcon\ (hcon_l - hcon_e)}{Mw}$$

The average condensate temperature is a function of enthalpy and pressure and therefore equation (3.14) may be re-arranged to find the leaving condensate temperature for the heater.

This form of heater representation does have limitations insofar that the shell side thermodynamic state is based on the saturation condition pertaining to the turbine steam tapping point pressure, minus the bled steam line pressure loss. No allowance is made for additional steam inputs such as flash steam which is required for the Heysham 2 configuration. One other limitation is that perfect drainage is assumed by assigning the drain flow equal to the bled steam flow. In this respect there is no water level representation. One of the requirements for the Heysham 2 heater model is the determination of water level. If the water level rises significantly in the heater shell, possibly in response to a tube leak, isolated drain route or severe transient response, then there is the risk that water could find its way back to the turbine bleed tapping point with the risk of damaging the blading. The plant is arranged such that the operator is warned of this condition by a high water level alarm. If the water rises further then an automatic trip sequence is initiated which isolates the affected heater from the LP turbines, and re-routes the condensate via a bypass route.

A number of approaches were explored to find a satisfactory solution in representing shell side water/steam pressure, and providing a water level, and these are discussed below.

Method 1 considers both water and steam phases in the shell. If the masses of water and steam are solved by a dynamic conservation of mass equation, represented in the usual way, it is possible to compare the volumes of water and steam existing in the shell and compare this with the shell volume. Clearly the two should be equal. Knowledge of the shell pressure will provide the specific volumes of both water and steam (the shell is assumed to operated in a saturated condition and therefore saturated property values may be determined from any one thermodynamic property). The volumes of water and steam are calculated from the individual masses and specific volumes. Comparison with the shell side volume will indicate either an equality, in which case the assumed pressure is correct, or an inequality in which case the

pressure is incorrect. The calculation is implicit in nature and can be solved either by an integrator or implicit loop routine. If the loop is broken by an integrator, the shell side (primary side) pressure derivative is represented as follows:

$$\frac{dP_p}{dt} = k\,(V_w + V_s - V_{shell}) \tag{3.16}$$

Intuitively, it may be seen that if the sum of the water and steam volumes is too large, then this increases the pressure with the affect of reducing the specific volumes (particularly of the steam). On the next iteration of the equation set, the combined water and steam volume is reduced due to the reduction in specific volumes. This effect removes the error when the convergence has been obtained on a particular integration step. The stability of the solution is affected by the magnitude of the gain term 'k' which may be adjusted to provide a satisfactory dynamic response. In performing a separate mass balance for both water and steam phases, a mechanism is required for deducing the quantity of steam that is condensed across the tube bundle to the water phase. One approach is to assume that all the steam is reduced to the saturated water condition corresponding to the particular shell pressure. The energy lost (mostly latent heat because the steam is slightly superheated) must be given up to the tube bundle. Therefore an energy balance can be used to determine the mass flow rate of condensing steam, assuming the shell always operates in a saturated condition. The condensing steam mass flow rate may be determined from:

$$w_c = \frac{q_p}{h_p - h_f} \tag{3.17}$$

It should be noted that the rate of heat transfer from the primary side to the tube bundle (q_p) is modified to account for the reduction in htc when the water level rises. This phenomenon is attributed to the significant difference in htc between condensing and liquid phase heat transfer, typically in the ratio of 3:1 (Heysham 2 plant data). In normal operation the water level in the

heater is generally located in the drain pipe, and therefore the whole tube bundle is subject to condensing heat transfer. If the water level rises significantly into the shell due a particular fault situation, the tube bundle gradually becomes submerged in saturated water. To facilitate this effect, 'q_p' is related to the tube bundle surface areas which are exposed to both the water and condensing steam, and the temperature difference between the primary side water/steam and the tube bundle. 'q_p' may be represented as follows:

$$q_p = (htc_w A_w + htc_c A_c) (T_p - T_{tube})$$

Noting the relation between condensing steam and water htc (3:1) then 'q_p' becomes:

$$q_p = (A_w + 3 A_c) htc_w (T_p - T_{tube}) \qquad (3.18)$$

where equation (3.18) expresses 'q_p' in terms of saturated water htc. It can be appreciated that as the water level rises then the tube bundle surface area covered by the water rises. Consequently the tube bundle surface area covered by the condensing steam reduces. The nett effect is a reduction in 'q_p' with a corresponding reduction in condensing steam mass flow rate into the water space (equation 3.17). The reduction in condensing steam mass flow rate helps stabilise a high water level condition within the heater, should this occur via any particular fault situation.

Although the description above (method 1) has explored a means of determining the shell pressure and water level, there are outstanding aspects to be addressed such as the drain flows from the heaters. As this is applicable to all the heater representations that were studied, it will be discussed after the following description of alternative methods for determining shell pressure and water level in the heaters.

Method 2 determines the shell pressure and water level from a more rigorous thermodynamic

view point, NNC Ltd[1994]. This approach has been used to described the conditions inside the DA of the Sizewell B Nuclear PS. Some modification is required to allow for tube bundle heat transfer but the technique is essentially similar.

The rate of change of the shell water and steam internal energy can be represented by equation (2.2) (Chapter 2) as follows:

$$\frac{dU}{dt} = \frac{d}{dt}(Mu) = \sum wh - p\frac{dV}{dt} + q_h \tag{3.19}$$

As the water and steam mixture does no work on the system, this term is omitted. The internal energy (Mu) can be expanded in terms of other thermodynamic properties as follows:

$$Mu = Mh - pV = V(\rho h - p)$$

And so the rate of change of internal energy can be represented as

$$V\rho\frac{dh}{dt} + Vh\frac{d\rho}{dt} + \rho h\frac{dV}{dt} - V\frac{dp}{dt} - p\frac{dV}{dt} = \sum wh - p\frac{dV}{dt} + q_h \tag{3.20}$$

Note that the 'p dV/dt' term cancels from both sides of equation (3.20). Method 2 assumes that both phases are represented in a saturated condition and as such equation (3.20) may be expanded to include both phases. It is also convenient to formulate equation (3.20) in terms of water volume derivative which substitutes for steam volume derivative (being numerically equal but opposite in sign) and therefore reducing the number of terms. Including both phases in terms of both pressure and volume time derivative, noting that $V_g = V_{tot} - V_f$, equation (3.20) becomes:

$$V_f \rho_f \frac{\partial h_f}{\partial p}\frac{dp}{dt} + (V_{tot} - V_f)\rho_g \frac{\partial h_g}{\partial p}\frac{dp}{dt} + V_f h_f \frac{\partial \rho_f}{\partial p}\frac{dp}{dt} + (V_{tot} - V_f) h_g \frac{\partial \rho_g}{\partial p}\frac{dp}{dt} +$$
$$\rho_f h_f \frac{dV_f}{dt} - \rho_g h_g \frac{dV_f}{dt} - V_f \frac{dp}{dt} - (V_{tot} - V_f)\frac{dp}{dt} = \sum_f^g wh + q_h \tag{3.21}$$

Collecting terms, equation (3.21) becomes:

$$\frac{dp}{dt}\left(V_f \rho_f \frac{\partial h_f}{\partial p} + (V_{tot} - V_f)\,\rho_g \frac{\partial h_g}{\partial p} + V_f h_f \frac{\partial \rho_f}{\partial p} + (V_{tot} - V_f)\, h_g \frac{\partial \rho_g}{\partial p} - V_{tot} \right) - \frac{dV_f}{dt}(\rho_f h_f - \rho_g h_g) = \sum_f^g wh + q_h \tag{3.22}$$

At this point it is necessary to eliminate the water volume time derivative which may be done by considering dynamic mass conservation within the shell. The total water and steam mass in the shell (M_{tot}) may be represented as follows:

$$M_{tot} = M_f + M_g = \rho_f V_f + \rho_g V_g \tag{3.23}$$

The rate of change of water and steam mass in the shell then becomes:

$$\frac{dM_{tot}}{dt} = \rho_f \frac{dV_f}{dt} + V_f \frac{d\rho_f}{dt} + \rho_g \frac{dV_g}{dt} + V_g \frac{d\rho_g}{dt} = \sum_f^g w \tag{3.24}$$

Making the substitution for the density time derivative in terms of specific volume, and replacing in terms of pressure gives:

$$\frac{d\rho}{dt} = -\frac{1}{\upsilon^2}\frac{d\upsilon}{dt} = -\frac{1}{\upsilon^2}\frac{\partial \upsilon}{\partial p}\frac{dp}{dt}$$

Using this relation and re-arranging equation (3.24) to make dV_f/dt the subject gives:

$$\frac{dV_f}{dt} = \frac{\frac{dp}{dt}\left(\frac{M_f}{\upsilon_f}\frac{\partial \upsilon_f}{\partial p} + \frac{M_g}{\upsilon_g}\frac{\partial \upsilon_g}{\partial p}\right) + \sum_f^g w}{\rho_f - \rho_g} \tag{3.25}$$

Equation (3.25) is used to determine water volume in the shell. This relationship may be substituted into equation (3.22) to eliminate dV_f/dt and provide the rate of change of internal energy in terms of pressure. Once the terms have been re-grouped equation (3.22) is represented

as follows:

$$\frac{dp}{dt} = \frac{\sum_f^g (w\ h) + q_h - \sum_f^g (w)\left(\frac{h_f}{\upsilon_f} - \frac{h_g}{\upsilon_g}\right)\left(\frac{1}{\rho_f - \rho_g}\right)}{\sum_f^g \left(M \frac{\partial h}{\partial p}\right) - \sum_f^g \left(\frac{h\,M}{\upsilon} \frac{\partial \upsilon}{\partial p}\right) - V_{tot} + \sum_f^g \left(\frac{M}{\upsilon} \frac{\partial \upsilon}{\partial p}\right)\left(\frac{h_f}{\upsilon_f} - \frac{h_g}{\upsilon_g}\right)\left(\frac{1}{\rho_f - \rho_g}\right)}$$

(3.26)

These equations are configured such that the pressure derivative is calculated before the water volume derivative to avoid the implicit relationship. The partial properties are deduced from thermodynamic functions of water and steam respectively. Method 2 is theoretically more attractive compared with method 1 and it is interesting to note that the requirement for deducing the condensing steam mass flow rate in order to solve two separate mass conservation equations has now been eliminated, due to the nature of the solution. This has been replaced by the rate of heat transfer to the tube bundle 'qh' which is the rate of energy transfer required to condense the steam to saturated water conditions. Method 2 however is more expensive computationally.

Stachowski[1993] has considered the modelling of vessels containing both water and steam in a fossil fired drum boiler of a combined cycle gas turbine plant. This type of drum boiler is of a forced recirculation type. The drum is a cylindrical vessel which under normal operation contains both water and steam. Water exits the base of the drum and passes through an evaporator bank where a proportion is elevated to steam. This two phase mixture passes back into the drum where the water is removed in a moisture separator. The steam then exits the drum on route to the superheater banks. Stachowski[1993] makes allowances for both the water to be subcooled and the steam to be superheated. Both phases have independent energy equations and both heat and mass transfer are considered between phases including evaporation and

condensation.

Pressure is determined for the steam space which includes contributions from all of the water and steam flows that leave the steam space. If this approach is used to model the heater, a method is still required to determine the condensing steam flow across the tube bundle (which also arose with method 1). Another issue with this method, is that mass transfer rates between the water and steam are determined with the aid of pre-determined coefficients. Consider the situation where the steam is slightly superheated and the water subcooled. Then by definition there is both condensation and evaporation occurring between phases. To determine the nett rate of condensation/evaporation, Stachowski[1993] has defined the interface between phases to exist exactly at the saturation temperature. Rates of heat transfer are then deduced to and from the interface from both phases, and the difference determines the condensation/evaporation flow rate. The magnitude of this flow rate depends greatly on the values of htc selected and therefore becomes qualitative to some degree unless precise values can be established. It could be argued that to consider condensation/evaporation based on heat transfer directly between phases is insignificant compared with that of the condensation flow rate across the tube bundle, and in this respect, the more simplified approach of method 1 would be just as valid.

From the above discussion, it is evident that the last of the methods proposed has no advantage over the previous two methods except for the ability to cope with subcooled and superheated regions. The major disadvantage would be the selection of htc's for various heat transfer process that are considered, all of which are small compared with the heat transfer given up to the tube bundle. It was therefore considered appropriate to dismiss the last method as a viable approach for modelling the heater. Method 1 was eventually used for determining the pressure in the shell due to its simplicity, however, transient comparison with method 2 is undertaken in the section on transient performance (Full stand alone model used to test heater 4 under quadrant trip

conditions).

During the development phase of testing the heater model, within a cascaded system of heaters and flash vessels, Figure (3.3), it became apparent that the system would not function correctly off design conditions. When a change of boundary conditions occurred that reduced the pressure in the heater shells, the water levels in many of the heaters and flash vessels would move to unrealistic positions (completely dry drain pipes). The problem was traced to the drain flow calculation, which used standard hydraulic relationships to determine mass flow rate. The mass flow rate is considered to be a function of both pressure drop and gravitational head as follows:

$$w_d = \sqrt{\frac{\rho}{k}(\Delta p + \rho\, g\, \Delta z)} \qquad (3.27)$$

The resistance coefficient 'k' may be determined from knowledge of the plant conditions. Shell pressures in the steady state are functions of the plant load level. When the model boundary conditions were changed to reflect a reduction in load level, the shell pressures reduced accordingly. However, the change in drain flow was attenuated by using a saturated water density in equation (3.27). Subsequent investigations revealed that the drain water flow can under certain conditions entrain steam when the water level is near or in the drain pipe. This effect increases as the water level falls further with proportionally more entrained steam in the drain flow. It can be appreciated that if a two phase mixture density is used which is a function of drain water level, then this will allow larger changes in drains flow passing the heater drain orifice plate, compared with a near constant saturated water density.

To include the effects of two phase drain flow requires at a minimum equation (3.27) to use a two phase mixture density. The problem then arises of how to specify the mixture quality at the drains orifice plate. In light of the fact that it was not possible to perform any tests at the plant

to predict this phenomenon, it was decided to relate the mixture quality at the drains orifice linearly to the water level in the drain. If the water level resides at the top of the drain pipe, then the drain quality is assumed to be zero, and therefore the drain contains single phase saturated water. If the water level reaches the drain orifice plate then the mixture quality is set to one, and the drain contains dry saturated steam.This was initially completed with a typical calculation for two phase mixture density based on the fraction of saturated water and steam present:

$$\rho_x = \frac{1}{\upsilon_f + x\,(\upsilon_g - \upsilon_f)} \tag{3.28}$$

Using this relationship unfortunately has the affect of dramatically reducing the mixture density for very small values of quality. The relationship (equation (3.28)) is highly non linear and this affects the water level such that once in the drain, very little movement occurs. The mixture density was subsequently modified to produce a linear variation with dryness fraction:

$$\rho_x = \rho_f + x\,(\rho_g - \rho_f) \tag{3.29}$$

The use of equation (3.29) allows a smoother transition between the shell and drain pipe, and in the limit produces identical values for the density of saturated water and steam. Ideally, use of equation (3.28) is preferential, however unless accurate predictions of dryness fraction are available, it is not sensible to use this relationship because of the non-linearity involved.

The drains flow calculation is based on a standard hydraulic relationship which includes the effects of pressure difference and gravitational head, equation (3.27). The question of whether this is suitable for two phase applications can be addressed by reference to work such as Liu *et al.*[1988]. Liu *et al* have conducted theoretical and experimental investigations relating to steam - water mixtures passing sharp edged orifices. It is interesting to note that the mass flow rate is predicted by the a relationship of the following form:

$$w_d = A_d \sqrt{\frac{2\rho_f \Delta p}{k\, k_m\, (1 + x(\frac{\rho_f}{\rho_g} - 1))}} \qquad (3.30)$$

The constant 'k' is a function of pressure ratio which determines the effects of compressibility. This is deduced from experimentation and it is often assumed that it is linear over pre-defined pressure ranges (where working pressures are significant when compared to the critical pressure for water, however at low pressure it is practically constant), although in general it is non-linear. k_m is a function of orifice to pipe diameter. Comparison of equation (3.30) with (3.27) highlighted the fact that these relationships are identical in form if equation (3.28) is re-arranged as follows:

$$\rho_x = \frac{\rho_f}{1 + x\,(\frac{\rho_f}{\rho_g} - 1)} \qquad (3.31)$$

Substituting for ρ_x in equation (3.27) it can be seen there is essentially no difference apart from the gravitational component. In this respect the use of equation (3.27) to define drains flow is justified.

Other researchers such as Lin *et al.*[1992], Rooney *et al.*[1973] consider more complex functional relationships to determine the hydraulic characteristics of orifices passing two phase flow. These include separated phase models, as opposed to a homogeneous model which has been used above. These models still rely on the basic premise that the pressure drop is proportional to the square of the flow rate. However sophisticated the flow model used, the accuracy of the flow rate prediction will always be limited by the uncertainty of the dryness fraction at the orifice plate for this application.

In the evolution of the physical relationships describing the heater performance, htc's have been

merely stated as a component of the rate of heat transfer from the primary fluid to the tube material, and from the tube material to the secondary fluid. Clearly, it is important for the htc's to accurately represent the physical situation within the heater. NNC Ltd[1994] have used a simplified relationship for heat transfer coefficient based on the well known Dittus Boelter correlation, Holman[1992a] which relates Nusselt number to Reynold's and Prandtl number. The relationship NNC Ltd[1994] has used, omits the dependence of the Prandtl number. The htc used by NNC Ltd for both the primary and secondary fluid is as follows:

$$htc \propto w^{IND} \tag{3.32}$$

The 'IND' exponent is itself made a function of flow rate which is indicative of load level. On reflection, it is difficult to see why the more general relationship such as that described by Dittus Boelter has not been used, which would include directly the effects of fluid temperature.

All the htc correlations mentioned so far are appropriate for liquid to tube heat transfer. However, the condensing htc could be more accurately defined by relationships such as that described by McAdams[1954] for condensing heat transfer across tube banks as follows:

$$htc_c = 0.725\left(\frac{K_{th}^3\ \rho^2\ g\ h_{fg}}{N\ d\ \mu\ \Delta T}\right)^{0.25}$$

It can be seen that this correlation does not include any flow dependency. It has been found by NNC Ltd[1994] that expressing the htc in terms of equation (3.32) has required prior knowledge of the heat rate at various load conditions so that individual terms may be fitted to the data to achieve the correct rate of heat transfer. The deviation between the LP feed train model and plant is tested in Chapter 4.

3.4.3 Drains Cooler Model

The purpose of the drains cooler (DC) is to elevate the condensate temperature by transferring

a proportion of the remaining heat energy from the LP heater drains water. The heater drains cooler is identical in design to the LP heaters although it is physically smaller. In operation the main difference is the input to it is saturated drains water instead of steam, a proportion of which flashes to steam when passing the inlet orifices. The energy and mass conservation equations are identical to that used for the heaters, however, additional calculations are required to determine the steam quality within the vessel. The enthalpy of the incoming mixture (drains from LP heater 1 and flash vessel 1) is deduced from steady state energy balance:

$$h_{sdc} = \frac{w_{dh1}\, h_{dh1} + w_{df1}\, h_{df1}}{w_{dh1} + w_{df1}}$$

The steam quality may be deduced from:

$$x = \frac{h_{sdc} - h_f}{h_{fg}}$$

The condensing steam flow is calculated in an identical way to that of the heater model, assuming the mixture inlet enthalpy is reduced to saturated water conditions. The proportion of incoming mixture that exists as dry steam is:

$$w_{gi} = x\ (w_{dh1} + w_{df1})$$

The proportion of dry steam that condenses across the tube bundle is:

$$x.w_{sw}$$

Where W_{sw} is the combined mass flow rate of the water steam mixture passing the tube bundle. Steam space mass conservation then becomes:

$$\frac{dMs}{dt} = w_{gi} - x.w_{ws}$$

A similar relationship is used for the water space mass conservation.

3.4.4 Flash Vessel Model

There are three flash vessels situated at the exit to LP heaters 2 to 4 respectively. Each flash vessel receives LP heater drains water and the drains from the upstream flash vessel (except for flash vessel 3), a proportion of which is flashed to steam across the inlet orifices. The steam in each flash vessel augments the LP heater operating at a slightly lower pressure, thereby improving the total quantity of heat transferred to the condensate. The flash vessels have been modelled using the following assumptions:

1 Steady state energy balance, a proportion of incoming drains flow is flashed to steam at the vessel pressure (identical to the DC model).

2 The vessel is adiabatic

3 Mass conservation for both phases (identical to the heater and DC models).

4 Saturation conditions prevail at all times (identical to the heater and DC models).

Pressure is determined in an identical way to that of the heaters by using a loop breaking integrator based on the volumes of both phases in the vessel. The flash vessel drain flow rate is based on pressure difference and potential head considerations, and is modified to reflect a level of steam entrainment should the water level fall into the drain pipe. This in fact is a necessity since the water level requires stabilising in a similar way to that of the heaters.

3.4.5 Deaerator Model

The DA model is based on the representation for the Sizewell B nuclear PS, NNC Ltd[1994], which has been examined in the section on LP heater model development (section 3.4.2, method 2). Energy and mass conservation equations are solved dynamically in terms of vessel pressure and water volume. Inputs include condensate feed flow from the LP heater path, and the bled steam from the LP turbine inlet. The DA forms the last item of plant to be modelled before the

start of the HP feed system and therefore requires exit flow rate as a boundary condition.

3.4.6 Condenser Model

The three main condensers have been modelled individually such that asymmetries in the dynamic response can be studied in detail. The physical modelling is identical to the DA with the addition of tube heat transfer included. Heat transfer to the cooling water (CW) is based on the LMTD approach which is modified to include tube material stored energy, which is identical to that used for the LP heaters. CW exit temperature is therefore predicted.

The condensers are assumed to operate in a saturated condition corresponding to the vessel pressure. Allowance is made for sub-cooling of the exit condensate by way of a user supplied temperature drop. The heat lost elevates the CW exit temperature to some degree, but since CW mass flow rate is considerably larger than the condensate flow rate to the DA, it is very small by comparison. Water level is determined from water volume and knowledge of the condenser geometry.

The condensate exit from all three condensers form the start of the condensate feed system. The plant configuration is such that asymmetries exist in the boundary conditions to each condenser, and these are listed in the following table.

Table 3.2 Condenser boundary conditions

CONDENSER	MODEL INPUTS
A	Drain flows: 1 Heater drains cooler 2 TMEC primary drain 3 LP heater 3 & 4 diverted drains
B	Drain flows: 1 TMEC primary drain Insurge flow (DA level low) LP Turbine B exhaust
C	Drain flows: 1 Heater drains cooler 2 TMEC primary drain 3 LP heater 3 & 4 diverted drains

3.4.7 Condensate Feed System Model

This component model has been assembled to accurately reflect the combined flow resistances of the previously described condensate feed components. The combine flow resistance must include all components from the condenser outlet hot well to the DA inlet, see Figure 3.3. This also includes additional resistances which represent the condenser level control valves (WC-244 & WC-244Y) which are situated at the exit of the condensate extraction pumps, see Figure 3.3. These valves move under control action and therefore represent a variable resistance in the feed path. Similarly, the DA level letdown valve (WC-253) is represented, which returns condensate to the RFW tanks. The resistance to the LP heater bank allows for a bypass route should the any particular heater trip on high water level (The LP turbines blades must be protected from water ingress). The sum of all resistances, gravitational head, and the condensate extraction pump head/flow characteristic are used to determine condensate flow rate. The condensate flow rate is represented by a loop breaking integrator and is used to satisfy conservation of mass in the system.

3.5 CONTROL SYSTEM MODELS

Within the LP feed system, there are four large water storage vessels (condensers and DA). Given that the plant changes its operating conditions with time, the requirement exists to maintain the vessel water levels on a continuous basis. Level control is implemented in both the DA and the condensers, and is detailed in the following subsections. Both control systems are represented in the LP feed system model.

3.5.1 Deaerator Level Control

The DA level is maintained by adding or removing condensate from the LP feed train. A low level is restored by introducing a make-up flow to main condenser 'B', supplied from the Reserve Feed Water (RFW) tanks, via control valve WC-343. A high level is reduced by redirecting a proportion of condensate down stream of the condensate polishing plant, back to the RFW tanks via control valve WC-253.

Both make-up and let-down valves respond to proportion plus integral control action. The level measurement for make-up and let-down controllers is provided by two independent transducers, each with a measurement range of 355.6 mm. Each measurement device is separated by 152.4 mm in the vertical plane.

The make-up measurement transducer tapping point is situated 3.046 m from the DA floor. The setpoint is 177.8 mm above this which equates to 3.2238 m above the DA floor. In operation, if the DA water level is below the setpoint, the control action will open control valve WC-343 to restore the water level. If the DA water level exists above the setpoint, control valve WC-343 will be fully closed, and the make-up control system will be in a saturated condition. The model

includes desaturation logic for this event.

The let-down transducer is situated 152.4mm above the make-up transducer. The setpoint is 177.8 mm above this value which equates to 3.376 m above the DA floor. If the DA water level exists above this value, control action will open valve WC-253 to restore the high water level. If the level is below the setpoint, then the control valve will be fully closed and the let-down control system will be in a saturated condition.

If the water level exists in a range 3.3 m ± 76.2 mm, then from the preceding description, both controller exist in a saturated condition with both control valves fully closed. In this respect, there is a 76.2 mm deadband, either side of the normal working level, which is built in to the DA water level control action. This prevents interaction between controllers at the normal working level.

3.5.2 Main Condenser Level Control

The water level in condenser 'B' is controlled by two valves in parallel (WC-244 & WC-244Y), situated in the condensate feed path, see Figure 3.3. At high load conditions, the main 12 inch valve (WC-244) will be controlling the level, the small valve WC-244Y remains fully open at above 45% load due to control action. This is achieved by different setpoints for both valves. At low load the main control valve is closed, and level control is achieved with the smaller valve which provides a better dynamic response at these conditions. Both valves operate under proportional plus integral control action.

Although level control is maintained in 'B' condenser only, this does affect both 'A' and 'C' condensers due to the common exit plenum. In general, providing the plant is operating normally, any differences in the levels of condensers 'A' and 'C' will tend to diminish due to

differences in gravitational heads. Providing the shell pressures are similar in magnitude, excess head in either condenser will produce an increased discharge flow to the common plenum, causing an equalising effect in condenser levels.

3.6 CLOSURE

A description of the research and model development has been given in order to analyse the AFRO response of the Heysham 2 power station. Most of the effort has been directed towards development of a suitable LP heater model, which is capable of showing dynamically the response to the AFRO mode of operation. This has necessitated a detailed examination of conservation of mass and energy for vessels containing a two phase water/steam mixture. Of particular importance is the necessity to represent a two phase drains flow. Without this, the cascaded heater/flash vessel system is unstable when standard single phase liquid pressure / flow models are used.

These component models have been developed to provide a mathematical description of the LP feed system. To test the validity of the composite LP feed system model and its suitability for predicting both the plant steady state and transient response, comparison with the plant is made in Chapter 4.

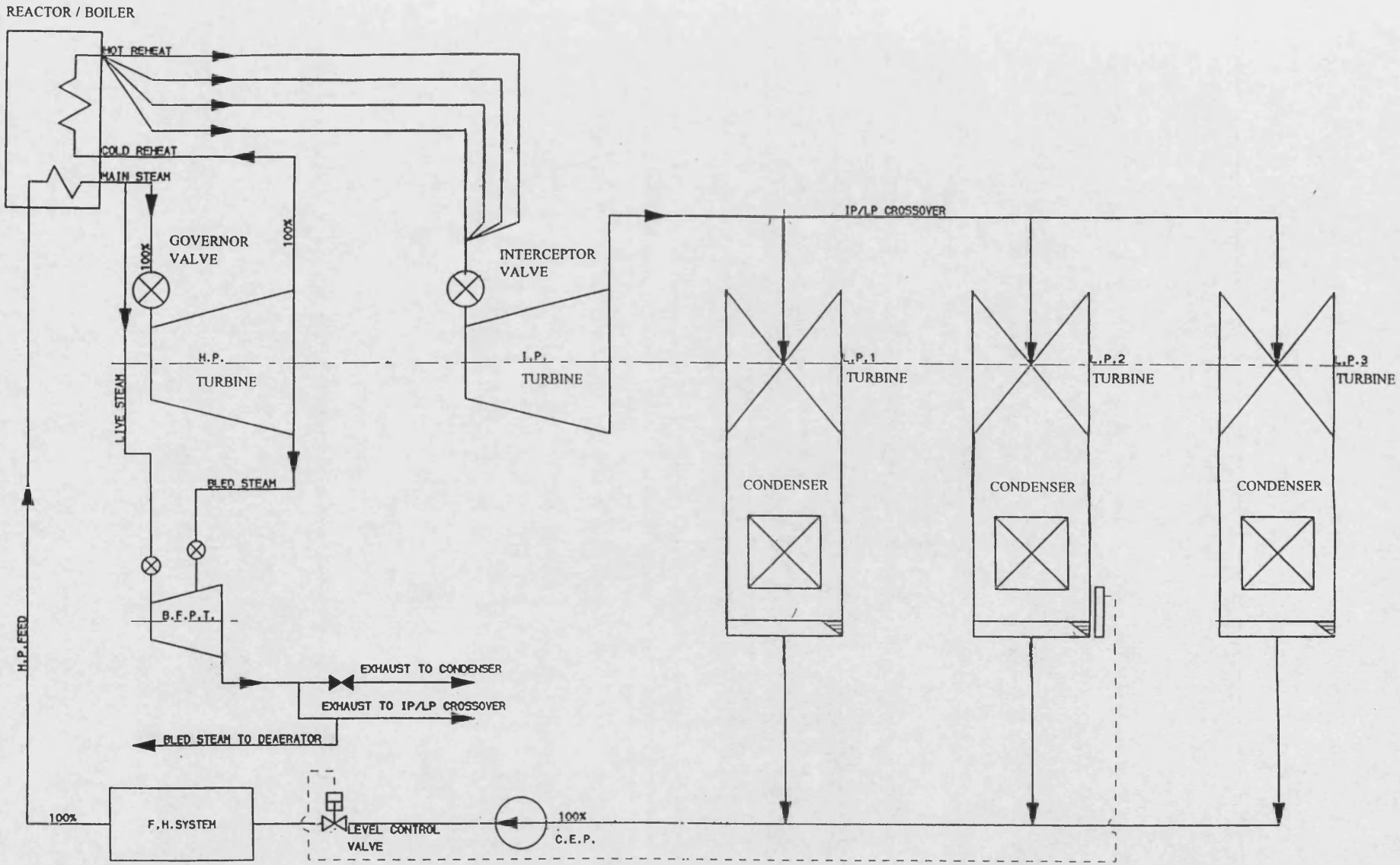

PLANT OVERVIEW FIGURE 3.1

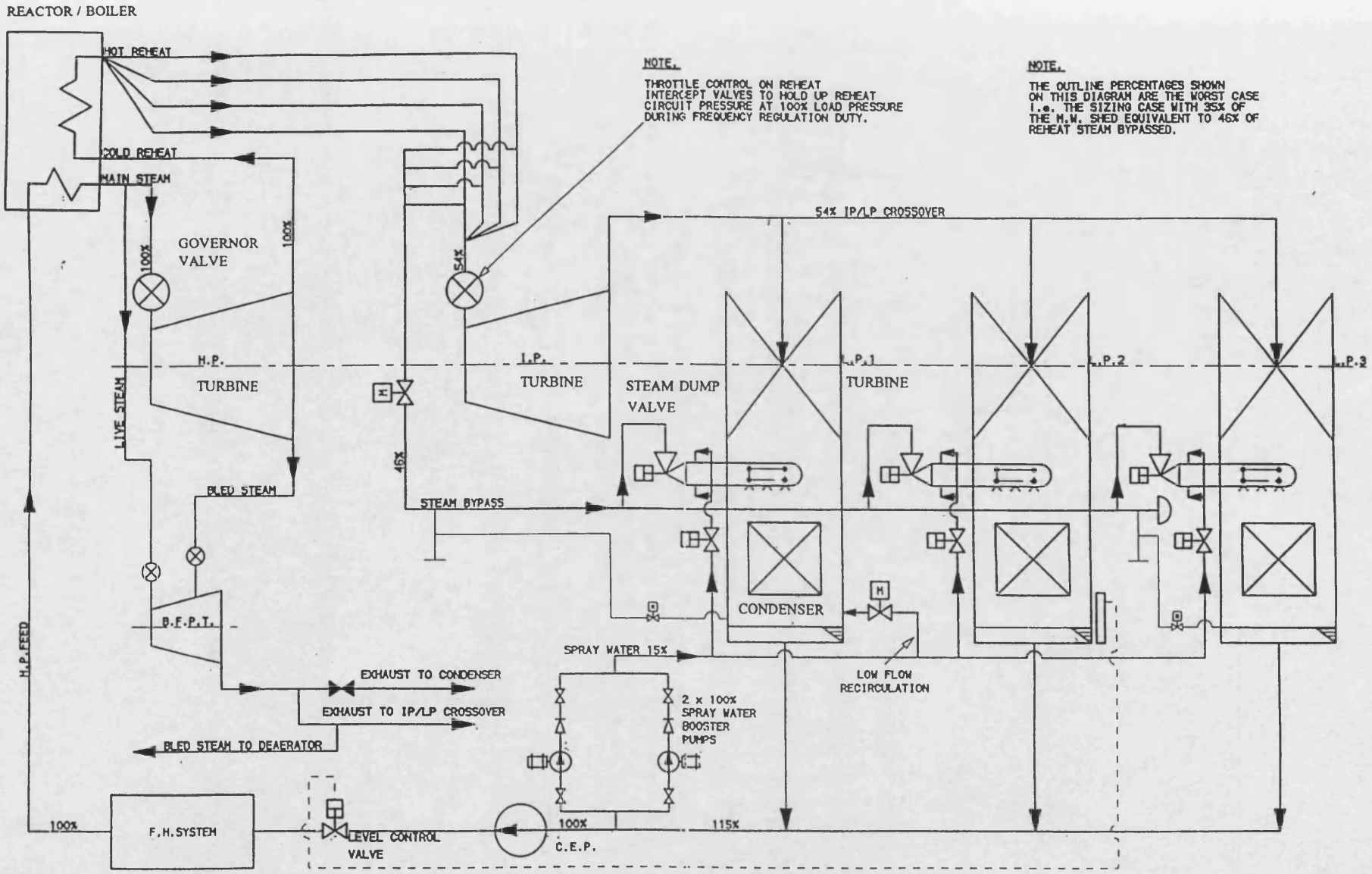

FIGURE 3.2 PLANT OVERVIEW WITH PROPOSED MODIFICATION

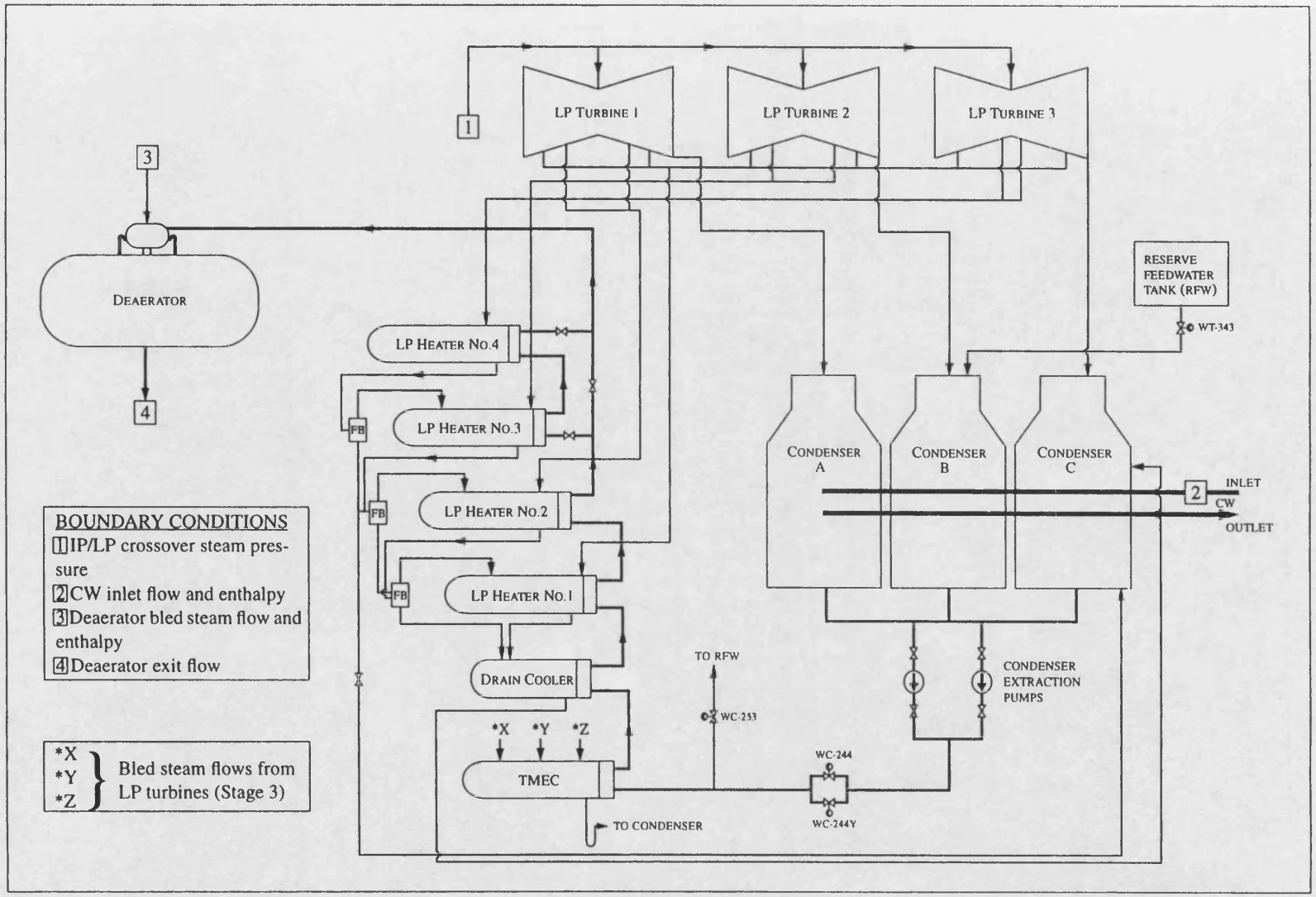

FIGURE 3.3

HEYSHAM 2 – HEBDYM CONDENSATE/FEEDHEATER MODEL

CHAPTER 4

POWER GENERATING PLANT - MODEL ASSESSMENT

4.1 INTRODUCTION

The purpose of this Chapter is compare both the steady state and transient performance of the composite low pressure (LP) feed system model described in Chapter 3, with that of the Heysham 2 plant. It is essential that the model performance corresponds closely with performance data from the plant, as it will be used to predict the Automatic Frequency Response Operation (AFRO) plant response.

4.2 MODEL VALIDATION

4.2.1 Steady State Comparison

The model has been compared with Heysham 2 Unit 7 acceptance tests, NEI Parsons Ltd[1989], at three test load conditions. These acceptance tests were undertaken during the commissioning phase of the plant prior to normal operations. As such these plant data provide the steady state performance in an 'as clean' condition. The predicted model variables have been compared with plant data, and the results recorded in Tables 4.1 to 4.3. It can be seen that the model results correspond closely with the plant data, with one notable area of divergence being the low predicted condenser cooling water (CW) exit temperature at the lower load conditions. However the condenser condensate outlet temperature and flow rate correspond well with plant data, which suggests that the correct level of heat transfer is taking place. On further inspection, it is clear that in order to maintain correspondence in CW exit temperature, a reduction in CW flow rate would be required. It should be noted that for the low load cases, the CW flow rate applicable to the high load condition has been used in the absence of plant data, as it is normal operational practice for CW flow rate to be independent of plant loading. However, to explore the sensitivity of the predicted CW exit temperature to reductions in CW flow rate, two

additional steady state calculations were made with 15% and 30% reductions respectively. The predicted CW exit temperatures do match more closely the acceptance test conditions as shown in the last two columns of Table 4.3b, but in the case of the 30% reduction in CW flow rate, it raised the condenser condensate exit temperature by 3 °C, which is 2.5 °C above plant conditions. Subtle adjustments in condenser CW flow rate and heat transfer would improve the correspondence, however model comparison with other plant data show variations of less than 1 °C from the original case, due in part to the reduction in heat pick up by the heaters as a consequence of elevated condensate feed temperatures. It should be noted that discrepancies of the order of 1 - 2 °C are within the tolerance of ± 1.5 °C for Class 1 E-type thermocouples, which were used for all steam, feed water, condensate and drains temperature measurements. In this respect the steady state comparison may be judged as agreeing well for the load range studied.

It is worth reflecting on the deviation of both the Prandtl number dependency on CW heat transfer, and the condensing tube heat transfer described by Hodman[1992], to that of the more simplified correlations used in the LP feed train model. Using the heat transfer correlations stated above would make these coefficients dependent on thermal conductivity for both primary and secondary fluids, and specific heat capacity for the condensing heat transfer (primary side). Future development of the LP feed train model should consider comparison with plant data with these correlations included.

4.2.2 Transient Comparison

Transient comparison has been made with a Unit 7 boiler quadrant trip, leading to a rapid change in total turbine steam flow, which occurred on 1st February 1997. This plant transient is ideal for testing the LP feed train model since the condensers and feed heaters experience large changes in steam flow. The quadrant trip event can occur for a number of reasons (plant

parameters exceeding trip margins), which results in the cessation of one of the four boiler quadrants.

4.2.2.1 Initial Condition Prior to the Quadrant Trip Event

As a precursor to the transient analysis, the LP feed train model was set up with plant conditions prior to the quadrant trip event to achieve a representative steady state condition. It should be appreciated that some plant variables (in particular boiler feed pump turbine (BFPT) steam flows) were not recorded and therefore to establish a set of boundary conditions for the LP feed train model does require some logical deductions which are explained below.

The model requires the following boundary conditions:

1 Intermediate/Low pressure (IP/LP) crossover pressure and enthalpy

2 CW flow rate and inlet enthalpy

3 Deaerator (DA) bled steam flow rate and enthalpy

4 DA exit flow rate

Items 1 and 2 above are used to determine the LP turbine and condensate feed flow rates, together with the condenser pressures. The specification of item 3 allows the DA thermodynamic conditions to be determined and hence the saturation pressure within the vessel. For the initial steady state, the DA outlet mass flow rate is set equal to the combined condensate and bled steam flows.

Due to the absence of plant data for steam flows to the IP/LP crossover and DA from the BFPT exhaust, the model bled steam flow boundary condition to the DA was based on taking approximately 50% of the BFPT steam flow exhaust, which is similar to the 672 MW acceptance test conditions, see section 4.2.1.

The initial model results for these boundary conditions predicted an increase in the level of total steam flow to the condenser as a result of an increase in IP/LP crossover pressure compared with the acceptance test conditions. This was reflected in:

1 An excess of DA feed water (FW) exit flow in relation to the measured total boiler feed flow.

2 A low DA saturation pressure.

To satisfy the DA thermodynamic conditions such that the correct vessel pressure and exit flow are maintained, the following changes are required.

a) An increase in bled steam flow rate and enthalpy from the BFPT. It was necessary to raise the level of the bled steam enthalpy to a value which coincided with the Unit 7 acceptance test data, in order to restrict the increase in bled steam flow rate to a sensible magnitude.

b) A reduction in condensate feed flow rate to the DA. This was achieved by increasing the turbine stage resistances, in some cases by up to 10% such that an overall reduction in steam/feed flow was obtained.

In addition, the quadrant trip data does not include the level of high pressure (HP) turbine gland steam flow to the DA, which, when included in the model, elevates the total bled steam energy input. Calculations using acceptance test gland steam temperature and flow rate (3 $kg.s^{-1}$) together with a bled steam flow rate of 20 $kg.s^{-1}$ (compared with a measured BFPT exhaust steam flow of 28 $kg.s^{-1}$), satisfy both the DA pressure and exit flow rate. Therefore a total bled steam flow to the DA of 23 $kg.s^{-1}$ is the initial steady state value adopted for all of the dynamic simulations discussed in the rest of the section. With no available plant measurement of steam flows to the DA, the BFPT bled steam flow has been used to provide the transient changes to the DA. A steady state comparison of the model and plant conditions prior to the quadrant trip event are presented in Table 4.4a and 4.4b.

4.2.2.2 Transient Comparison of the Quadrant Trip Event

The main forcing function to the LP feed train from this event is the rapid reduction in IP/LP crossover steam pressure, as shown in Figure 4.1a. Also shown in this Figure is the bled steam supply flow which is inferred from the BFPT exhaust flow as previously stated. In addition, the DA outsurge valve control action (Figure 4.5a) has been suppressed until the water level reaches 3.535m as opposed to the originally supplied control data value of 3.37m (Figure 4.4a). Moving the outsurge initiation prevents an unwanted model control action at the start of the transient in order to align with the logged plant data. It would appear that if the control data is correct, then this apparent discrepancy could be due to an anomaly in the DA level measurement transducer.

It can be seen from Figures 4.1b to 4.6 that most of the model variables correspond closely with the plant dynamic response. This is typified in heater number 4 feed water exit and drain temperatures (Figures 4.2a and b) and condenser pressure (Figure 4.6b). The temporary recovery of the condensate feed water exit temperature from heater 4 (this phenomenon occurs at the exits from all heaters), occurring at 750 seconds is due to the action of the outsurge valve which transiently removes condensate from the inlet to the heater banks. This reduces the condensate flow rate through the heaters temporarily thus inducing a rise in temperature. DA and condenser levels (Figure 4.4a am 4.6a) also compare well, having a very similar response to the plant. Correspondence is also maintained as the plant settles out to a new steady state condition, some 3000 seconds after the initiation of the quadrant trip event. However, not withstanding the close dynamic comparison, there are two aspects which warrant further discussion, which are itemised below.

1 Transiently, the plant DA exit FW temperature reduces more rapidly than the model prediction (Figure 4.6b), however the initial and final values compare well. This may be explained by the inferred transient boundary conditions, most likely related to the

DA bled steam conditions. The overall transient change in the model and plant condenser level control valve positions compare well, thus yielding confidence in the predicted level of condensate feed flow to the DA.

2 There is a continual cycling of the plant condenser level control valve WC-244 position, the amplitude of which corresponds to 5% of full travel (Figure 4.5b). This behaviour is not exhibited by the model, but is possibly due to non-linearities in the control hardware such as hysteresis or anomalies in the controller settings.

An improvement in DA exit feed temperature prediction can be achieved (Figure 4.10b) if the DA bled steam boundary condition is modified. A range of plant and model variables are shown in Figures 4.7 to 4.12 respectively with modified boundary condition. Figure 4.7a highlights the revised bled steam flow boundary condition, which has been reduced in magnitude, for a period of 500 seconds at the start of the quadrant trip event, to the level of the HP turbine gland steam flow of 3 $kg.s^{-1}$. Subsequently it is raised back to the original boundary condition value of 12.5 $kg.s^{-1}$. It should be noted that the DA FW exit flow boundary condition was reduced by 3% during the post quadrant trip period, in order to offset an increased change in DA level, which occurred as a consequence of the modified bled steam flow boundary condition. It is evident that a variation in the DA bled steam level boundary conditions can affect the DA thermodynamic state significantly, due to the high energy content relative to the incoming condensate flow. Justification for the bled steam flow modification can be argued on the following basis:

1 The original value is based on the BFPT bled steam supply flow in the absence of plant data. The true value of the DA bled steam flow will be dependent on the IP/LP crossover, BFPT exhaust and the DA pressures. In this respect they form the boundary pressures of a flow network. Clearly transient variations in these pressures during the

quadrant trip event could significantly affect the level of bled steam flow. For example, it could be inferred from the Figures that during the initial period following the quadrant trip, the DA pressure is higher than the IP/LP crossover and BFPT exhaust pressures, thus preventing any bled steam flow to the DA, except for the HP turbine gland steam flow.

2 The change in the DA thermodynamic state could not be achieved by adjustments to the condensate feed flow alone. Sensitivity studies have shown that step changes to the condensate feed flow do not induce the rate of change of DA FW exit temperature exhibited by the plant. In addition, a much higher confidence exists in the variation of condensate feed flow, since the DA FW exit flow is provided by plant data, and the DA FW inlet flow is inferred from very similar changes in the predicted and plant condenser level control valve positions.

Apart from the DA thermodynamic conditions and the DA outsurge valve WC-253 position (Figure 4.11a), other model variables remained relatively insensitive to the change in DA boundary conditions.

4.2.3 Heater Dynamic Response

In Chapter 3, the merits of various LP heater model formulations were discussed. It should be recalled that method 1 (shell pressure determined from an implicit loop solution based on water/steam volumes) has been used to produce the transients discussed in the previous section for the quadrant trip event. For comparison purposes, the solution method 2 has been adopted to highlight any discrepancies in the 1st method of solution. Method 2 is more rigorous in nature and solves both mass and energy from dynamic conservation equations (see Chapter 3). Figures

4.13 to 4.17 show the transient response of heater 4 to the quadrant trip event using methods 1 and 2. It can be seen that all variables with the exception of the steam volume show an identical transient response. In this respect the choice of solution method 1 seems justified as shell pressure and condensate exit temperature are identical. The more rigorous solution used in method 2 does however have the advantage of producing a smoother transient response for the steam volume and should be considered if method 1 becomes unstable in a particular operating region.

4.3 CLOSURE

Comparison of both the steady state and dynamic performance of the LP feed train model against plant data has indicated a close correspondence for most model variables. It is clear that the model is suitable for analysing a variety of situations that the plant could be subjected to, including the AFRO mode of operation for which it has been specifically developed.

Comparison of the quadrant trip event could have been significantly improved if the BFPT steam flow to the DA had been recorded. This would avoid a qualitative assessment of the mass and energy levels received by the DA and thus define the DA model boundary explicitly. The changes made to the DA boundary conditions have been justified on the basis of an assessment of DA, BFPT exhaust and IP/LP steam pressures, and their effect upon the bled steam flow in the initial period following the quadrant trip.

Refinements to the model should be investigated with respect to the heat transfer correlations used. Using more exacting heat transfer correlations for condensing heat transfer could well find improvements to the steady state mappings discussed in section 4.2.1.

Further examination of the apparent hunting exhibited throughout the plant

condenser/feedheating system, which is evident in the condenser level and control valve position (WC-244) would improve the correspondence between model and plant. This behaviour could possibly be due to incorrect control system data or non-linearities in the control system hardware which is not reproduced in the model.

Table 4.1a Boundary Conditions at the 672 MW Unit 7 Acceptance Test Conditions

Parameter	Units	Acceptance Test data
IP/LP cross over steam pressure	bara	5.265*
IP/LP cross over steam temperature	°C	262.98*
CW inlet water temperature	°C	7.12*
CW flow rate	$m^3.s^{-1}$	19.65
CW inlet pressure	bara	2.0
Deaerator bled steam flow rate	$kg.s^{-1}$	20.41
Deaerator bled steam temperature	°C	190.0

* *mean value*

Table 4.1b 672 MW Unit 7 Acceptance Test Plant Data to Model Comparison

Parameter	Units	Plant Data	Model Data
LP 1 Cylinder measurements	bara		
LP 2 heater pressure at turbine cyl.		0.8499	0.854
LP 1 heater pressure at turbine cyl.		0.4055	0.40
LP 2 Cylinder measurements	bara		
LP 3 heater pressure at turbine cyl.		1.81	1.82
LP 1 heater pressure at turbine cyl.		0.392	0.39
LP 3 Cylinder measurements	bara		
LP 4 heater pressure at turbine cyl.		3.156	3.16
LP 1 heater pressure at turbine cyl.		0.392	0.40
CW exit temperature	°C	18.14	17.2
Condenser pressure	mbar (a)	35.29	35.8
Condenser FW outlet temperature	°C	24.84	25.6
TMEC FW outlet temperature	°C	44.81	44.6
TMEC drains temperature	°C	47.61	47.4
Heater 4 FW exit temperature	°C	132	131.8
Heater 4 drain temperature	°C	134.4	134
Condensate FW flow rate to DA	$kg.s^{-1}$	482	480.3
Deaerator pressure	bara	5.149	5.23
Deaerator FW exit temperature	°C	152	153.5

Table 4.2a Boundary Conditions at the 528 MW Unit 7 Acceptance Test Conditions

Parameter	Units	Acceptance Test data
IP/LP cross over steam pressure	bara	4.149*
IP/LP cross over steam temperature	°C	244.9*
CW inlet water temperature	°C	6.25*
CW flow rate	$m^3.s^{-1}$	19.65 (assumed from 672 MW test)
CW inlet pressure	bara	2.0
Deaerator bled steam flow rate	$kg.s^{-1}$	15.233
Deaerator bled steam temperature	°C	175.0

* *mean value*

Table 4.2b 528 MW Unit 7 Acceptance Test Plant Data to Model Comparison

Parameter	Units	Plant Data	Model Data
LP 1 Cylinder measurements	bara		
LP 2 heater pressure at turbine cyl.		0.6932	0.681
LP 1 heater pressure at turbine cyl.		0.349	0.319
LP 2 Cylinder measurements	bara		
LP 3 heater pressure at turbine cyl.		1.476	1.45
LP 1 heater pressure at turbine cyl.		0.3229	0.313
LP 3 Cylinder measurements	bara		
LP 4 heater pressure at turbine cyl.		2.582	2.5
LP 1 heater pressure at turbine cyl.		0.3206	0.32
CW exit temperature	°C	16.33	14.5
Condenser pressure	mbar (a)	N/A - no data	29
Condenser FW outlet temperature	°C	21.69	21.2
TMEC FW outlet temperature	°C	41.99	40.7
TMEC drains temperature	°C	43.7	43.2
Heater 4 FW exit temperature	°C	124.43	124.3
Heater 4 drain temperature	°C	126.43	126.4
Condensate FW flow rate to DA	$kg.s^{-1}$	386.9	384
Deaerator pressure	bara	4.114	4.13
Deaerator FW exit temperature	°C	143.93	144.7

Table 4.3a Boundary Conditions at the 460 MW Unit 7 Acceptance Test Conditions

Parameter	Units	Acceptance Test data
IP/LP cross over steam pressure	bara	3.714*
IP/LP cross over steam temperature	°C	234.4*
CW inlet water temperature	°C	7..07*
CW flow rate	$m^3.s^{-1}$	19.65 (assumed from 672 MW test)
CW inlet pressure	bara	2.0
Deaerator bled steam flow rate	$kg.s^{-1}$	13.235
Deaerator bled steam temperature	°C	168.0

* *mean value*

Table 4.3b 460 MW Unit 7 Acceptance Test Plant Data to Model Comparison

Parameter	Units	Plant Data	Model Data Case 1	Case 2 70%CW flow rate	Case 3 85%CW flow rate
LP 1 Cylinder measurements	bara				
LP 2 heater pressure at turbine cyl.		0.636	0.614		
LP 1 heater pressure at turbine cyl.		0.3334	0.228		
LP 2 Cylinder measurements	bara				
LP 3 heater pressure at turbine cyl.		1.346	1.304		
LP 1 heater pressure at turbine cyl.		0.2954	0.283		
LP 3 Cylinder measurements	bara				
LP 4 heater pressure at turbine cyl.		2.326	2.247		
LP 1 heater pressure at turbine cyl.		0.2934	0.289		
CW exit temperature	°C	17.54	14.4	17.64	15.8
Condenser pressure	mbar (a)	N/A - no data	28.8	35	31.5
Condenser FW outlet temperature	°C	22.6	21.96	25	23.2
TMEC FW outlet temperature	°C	41.96	39.4	40.5	39.8
TMEC drains temperature	°C	43.35	41.8	42.9	42.3
Heater 4 FW exit temperature	°C	121.28	121	121	121
Heater 4 drain temperature	°C	123.07	122.9	122.9	122.9
Condensate FW flow rate to DA	$kg.s^{-1}$	347.9	346.8	346.8	346.8
Deaerator pressure	bara	3.699	3.68	3.68	3.68
Deaerator FW exit temperature	°C	140.06	140.7	140.7	140.7

* *mean value*

Table 4.4a boundary Conditions Prior to the quadrant Trip Event on Unit 7

Parameter	Units	Plant Test Data
IP/LP cross over steam pressure	bara	5.5949*
IP/LP cross over steam temperature	°C	210.0*
CW inlet water temperature	°C	6.25*
CW flow rate	$m^3.s^{-1}$	15.43 (to match CW exit temp)
CW inlet pressure	bara	2.0
Deaerator bled steam flow rate	$kg.s^{-1}$	23.04 (to satisfy DA conditions)
Deaerator bled steam temperature	°C	177.2

Table 4.4b Quadrant Trip Plant Data to Model Comparison

Parameter	Units	Plant Data	Model Data
CW exit temperature	°C	17.15*	17.4
Condenser pressure	mbar (a)	45.3	45.1(condenser A)
Condenser FW outlet temperature	°C	28.5*	29.6(condenser A)
TMEC FW outlet temperature	°C	47	45.6
TMEC drains temperature	°C	50.5	48.3
Heater 4 FW exit temperature	°C	132.5	131.5
Heater 4 drain temperature	°C	134.9	133.6
DA Condensate exit FW flow rate	$kg.s^{-1}$	525	523.6
Deaerator pressure	bara	N/A	5.38
Deaerator FW exit temperature	°C	155	154.6

* mean value

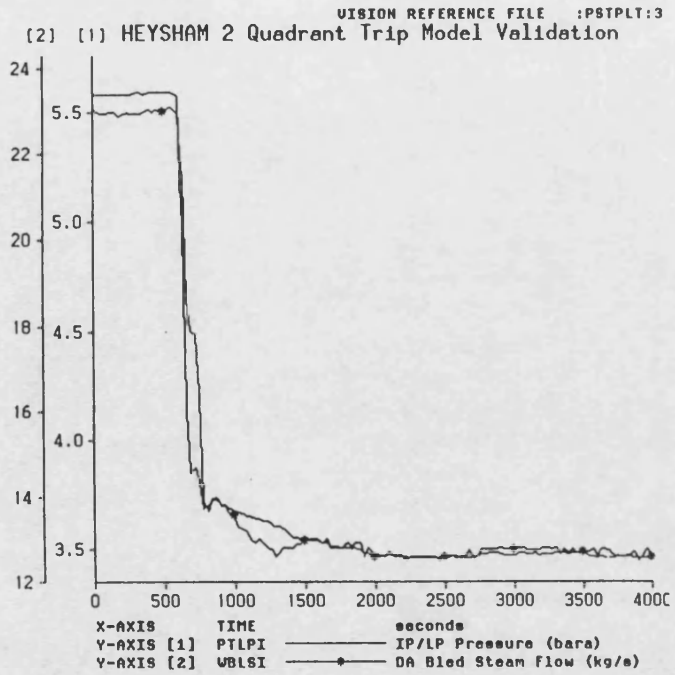

Boundary Conditions Figure 4.1a

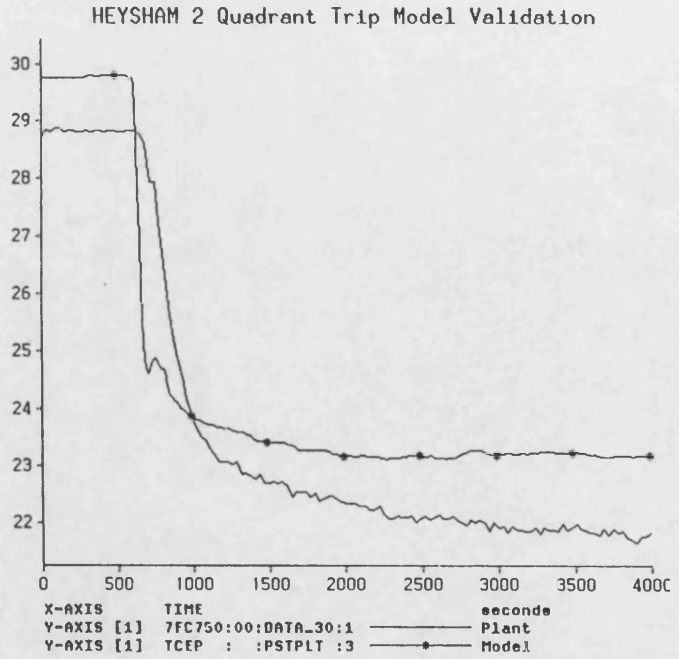

Condenser Extn Pump Exit Temp (deg C) Figure 4.1b

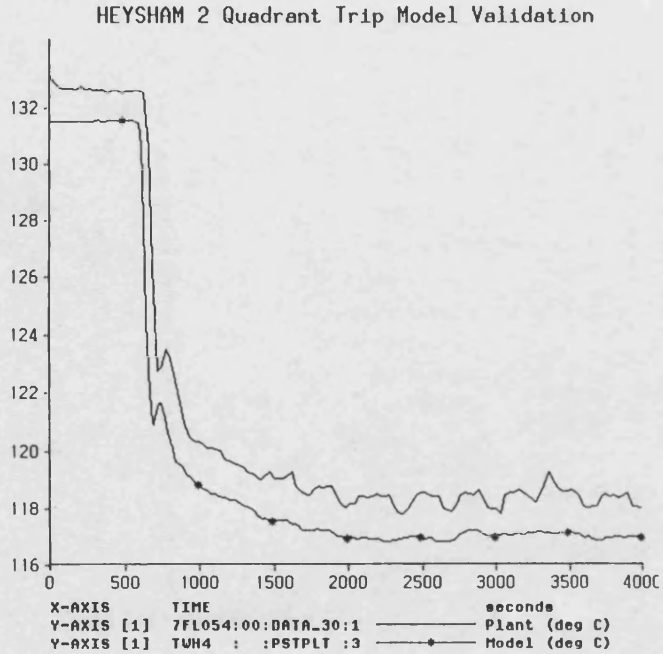

Heater 4 FW Exit Temperature Figure 4.2a

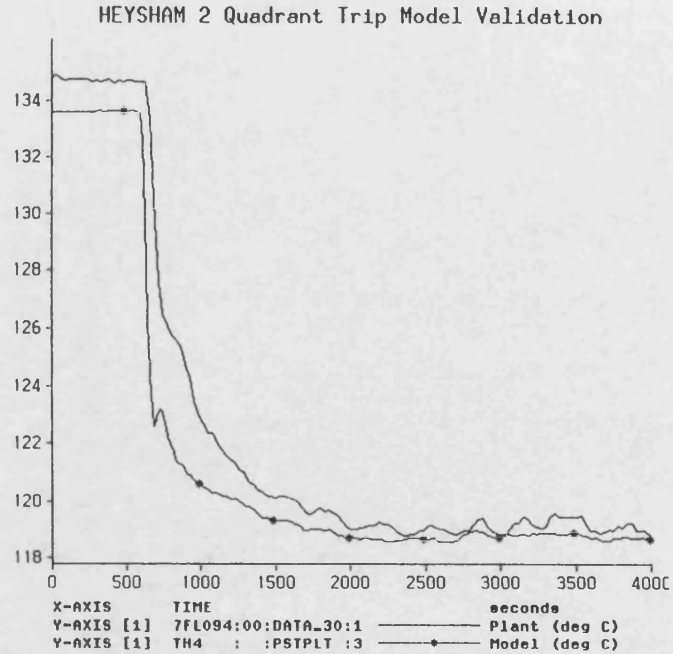

Heater 4 Drain Temp Figure 4.2b

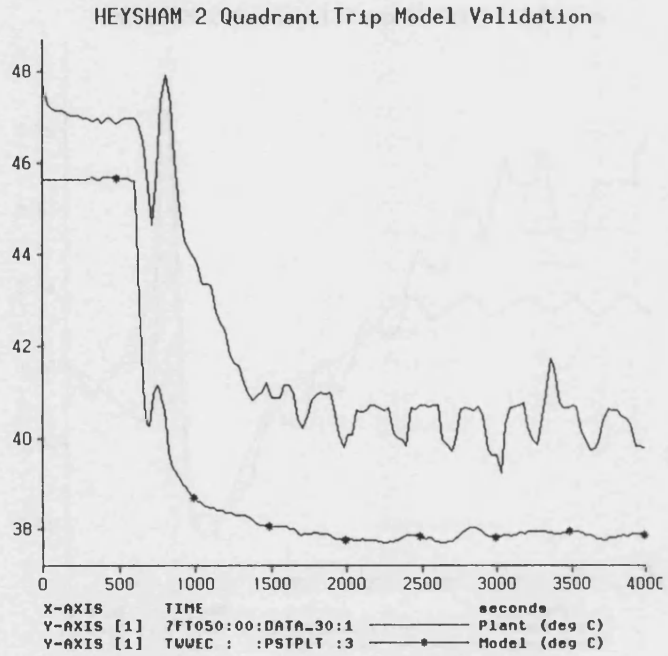

TMEC FW Exit Temperature Figure 4.3a

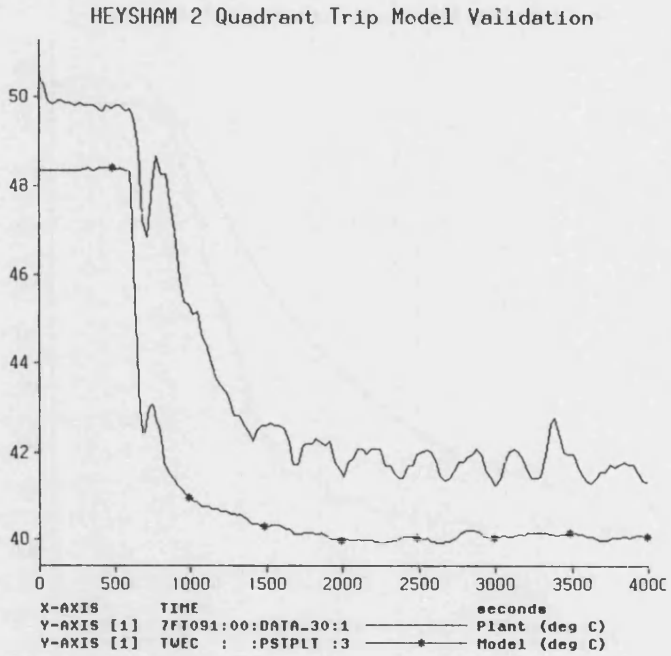

TMEC Drain Temperature Figure 4.3b

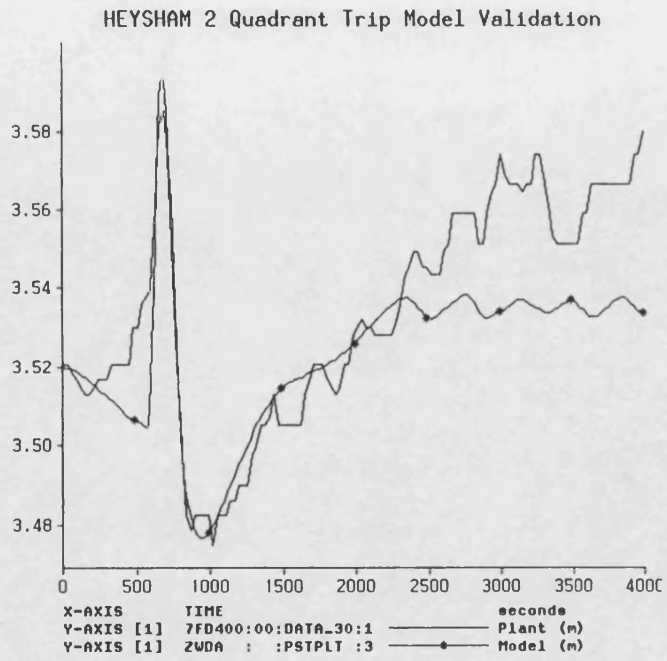

Deaerator Level Figure 4.4a

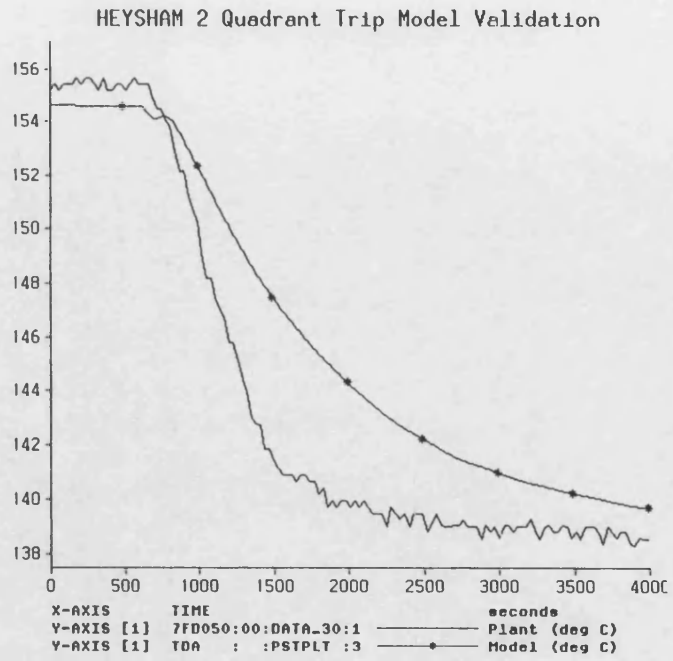

Deaerator FW exit Temperature Figure 4.4b

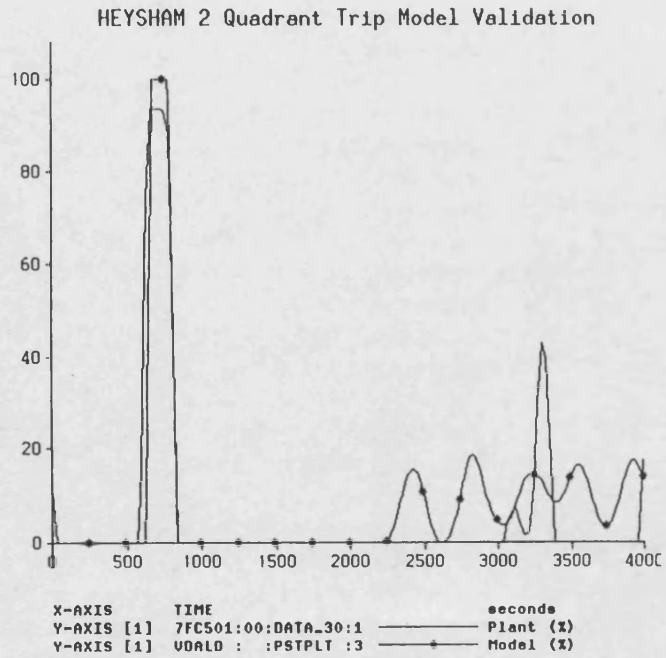

Outsurge Valve (WC-253) Position Figure 4.5a

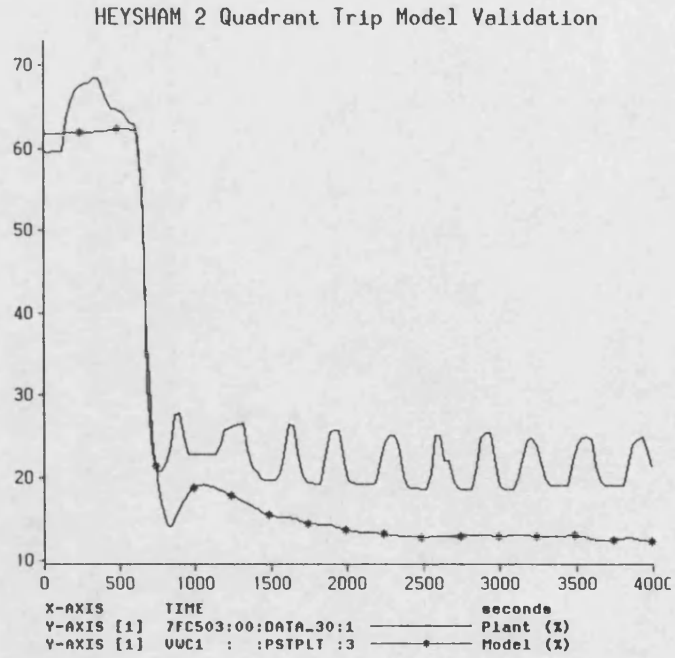

Control Valve (WC-244) Position Figure 4.5b

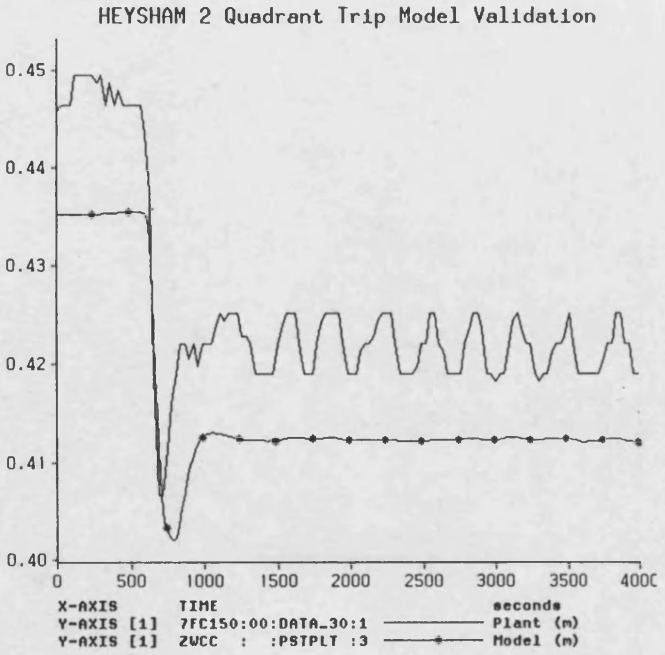

Condenser (C) Level Figure 4.6a

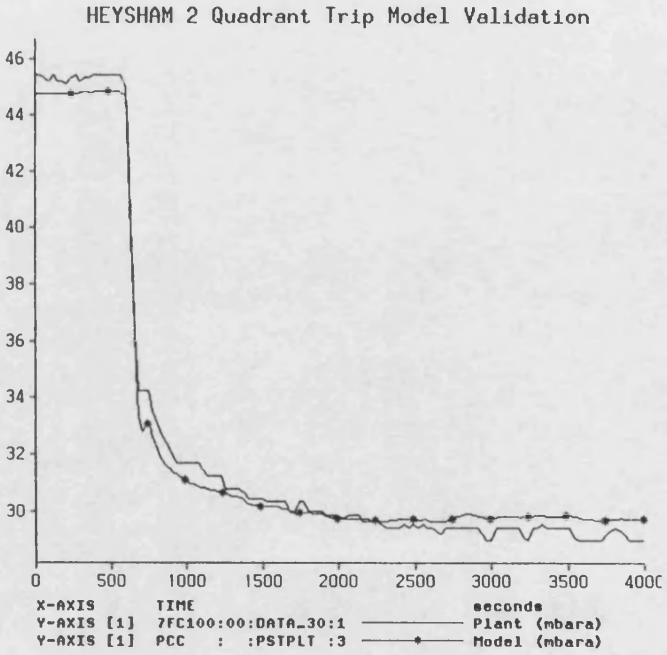

Condenser (C) Pressure Figure 4.6b

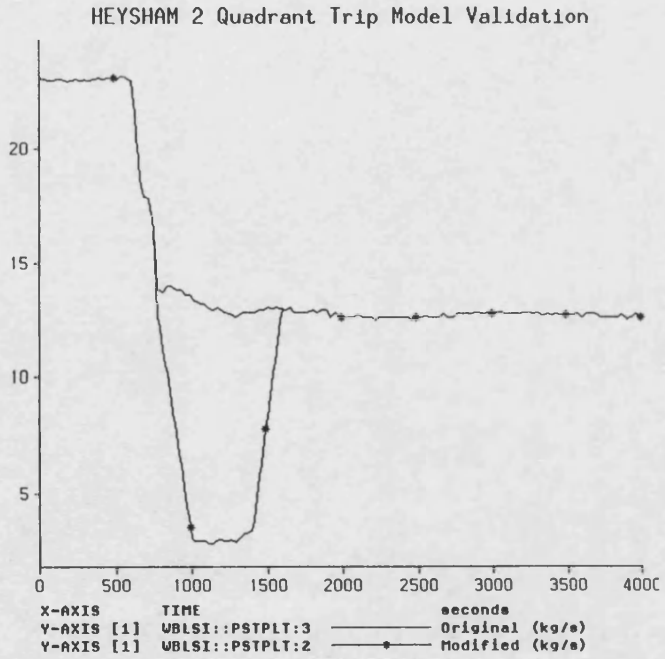

DA Bled Steam Flow Boundary Conds Figure 4.7a

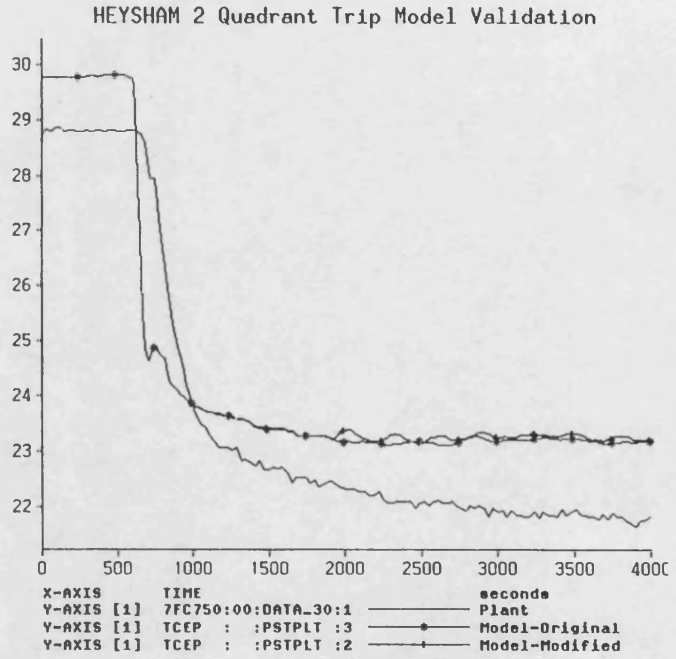

Condenser Extn Pump Exit Temp (deg C) Figure 4.7b

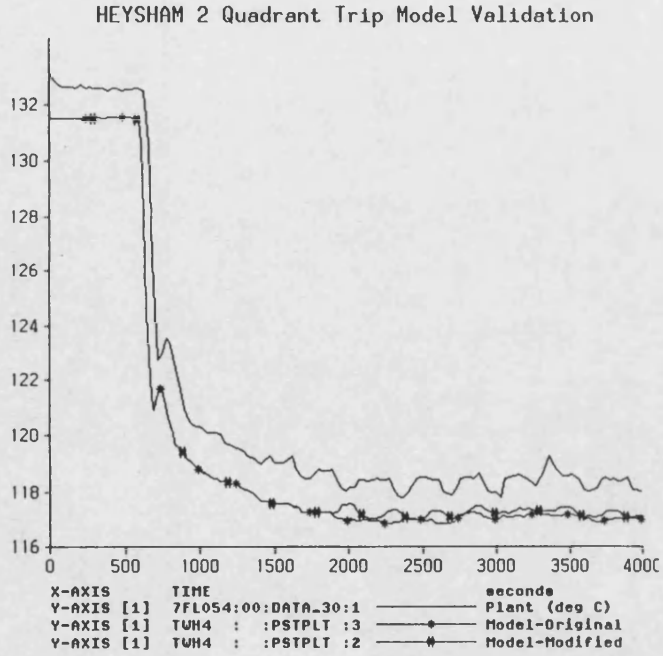

Heater 4 FW Exit Temperature (deg C) Figure 4.8a

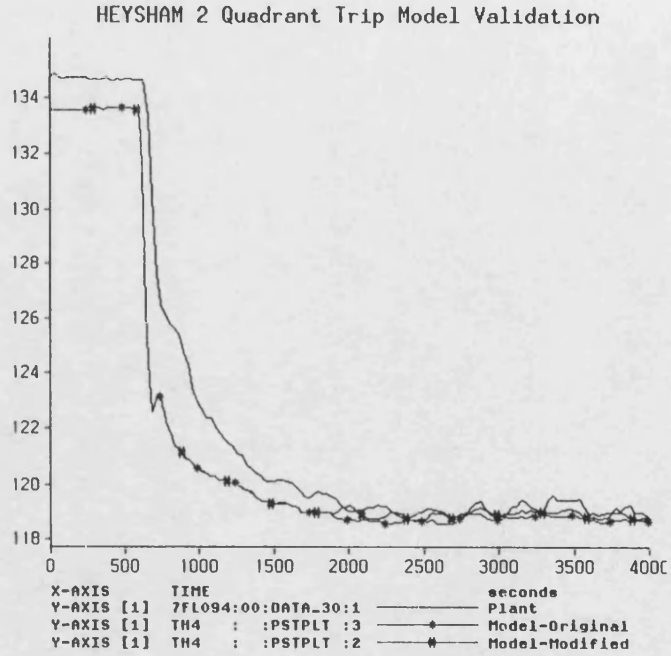

Heater 4 Drain Temp (deg C) Figure 4.8b

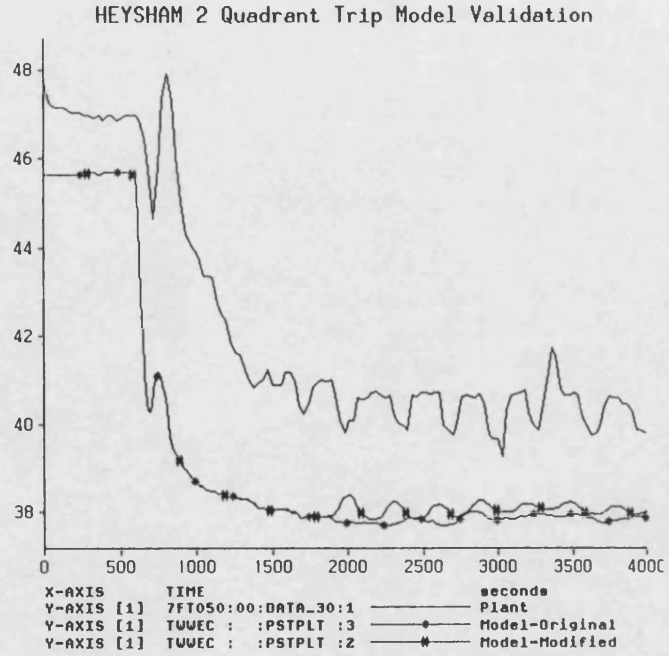

TMEC FW Exit Temperature (deg C) Figure 4.9a

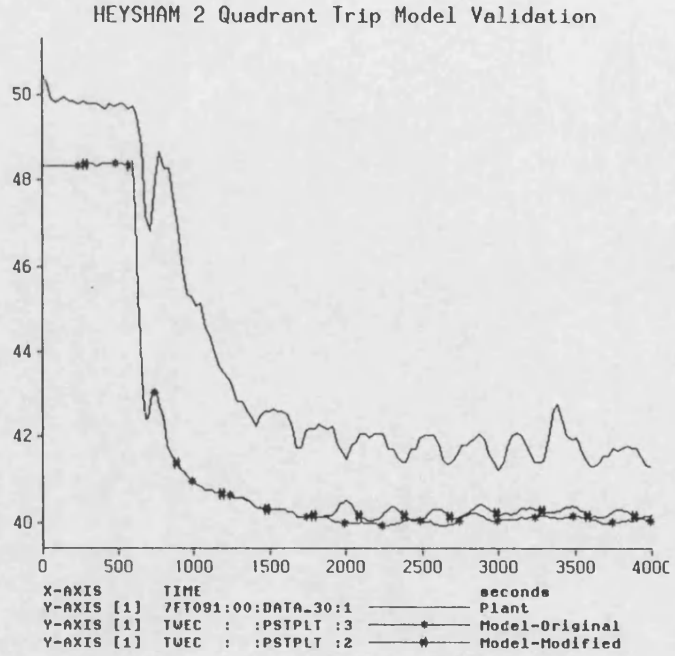

TMEC Drain Temperature (deg C) Figure 4.9b

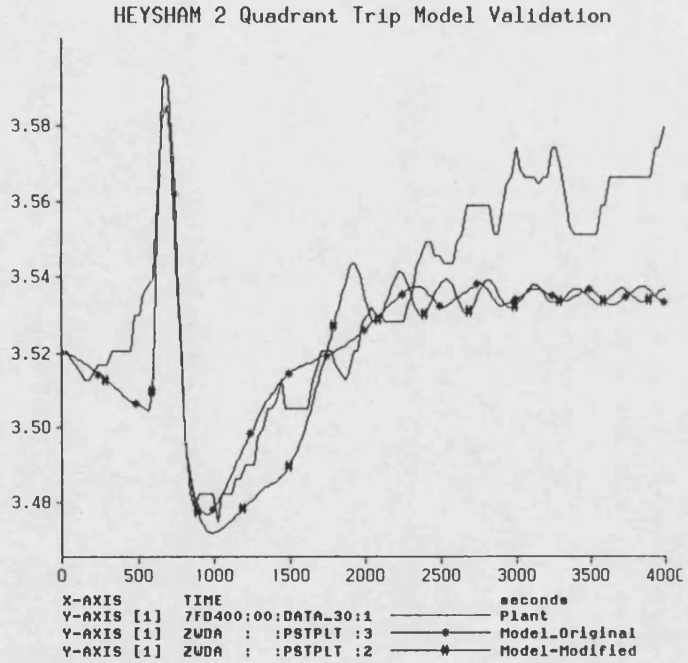

Deaerator Level (m) Figure 4.10a

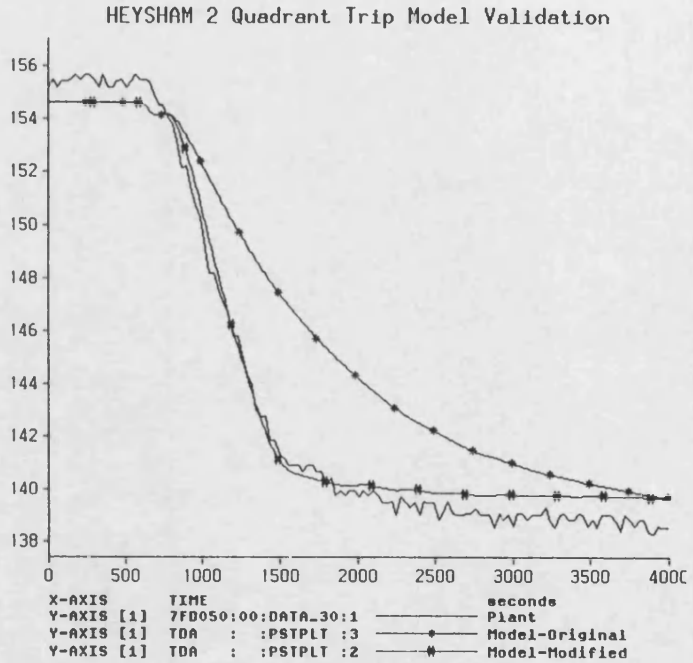

Deaerator FW exit Temp (deg C) Figure 4.10b

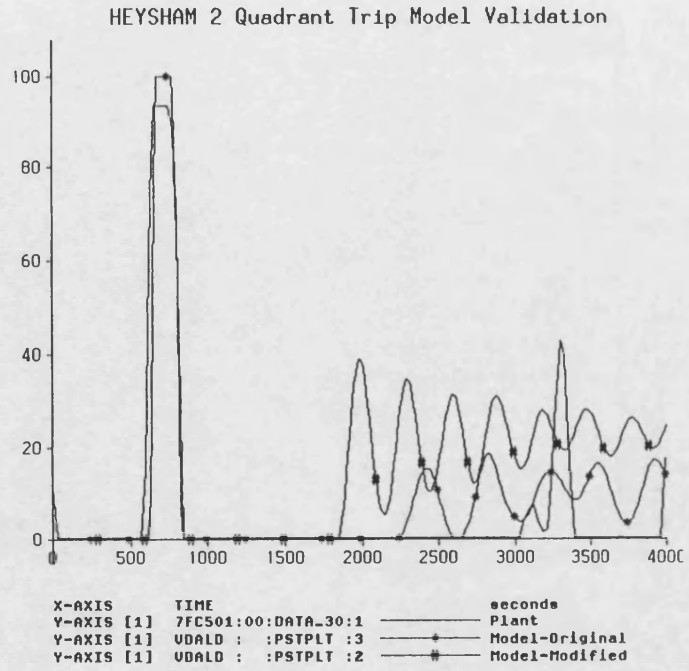

Outsurge Valve (WC-253) Position (%) Figure 4.11a

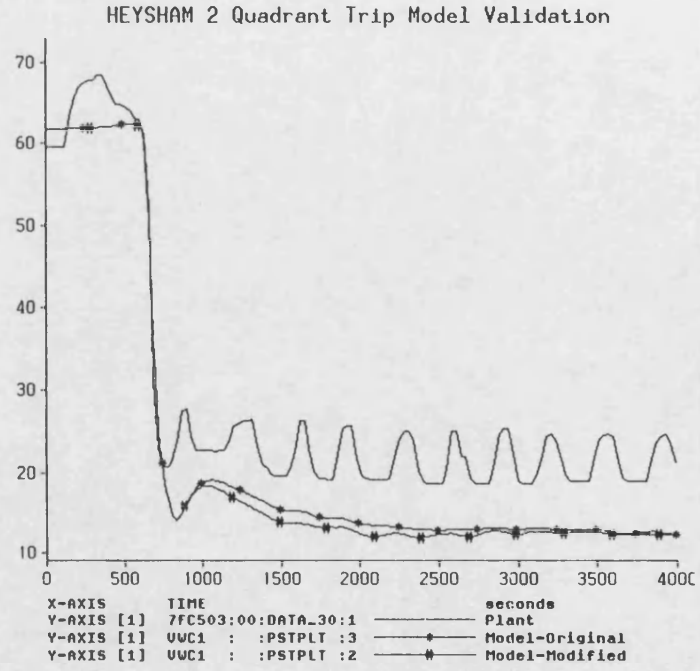

Control Valve (WC-244) Position (%) Figure 4.11b

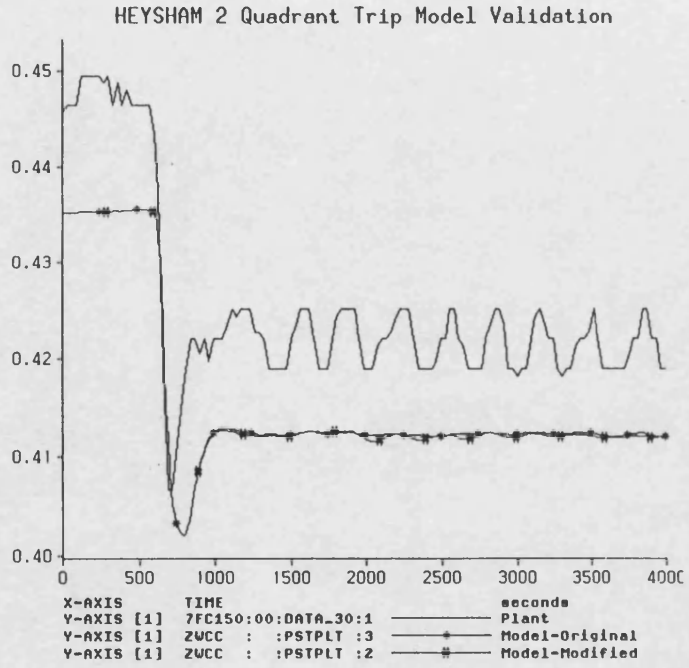

Condenser C Level (m) Figure 4.12a

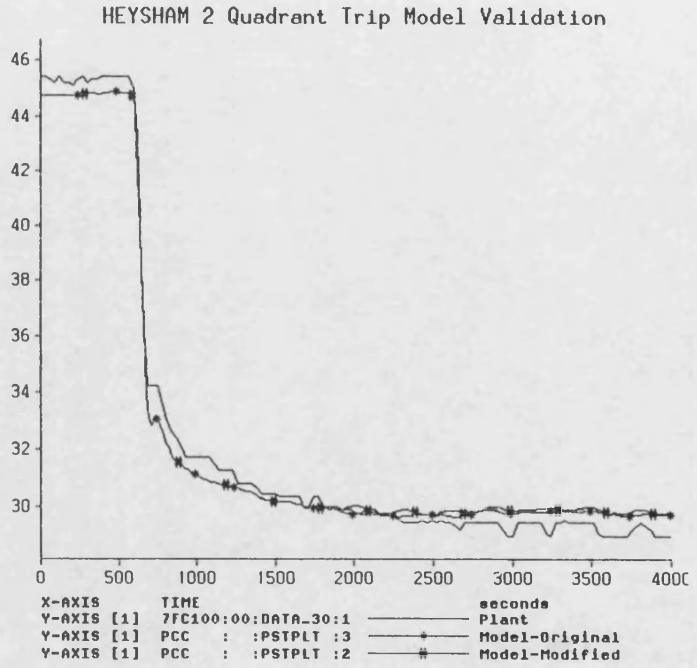

Condenser C Pressure (mbara) Figure 4.12b

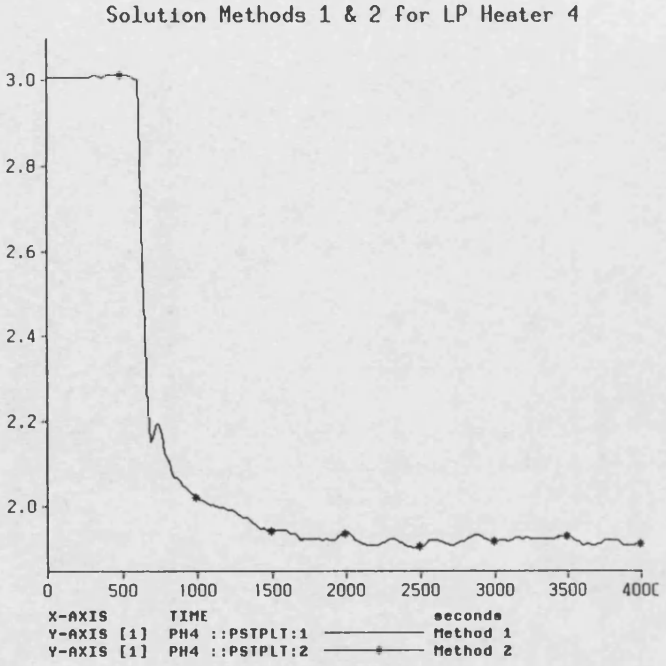

Shell Pressure (bara) Figure 4.13

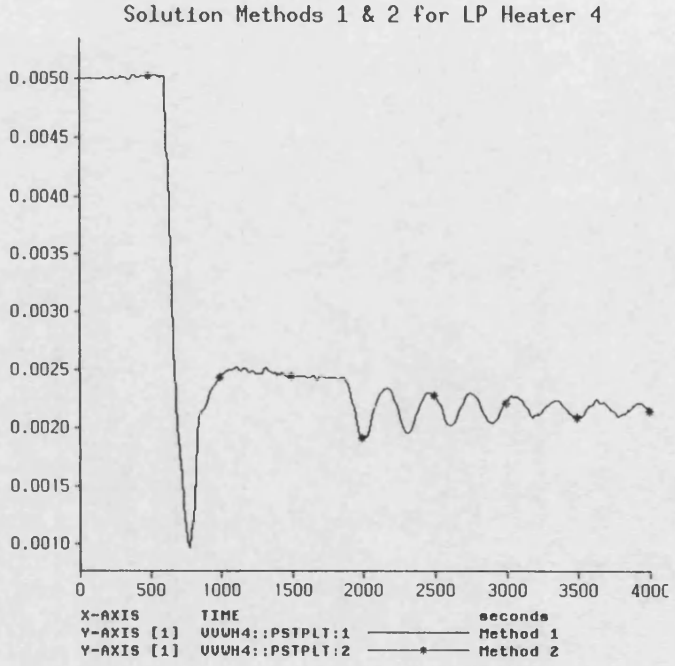

Shell Water volume (m^3) Figure 4.14

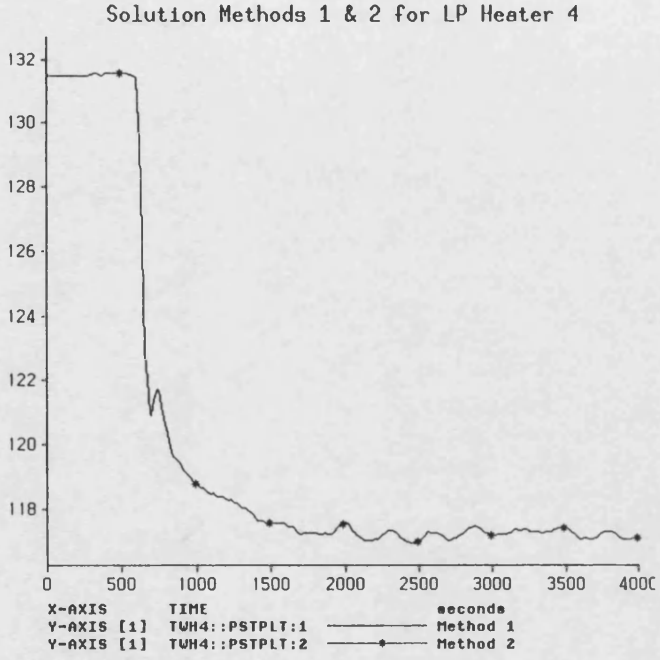

Condensate Exit Temperature (deg C) Figure 4.15

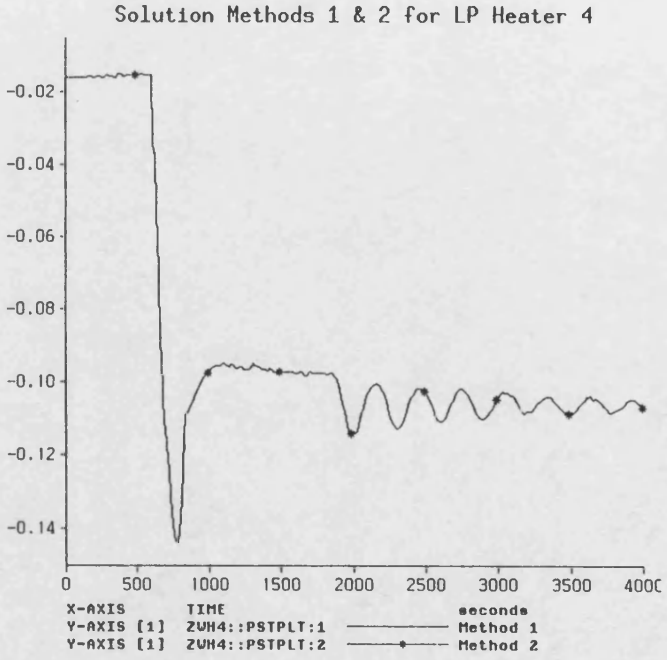

Shell Side water Level (m) Figure 4.16

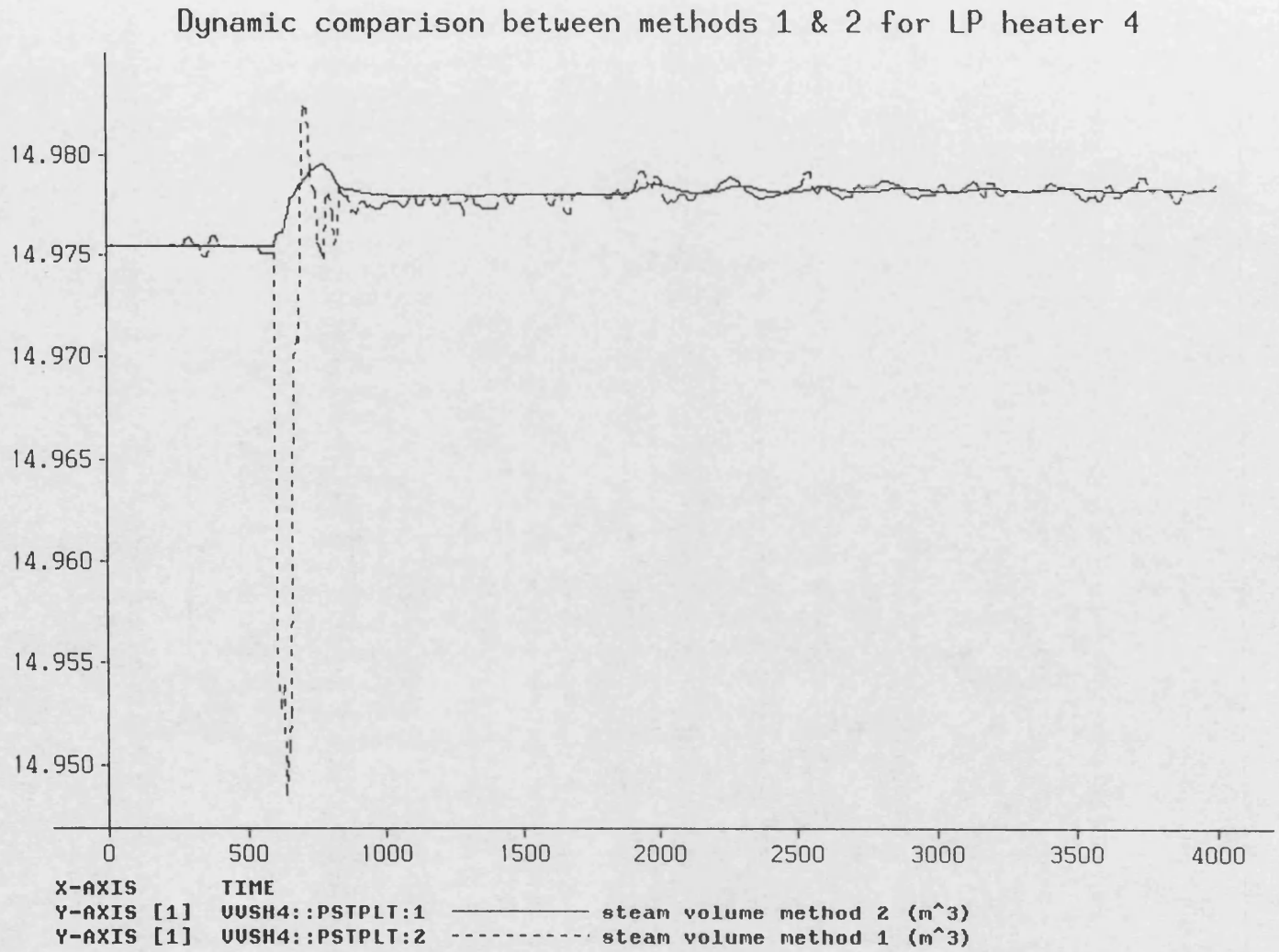
Dynamic comparison between methods 1 & 2 for LP heater 4
14.980
14.975
14.970
14.965
14.960
14.955
14.950
0
500
1000
1500
2000
2500
3000
3500
4000
X-AXIS TIME
Y-AXIS [1] UUSH4::PSTPLT:1 steam volume method 2 (m^3)
Y-AXIS [1] UUSH4::PSTPLT:2 steam volume method 1 (m^3)

FIGURE 4.17

CHAPTER 5

HYDRAULIC FLUID POWER SYSTEMS - MODEL DESCRIPTION

5.1 INTRODUCTION

The purpose of this Chapter is to apply the theoretical approach developed in Chapter 2 to simulate hydraulic fluid power systems. Information is required concerning the hydraulic characterisation of the components, and in particular how the hydraulic performance of the components is affected by temperature variation. Another aspect which requires attention is discretising of the distributed effects for the component models. For example, it is possible to consider a hydraulic pump as a purely resistive device, providing a flow rate for a given pressure boundary condition, which is typically practised using the Bath*fp* simulation package (which was used for the research in this Chapter). This imposes functional requirements on the connecting models regarding variable transfer and suitability.

The first step in simulating a hydraulic circuit in Bath*fp* requires characterisation of circuit components as individual models. This is achieved by fitting characteristics to experimental data over the operating range, and then implementing the conservation equations for mass and energy developed in Chapter 2 where necessary for each component model. The modelling approach is based on providing a consistent equation set for components in a circuit. The nature of Bath*fp* is such that each component model must be capable of linking to adjacent models at the circuit building stage, Richards and Tilley[1991]. This requires that the boundary conditions for each model must be consistent in terms of variable transfer. Otherwise, the completed circuit would be inconsistent and not function correctly. This approach has led to components such as valves and pumps calculating flow rates with knowledge of the pressure boundary conditions supplied by adjacent component models (pipes). This approach has been adopted here. It is interesting to note that Harris[1990] addressed a similar issue when formulating mathematical models for

inclusion in the software simulation environment HASP. However, because of the approach used in HASP where two integration schemes were used, one for the hydraulic states and one for the thermal states, a number of problems arose. Harris decided that the method used in HASP for simulating thermal hydraulic systems was unsuitable for reverse flow conditions because of problems with variable transfer between common blocks. As such, Harris chose to ignore this particular situation for the purposes of his research. This is not the case with Bath*fp* which can cater for reverse flow situations in thermal hydraulic systems, which is necessary when more complex circuits are studied.

5.2 CIRCUIT DESCRIPTION

For the purpose of examining the theoretical approach in Chapter 2, a small self contained hydraulic circuit was constructed, see Figure 5.1. The elements of the circuit comprised a Truninger (model 5-H1-40) two stage internal gear pump driven by an electric induction motor, with a nominal speed of 1440 rev.min^{-1} and a maximum electrical power of 11 KW. To load the pump and therefore generate heat in the circuit, a small variable restrictor valve was placed between the pump and the oil cooler. The oil cooler was a three-pass shell-in-tube Bowman counter flow heat exchanger capable of a maximum flow rate of 140 L.min^{-1} and 85 L.min^{-1} for the hot and cold fluids respectively. A reservoir was placed between the oil cooler exit and the pump inlet. The reservoir is rectangular in shape with a total volume of 225 litres. A relief valve was situated at the pump outlet to safeguard the circuit.

5.3 HYDROSTATIC PUMP MODEL

The requirement of a hydrostatic pump model is to provide an accurate value of flow rate for a given speed and pressure boundary conditions, and to provide the outlet temperature of the working fluid for the range of operating efficiencies encountered. Experimental data from the rig was gathered and used to produce both volumetric flow rate and torque loss models. These

were generated as nonlinear functions of the fluid conditions, as opposed to describing the performance with the standard Wilson [1948] linear model. The pump was driven by an electrical induction motor. The change in speed over all operating conditions amounts to 3% of the nominal speed. For this reason both torque and flow loss models developed below ignore speed dependence. This assumption is based on experimental evidence by McCandlish and Dorey [1984] who tested a number of gear pump units and established general performance trends. Figure 5.2 shows the typical flow loss verses speed characteristic from a gear pump tested by McCandlish and Dorey. The change in flow loss is more evident at high discharge pressure in contrast to low discharge pressure condition where there is a negligible change. Clearly a 3% change in speed anywhere in the operating range produces a negligible change in flow loss. A similar deduction can be made for the variation in torque loss over the operating speed range for the same gear pump unit (Figure 5.3).

The discharge flow rate from the pump can be considered typically as the sum of the theoretical flow (ωD) minus the loss flow. An approach similar to McCandlish and Dorey [1984] has been used to develop a flow loss model insofar that the flow loss can be linearised at constant viscosity by expressing $Q_l = K_1 (P^n)_{\mu = const}$. K_1 can then be made a function of viscosity. This leads to a flow loss model of the form:

$$Q_l = P^{0.917} \left(0.2037 - 6.0148 * 10^{-3} \mu + 4.899 * 10^{-5} \mu^2 \right) \qquad (5.1)$$

Figure 5.4 shows the pump loss flow prediction against discharge pressure, along with the experimental data. Although the prediction is reasonably good over the operating range, it can be seen that little loss in accuracy would result if the flow loss is considered proportional to pressure, as the Wilson flow loss model suggests. However the variation in flow loss with viscosity is nonlinear which is a deviation from the Wilson assumption.

The pump shaft torque can be considered as the sum of the theoretical torque (*PD*) plus the loss torque. The Wilson torque loss model allows for frictional losses proportional to both viscosity and load. However experimental results showed that the torque loss had very little dependence on discharge pressure for the range studied (30 - 150 bar). The torque loss is thus represented as a function of viscosity only as shown below:

$$Tq_l = 2.04 - 0.1384\mu + 6.78*10^{-3}\mu^2 \qquad (5.2)$$

Figure 5.5 shows both experimental and model torque loss (equation 5.2) against pressure for a number of different oil viscosities.

For the circuit in question, it would be feasible to represent the pump as a steady state device providing flow rate and temperature, and allow the pipes and reservoir to perform the dynamic calculations for pressure and temperature. This approach has been successfully used by Harris [1990] by virtue of the fact that if the pump is small in relation to other circuit components, then the time frame of the pump transient thermal response occurs at a significantly faster rate than that of the reservoir. This is acceptable as the reservoir will dominate the thermal response characteristics in this circuit due to its size. However, the penalty in adopting this approach is the assumption of adiabatic pump conditions, resulting in implicit relationships between temperature and heat transfer. For the purposes of this research, a more flexible approach has been adopted by implementing a dynamic equation for temperature. Equation (2.23) may be used for this purpose with a suitable expression for pump work input. Heat transfer from the pump has been neglected on the basis that the heat dissipation is small in relation to other circuit components. This is not to say that it is never unimportant. In certain circumstances where fluid power circuits have no oil cooler and rely on convection from component surfaces to dissipate heat, then heat transfer from component surfaces must be considered. The effect of the pressure

derivative in equation (2.23) has been neglected for the pump as the continuity equation is not solved within the pump model when considering it as a purely resistive device. The pump work input can be expressed in terms of the unit pressure drop, discharge flow rate and overall efficiency as follows:

$$W_s = \frac{Q_d\,(p_e - p_l)}{\eta_o} \tag{5.3}$$

The pump outlet temperature derivative can then be expressed as:

$$\frac{dT_l}{dt} = \frac{vw_e}{VCp}[v(1 - \beta T - \frac{1}{\eta_o})(p_e - p_l) + Cp(T_e - T_l)] \tag{5.4}$$

The overall efficiency is deduced from the previously defined expressions for pump flow and torque loss.

5.4 HYDRAULIC PIPE MODEL

The hydraulic pipe models utilise both conservation equations (2.7 and 2.23). The assumptions are that the pipe volume remains constant and no work is done on or by the fluid. Therefore, only heat transfer to the surroundings and the thermodynamic conditions of the fluid at entry to the pipe are responsible for changing the pipe fluid temperature. Equations (2.7 and 2.23) are required to be solved simultaneously at any particular time step. The implicit relationship may be removed by substitution which yields a modified pipe fluid temperature derivative. Further modification to the temperature derivative has been made to overcome duplication of pressure at the connecting ports. This has arisen because the difference in fluid enthalpy is represented as a function of both pressure and temperature difference between adjacent models and the pipe model. Therefore to solve the energy equation in its present form it is necessary to pass both pressure and temperature between adjacent component and pipe models. This is clearly an

unwanted feature. For example, a pipe receiving both flow rate and fluid temperature from a pump does not require pump discharge pressure as this is already a boundary condition calculated by the pipe. Therefore, the difference in fluid enthalpy between pump discharge and connecting pipe can be entirely represented by temperature alone. This analogy can be extended to multiple pipe connections if the outlet fluid temperature from one pipe is suitably modified to account for the isenthalpic temperature rise due to frictional losses. The pipe fluid temperature derivative can then be represented as follows:

$$\frac{dT}{dt} = \frac{v\,[w_e Cp(T_e - T_l) + q_h + \frac{\beta T\, B_m}{\rho}(w_e - w_l)]}{V(Cp - v\beta^2 T\, B_m)} \tag{5.5}$$

The problems associated with variable transfer between component models as described above could be removed completely if fluid enthalpy is used to represent conservation of energy. Unfortunately, this requires a thermodynamic property map for the oil under test so that the partial properties may be established, which is unavailable at the present time. In general it is found that only transport properties exist for most fluids used in fluid power systems (with the exception of water).

The continuity equation remains as equation (2.7). Heat transfer from the pipe model is accounted for by assuming a lumped pipe material temperature. The pipe material derivative then becomes proportional to the net rate of heat transfer between the fluid and pipe wall, and the pipe wall and atmosphere, and inversely proportional to the material heat capacity. Heat transfer coefficients are represented using standard relationships for circular pipes, Rogers and Mayhew[1980b]. Radiation heat transfer is represented from the pipe outer surface to atmosphere. Radiation heat transfer is considered in this instance due to the fact that the level

of free convection to atmosphere from the pipe surface is in the same order of magnitude, typically 10 to 50 $W.m^{-2}.k^{-1}$ for the range of temperatures encountered. To close the equation set requires mass flow rate which is either provided by an adjacent model or calculated from steady state momentum considerations assuming the pressure loss in the pipe due to friction is a function of Reynolds number and friction factor for the turbulent flow region. Both laminar and turbulent flow regimes are represented.

5.5 LOADING VALVE MODEL

The loading valve used in the circuit is an adjustable restrictor valve. The standard orifice flow equation is used to represent the pressure flow characteristic as follows:

$$Q = A\ Cd \sqrt{\frac{2\Delta p}{\rho}} \tag{5.6}$$

Because there is no valve position reference available for intermediate positions, the discharge coefficient and the valve area are combined to form a single orifice flow coefficient (Cr). The orifice flow coefficient is first characterised at a reference oil viscosity (at ambient temperature) for a given range of working pressures (Figure 5.6). Typically the valve discharge coefficient will be a function of Reynolds number, so for a variety of different valve openings, the variation in Cr was observed with respect to change in circuit temperature/viscosity (Figure 5.7). It was not possible to determine Cr explicitly as a function of Reynolds number because the orifice flow velocity could not be determined experimentally. The data are linearised by using a logarithmic relationship between Cr and viscosity. This is combined with the correlation of Cr at the reference viscosity ($Cr_{\mu,ref}$) to obtain the actual orifice flow coefficient Cr. The following relationships are used:

$$Cr_{\mu_{ref}} = -2.603*10^{-2} + 1.39*10^{-3}\Delta p - 2.34*10^{-5}\Delta p^2 + 1.61*10^{-7}\Delta p^3 - 3.92*10^{-10}\Delta p^4 \quad (5.7)$$

$$Cr = Cr_{\mu_{ref}} e^{-B(\mu_{ref} - \mu)} \quad (5.8)$$

Where B is the slope of the linearised Cr verses viscosity(eqn 5.8).

The valve thermal performance can be implemented in a number of ways and many of the arguments sighted for the pump thermal performance model are relevant here. For example due to the small component size in relation to the other circuit components it is possible to assume isenthalpic expansion across the valve and a steady state temperature change on the basis that little heat is lost and that the thermal response is orders of magnitude faster than that of the reservoir. Therefore, the dynamic response of the valve will have negligible impact on the reservoir fluid bulk temperature. However to maintain flexibility, a valve model incorporating dynamic thermal effects and heat transfer were implemented for the current research. Equation (2.23) is used to define the valve outlet temperature derivative ignoring the work and pressure derivative terms as follows:

$$\frac{dT_l}{dt} = \frac{\upsilon}{Cp\ V}[w_e(\upsilon(1 - \beta T)(p_e - p_l) + Cp(T_e - T_l)) + q_h] \quad (5.9)$$

Analogous to the pipe model approach, heat transfer is accounted for by assuming a lumped material temperature. The valve material derivative then becomes proportional to the net rate of heat transfer between the fluid and valve body, and the valve body and atmosphere; and inversely proportional to the material heat capacity. As previously mentioned, heat transfer from the valve body is very small in relation to other circuit components and to an extent variation in

values for heat transfer coefficients would make little difference to the transient or steady state performance of the system as a whole.

5.6 RESERVOIR MODEL

Research conducted by Harris [1990] showed that the reservoir used in this study could be considered in a simplistic manner insofar that heat transfer to the surroundings is considered, but the wall temperature is assumed to be at the oil temperature. Experimental results based on cool down times validated this approach. Correlations for wall to air convective heat transfer coefficients showed good agreement with experimental results, and these were used to produce an overall convective heat transfer coefficient. Because the radiative and convective heat transfer could not be separated, the radiative component was assumed to be correct and adequately represented by being proportional to the 4th power of temperature. A value of emissivity equal to 0.9 was used for the radiation component and was considered representative for this case. This was taken into account when experimental results were being assessed to give a convective heat transfer coefficient value. Because of the large quantity of fluid in the reservoir, a dynamic temperature calculation is necessary. Unlike other components though, there is a negligible pressure differential across the reservoir. Equation (2.23) can then be used to formulate a fluid temperature derivative:

$$\frac{dT_t}{dt} = \frac{v}{VCp}[w_e Cp(T_e - T_t) - q_h] \tag{5.10}$$

The convective heat transfer coefficients for the reservoir surface to the surroundings can be represented as follows, Rogers and Mayhew [1980c]:

$$h = k_1 \left(\frac{\theta}{k_2}\right)^{0.25} \tag{5.11}$$

Where k_1 is a coefficient dependent on the orientation of the surface and whether heating or

cooling is taking place; and k_2 is a characteristic dimension. Clearly an overall heat transfer coefficient may be calculated as follows:

$$UA_{total} = A_{lid}(h_{lid} + h_{base}) + h_{wall}A_{wall} \quad (5.12)$$

Due to the open to atmosphere nature of the reservoir, the model can be assumed to be a constant pressure device. Allowing for variation in the fluid depth makes little difference to this assumption. However the model does use an integrator for pressure, with the derivative being set to zero. This technique avoids generation of implicit relationships between pressure and flow in the circuit and was a suitable place to include a loop breaking integrator. The above representation of the reservoir is simplistic insofar that it assumes perfect mixing of the oil, a point that proved not to be the case Harris[1990] and which is expanded upon in the analysis of results Chapter 6.

5.7 OIL COOLER MODEL

The oil cooler used is a three-pass shell and tube counter flow heat exchanger. The thermal performance of oil coolers can be examined in many ways. Heat transfer formulations range from complex polynomial expressions to the more basic NTU (number of transfer units) method. Of these the NTU method was chosen due to its generality and ease of implementation. It is also worth considering the other well known method for predicting heat transfer using the log mean temperature difference approach (see Chapter 3). The NTU approach is straight forward to implement, as only the inlet fluid conditions are required to predict the rate of heat transfer. The NTU approach does however require knowledge of the heat exchanger effectiveness, which can either be found from the manufacturer's data or experimentation. The outlet fluid temperature may be represented in steady state form as:

$$T_l = T_e - \frac{q_h}{(wCp)_{oil}} \quad (5.13)$$

Clearly if the cooler oil volume is significant with respect to the circuit oil volume then a dynamic equation would be needed based on equation (2.23). Heat transfer is represented by the NTU method as follows:

$$q_h = \epsilon Cmin(T_{hot(e)} - T_{cold(e)}) \tag{5.14}$$

Figure (5.8) shows the effectiveness of the cooler over a range of test conditions. It can be seen that providing the inlet temperature difference remains above 15 to 20°C then calculated values of effectiveness ϵ are approximately constant for each test condition. At reduced temperature differences, ϵ does appear to deviate from a constant value. Estimation of ϵ however at low inlet temperature differences will have associated with it progressively larger errors due to thermocouple tolerance (± 0.5°C). Consider the test condition exhibited in Figure (5.8) which is closest to the model/rig performance tests of Chapter 6. The cooling water flow rate was 52 $L.min^{-1}$ and the oil flow rate was 45 $L.min^{-1}$. For these flow conditions, and an inlet temperature difference of 20°C the rate of heat transfer q_h amounted to 3355W. When estimating q_h it is preferable to consider the temperature change of the fluid (oil) with the smallest heat capacity which will provide the largest temperature change, and therefore minimise the effect of the thermocouple error. At the aforementioned operating condition the temperature drop in the oil between inlet and outlet was 2.6°C. It is evident then that as the inlet temperature difference between both hot and cold fluids reduces below 10°C will correspond to an oil temperature drop approaching the accuracy of the thermocouples. Clearly the error in calculating q_h will affect the estimation of ϵ. The error in estimating ϵ was minimised by matching inlet and outlet thermocouples too less than ± 0.2°C. Confidence in the estimation of ϵ is clearly limited to the larger inlet temperature difference conditions which provided a consistently stable value for the instrumentation used. For these reasons, a constant value of ϵ was used for assessing model performance in Chapter 6 based on the experimental operating conditions for each transient. In principle characterising the heat exchanger for the lower inlet temperature difference conditions

is possible, however this would require thermocouples with a much finer tolerance than those available for the experimentation.

5.8 CLOSURE

A set of component models have been developed to represent the steady state and transient performance of the hydraulic fluid power circuit described above. These models use the fundamental conservation equations for mass and energy developed in Chapter 2 to provide the system states. Where necessary characterisations of the hydraulic relationships involving flow as a function of pressure and temperature have been used accurately to represent the individual circuit components and to close the equation set. Chapter 6 explores the validity of these models when assembled in the Bath*fp* simulation environment. The steady state and transient performance is assessed by comparison with rig data.

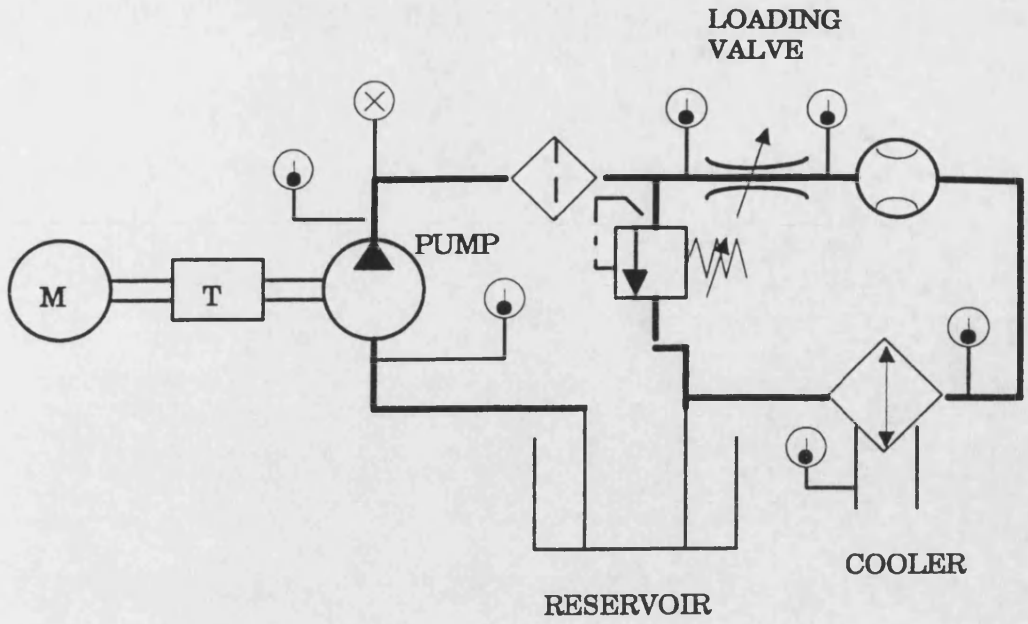

EXPERIMENTAL HYDRAULIC CIRCUIT FIGURE 5.1

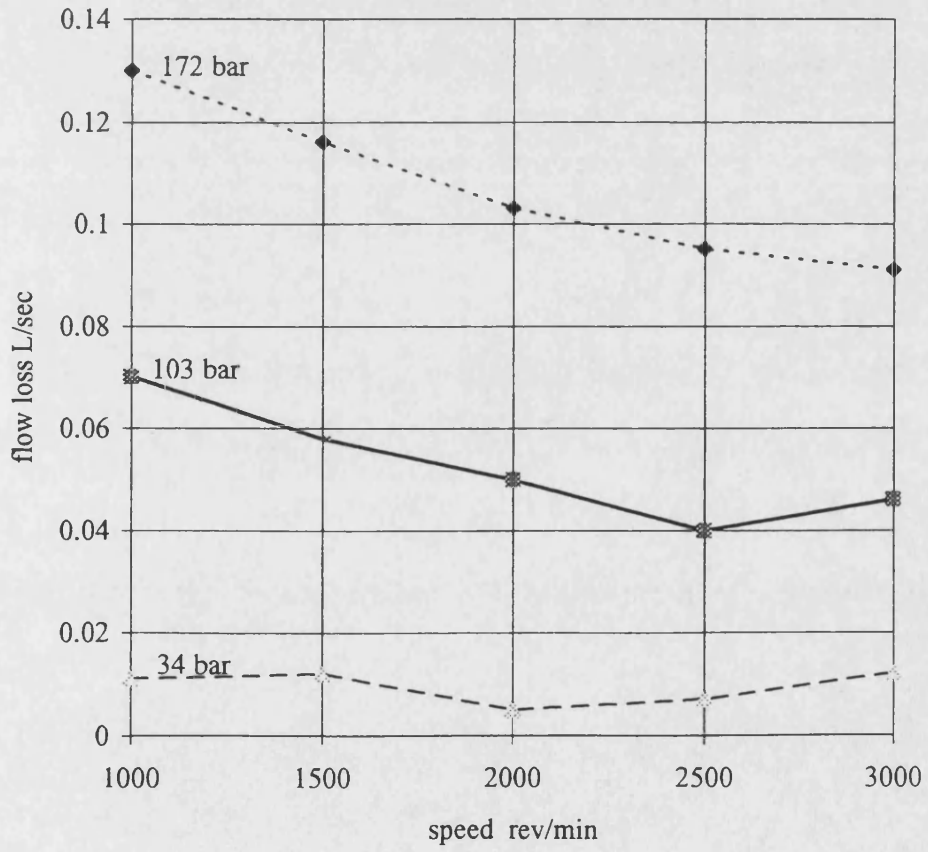

GEAR PUMP CHARACTERISTICS FIGURE 5.2

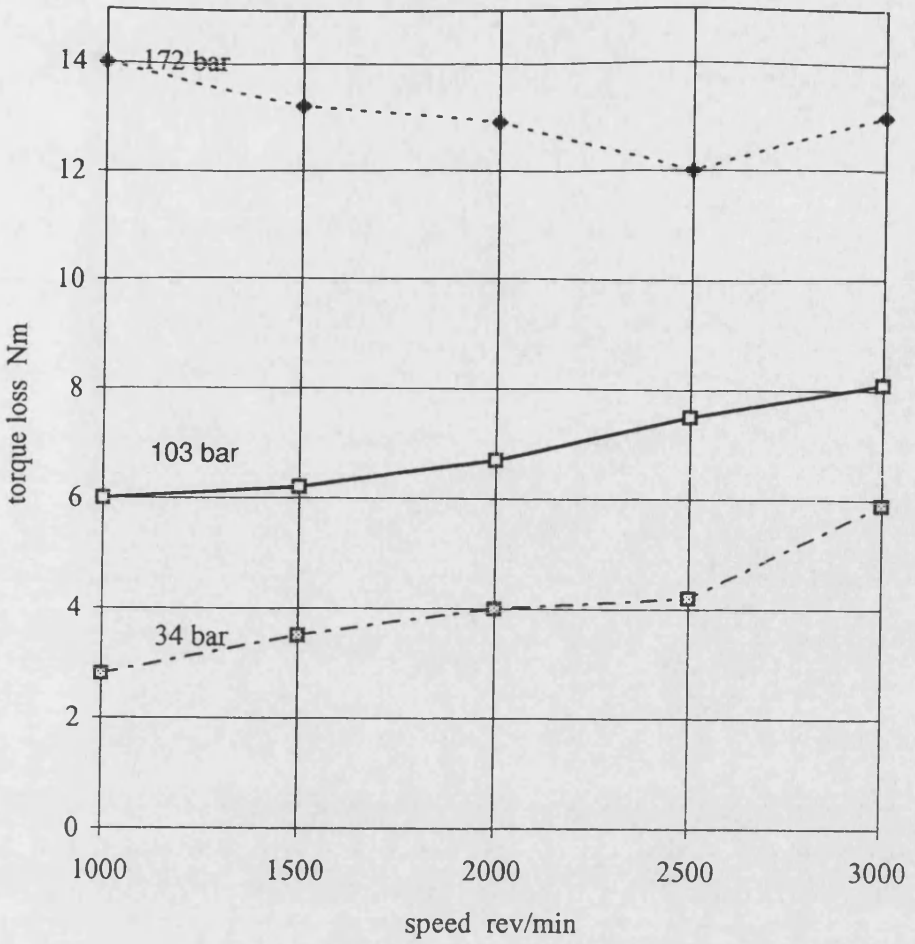

GEAR PUMP CHARACTERISTICS FIGURE 5.3

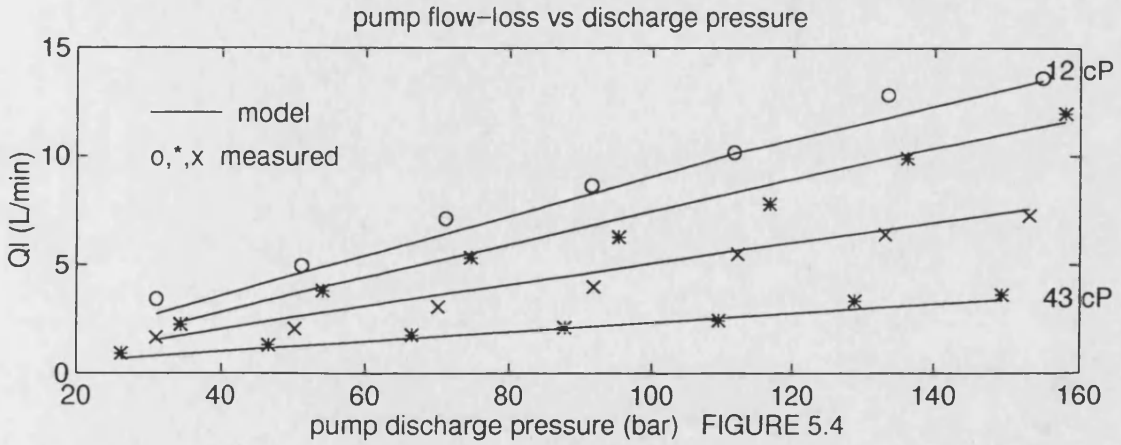

FIGURE 5.4

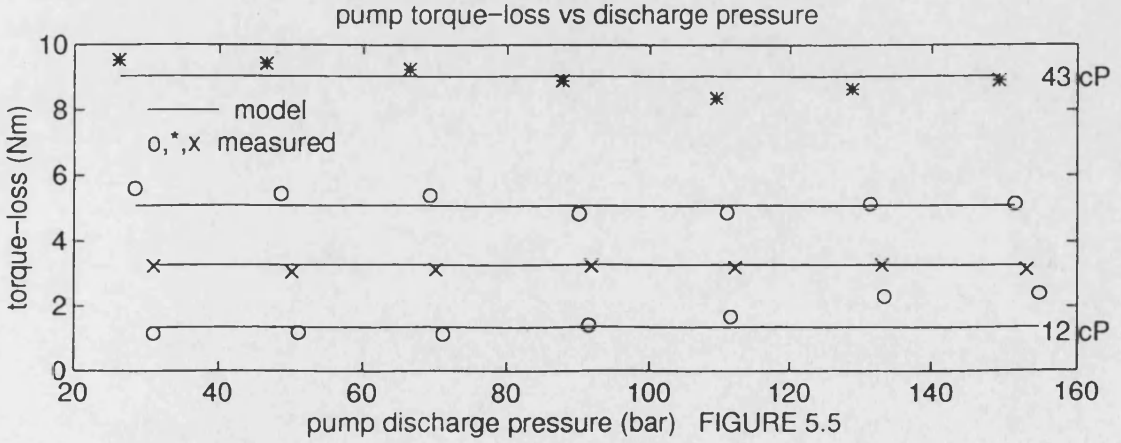

FIGURE 5.5

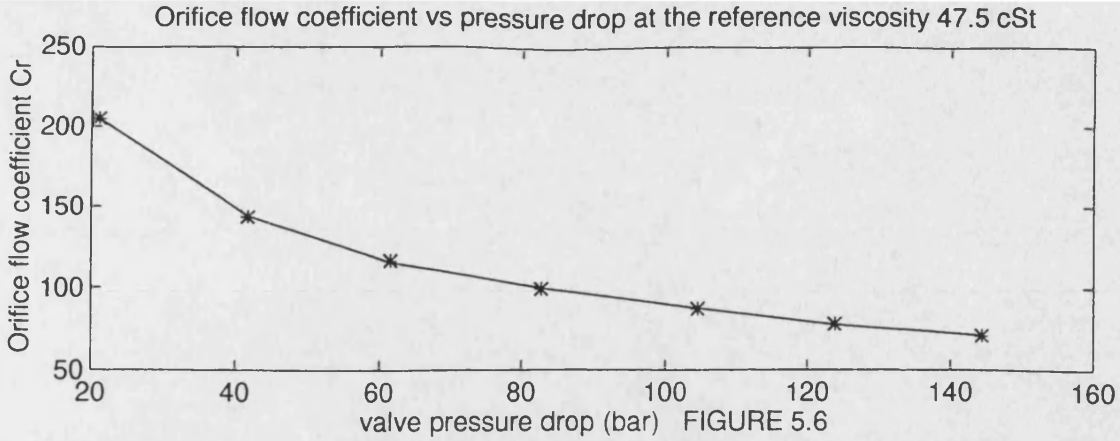

FIGURE 5.6

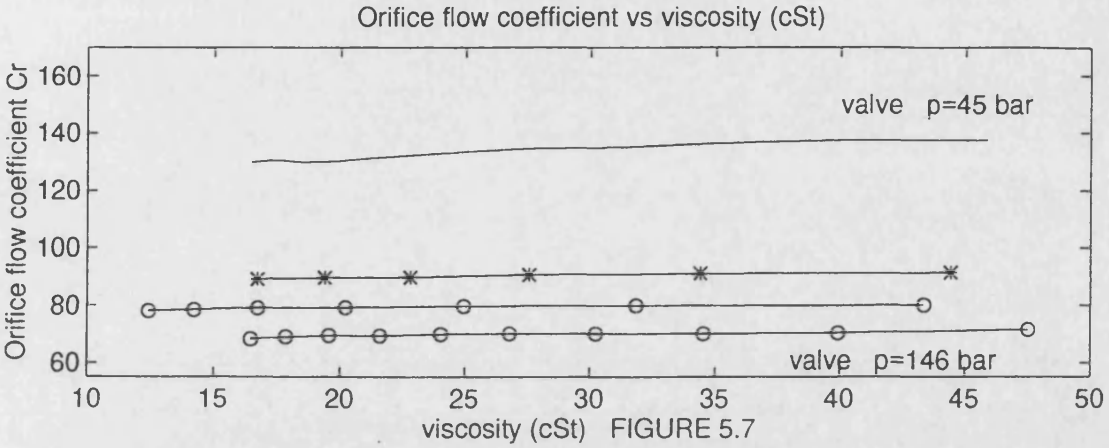

FIGURE 5.7

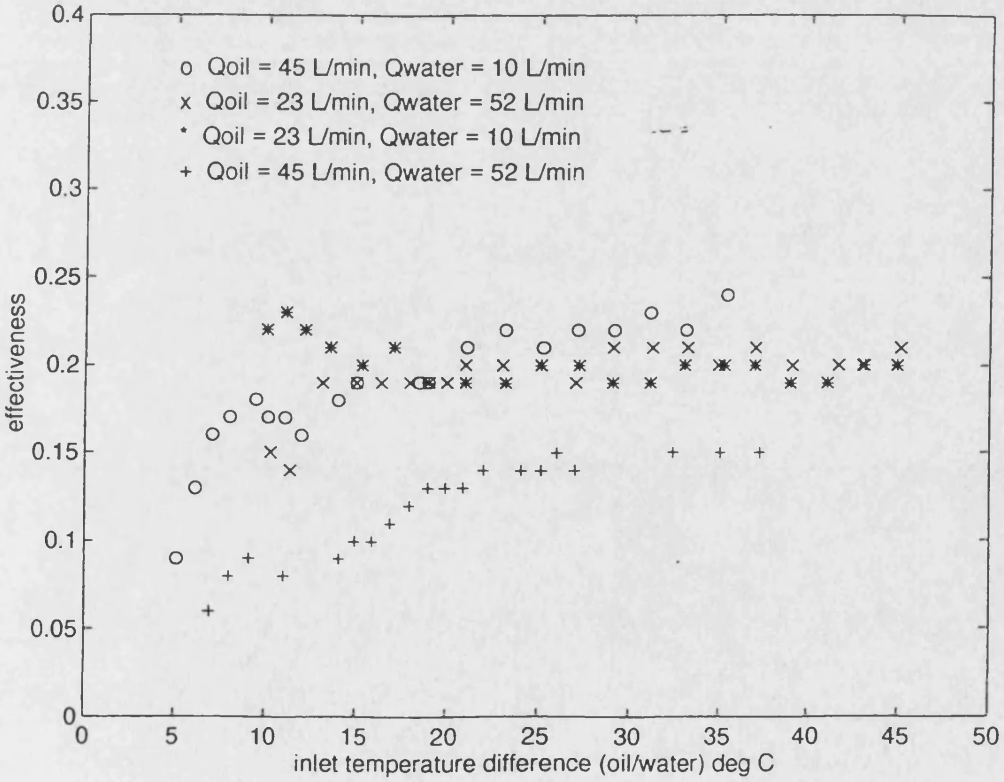

OIL COOLER EFFECTIVENESS FIGURE 5.8

CHAPTER 6

HYDRAULIC FLUID POWER SYSTEMS - INSTRUMENTATION AND MODEL ASSESSMENT

6.1 INTRODUCTION

The purpose of this chapter is to describe the experimental rig instrumentation and explore the suitability of the simulation approach for the hydraulic circuit described in Chapter 5. The quality of the instrumentation in terms of accuracy, resolution and repeatability has a fundamental effect on the simulation assessment. Ideally the instrumentation should be capable providing measured circuit parameters with sufficient accuracy such that testing of model predictions can be achieved quantitatively. The accuracy of model prediction is considered in detail in Appendix C.

To examine the circuit performance, three simulations were performed and then compared with experimental data as follows:

1. A circuit warm up by closing the loading valve and allowing the circuit temperatures to reach a pseudo steady state condition from ambient conditions.

2. A circuit cool down from an elevated steady state circuit temperature by opening the loading valve and thus reducing the circuit pressure and load.

3. Load cycling by repeated cycling of the loading valve differential pressure from an initial ambient temperature condition.

The above tests are considered to provide sufficient information regarding both the steady state

and dynamic characteristics of the circuit for validation purposes.

6.2 EXPERIMENTAL RIG INSTRUMENTATION

Data comprising pump pressure and torque, and circuit temperatures were gathered on a computer based data acquisition system. Electronic cards were matched to each transducer and ranged to give the required signal. Pump torque was measured with a transducer (TT2/4/CA) located in the pump drive shaft. The accuracy of measurement was ± 0.11% FSD (full scale deflection) which for the current application was ± 0.15Nm. The circuit pressure was measured at the pump discharge / valve inlet with an accuracy of ± 0.735 bar. Circuit temperatures were measured with T type thermocouples with an accuracy of ± 0.5 °C and a time constant of 0.25sec (plunge test into hot water).

Other circuit data which was required to characterise and monitor the system but did not form part of the computer data acquisition system are detailed as follows. The pump speed was measured using a light sensor digital hand tachometer with an accuracy of ± 1 $rev.min^{-1}$. The circuit oil flow rate was measured with a meter positioned down stream of the loading valve with an accuracy of ± 0.5% of measured value.

The cooler water flow rate was measured with a rotameter type flow meter. This was calibrated to provide flow rate for a given float position.

6.3 CIRCUIT WARM UP

Figure (6.1) shows the model/rig response to a step change in valve differential pressure from an initial steady state condition where the circuit oil temperature is at ambient conditions. It can be seen that model/rig circuit temperatures correspond very well giving approximately one degree difference throughout the transient. This difference is a similar magnitude to the limit of

the expected error determined in Appendix C. However, the hydraulic performance is less than ideal and this is due to a difference between the pump model flow rate prediction and the actual rig flow rate for the particular operating envelope, see Figure (5.4). Figure (6.2) shows the system characteristic (valve inlet pressure for the indicated viscosities) for a fixed valve position (warm up transient) and the pump flow loss characteristic. The locus of these intersecting points describes the pressure fall as the circuit temperature increases. In effect for the given pump pressure drop (90 - 95 bar), the loss flow is up to 0.5 $L.min^{-1}$ in error for the operating conditions that prevail. An improvement in the hydraulic performance is achievable by using a more accurate pump flow loss model. In Chapter 5 it was established that the pump flow loss could be adequately represented as a linear function of pump differential pressure multiplied by a non-linear function of viscosity. If this model is extended to incorporate a 3rd order polynomial in viscosity, and using multiple regression analysis to establish the coefficients yields a pump flow loss model of the form:

$$Q_l = P\,(\,0.172 - 8.45*10^{-3}\mu + 1.76*10^{-4}\mu^2 - 1.36*10^{-6}\mu^3\,) \qquad (6.1)$$

Figure (6.3) shows the new pump flow loss model fit compared with rig data. It can be seen that using this new pump flow loss model has improved the hydraulic simulation significantly compared with the original model (Figure (6.1) and (6.4)).This may be seen by examination of the model and rig pump discharge pressures, and oil cooler flow rates respectively. For both simulations the circuit temperatures are marginally above the rig measurement (approximately 1 to 1.5 °C) which shows that improvements to the hydraulic performance in this area has little effect on the thermal prediction.

6.4 CIRCUIT COOL DOWN

Figure (6.5) shows the model/rig response to a reduction in valve differential pressure from an

initial quiescent state (pump discharge pressure 92.5 bar), to a pump discharge pressure of 28 bar. It is evident that the hydraulic performance is very good, there being almost no difference between model and rig. The thermal performance is still good, however from Figure (6.5), the rig thermal transient response appears to now be faster than the model in contrast to the warm up transients. This phenomenon is attributed to thermal stratification within the reservoir as noted by Harris[1990] which effectively reduces the heat capacity of the reservoir oil. Harris has shown that for this type of reservoir, a reduction of oil inlet temperature on the cooling phase has induced buoyancy effects in the reservoir oil such that a layer of un-mixed fluid is maintained at the free surface. This accounts for the apparent reduction in oil heat capacity and hence a reduction in thermal response time for the system. Figure (6.6) shows a revised transient where the effective model reservoir oil heat capacity is reduced by 18% on the cool down phase to maintain a correspondence between model/rig transient thermal response.

It is clear that to maintain consistency for transient thermal response, requires the reservoir to be characterised over the operating envelope, or a more sophisticated model representation which can cope with thermal stratification effects. There is a small temperature difference at the end of the cool down period which can be attributed to the combined effects of small differences in the overall heat transfer and work input between model and rig, and also the effects of measurement inaccuracy.

6.5 LOAD CYCLING

Finally the transient performance for the rig is investigated for repeated cycling of the valve differential pressure. The variation in pump discharge pressure is illustrated in Figure (6.7) and compared with the model prediction. Again the hydraulic performance is very good, demonstrating that the pump and valve characterisation is acceptable over the range of operational pressures and temperatures. The thermal response however still exhibits the effects

of reservoir oil thermal stratification after the initial warm up period. Again this error can be minimised by adjustment of the model reservoir oil heat capacity at each subsequent loading condition (Figure (6.7)). The stratification effect will reduce the transit time of the oil in the reservoir and as such shows the importance of complete mixing. Correct reservoir design, including the use of baffles, return line diffusers and suction line strainers should help minimise this effect and ensure all the fluid is used within the system.

6.6 MODEL AND RIG COMPARISON

The accuracy of model prediction has been considered in Appendix C. This has involved an assessment of both the systematic and random errors involved when considering the temperature difference across the pump. The assessment has focussed on the pump because the prediction of its thermal performance is dependent on many of the measured circuit parameters. In this respect, the sensitivity of oil temperature, to errors in circuit parameters can be tested more fully. This does not diminish the role of the other component models. However, the importance of the pump model prediction is fundamental to determining the predicted circuit oil temperature (work done on the system).

It was shown in Appendix C that for a range of circuit operating conditions, the error in pump temperature difference was bounded at a maximum of ± 0.48 °C. Comparison with the total measurement error of ± 0.707 °C (based on two thermocouples at pump inlet and outlet) has shown that the pump model prediction could be considered more accurate than the measurement. Consider the pump operating at 100 bar discharge pressure, 20 °C and with an efficiency of 80%. The predicted oil temperature rise across the pump is 2.66 °C for these conditions. It is therefore possible for the measurement error to be as much as ± 26.5%. Clearly if an indication of pump heat transfer was attempted, based on pump oil temperature rise, this could give rise to large errors. It is fortunate that for the circuit under consideration, the pump heat transfer is

small in comparison with that of the oil cooler and therefore can be neglected.

Predicting circuit temperatures is not purely a function of the pump performance. When considering steady state conditions, then circuit temperatures will stabilise when the work done by the pump is balanced by the heat loss from the circuit. This requires not only an accurate pump model, but also an oil cooler model of similar pedigree.

6.7 CLOSURE

An approach to analysing the transient and steady state thermal hydraulic performance of hydraulic fluid power systems has been demonstrated. For the circuit studied, a good thermal correspondence is achieved between model and rig, when taking into account the possible systematic and random errors involved (Appendix C). It has been shown that this level of correspondence requires accurate hydraulic performance models which include the effects of temperature and therefore viscosity. The change in viscosity should not be under-estimated insofar that a 20 °C rise in oil temperature can halve the viscosity (the hydraulic oil used for this study was BP-HLP 32). This is demonstrated by the pump flow loss model and the loading valve hydraulic performance model discussed in Chapter 5. The circuit has provided a useful test bed for validation of the theoretical approach for typical components used in fluid power systems. To maintain consistency, models that solve the energy equation dynamically should also solve continuity dynamically to provide the dynamic cross coupling effect between pressure and temperature. However this becomes impractical to some degree where component models have been evolved to provide flow rate from pressure boundary conditions, and which therefore have no continuity equation. In this respect the sophistication of a model will be dependent on its intended application.

For the current circuit studied, the thermal response is dominated by the heat capacity of the

reservoir and the dynamic cross coupling effect between pressure and temperature will have negligible impact on the overall transient response. The dynamic cross coupling effect between pressure and temperature will be more noticeable in systems where large pressure fluctuations occur for a sustained period of time (such as the LP feed train examined in Chapters 3 and 4), and where the heat capacity of the system is small. An example of this could include systems where cyclical loading occurs via an hydraulic actuator. To successfully study and predict the dynamic response of these systems, would require improvement in thermocouple dynamic response, such that it is comparable with the pressure transducer dynamic response.

For the circuit studied, dominance of the system heat capacity in the thermal transient response, suggests that it is acceptable to base estimations of the response time on the thermal inertia of the system. In this respect, the modelling approach of Harris[1990] could be used without significant loss of accuracy being incurred for the circuit in Figure (5.1). It has been shown that providing there is an accurate thermal hydraulic characteristic for each component, then the steady state performance will also be predicted with confidence.

It was shown that the oil thermal stratification within the reservoir had a distinct affect on the transient response (figures 6.5 to 6.7) by effectively reducing the heat capacity of the system. This was noted when the oil entering the reservoir reduced in temperature, thereby inducing buoyancy effects such that a layer of un-mixed fluid is maintained at the free surface, Harris[1990].

It is considered that improvements to the model prediction would require the following extended research:

1 Examination of the phenomena of heat and mass transfer within a single phase fluid such that a more detailed reservoir model could be established. The possibility of extending the lumped parameter modelling approach to adjacent layers of fluid such that each layer constituted a control volume could be considered. Each control volume would perform mass, momentum and energy conservation.

2 Research into heat transfer correlations for the circuit components other than the oil cooler. This would have a second order effect but nevertheless improve the model prediction at all operating conditions. To access the heat transfer in detail from each component would require thermocouples with improved accuracy compared with that currently used for this study. This is due to the temperature rise across most components being typically less than a few °C.

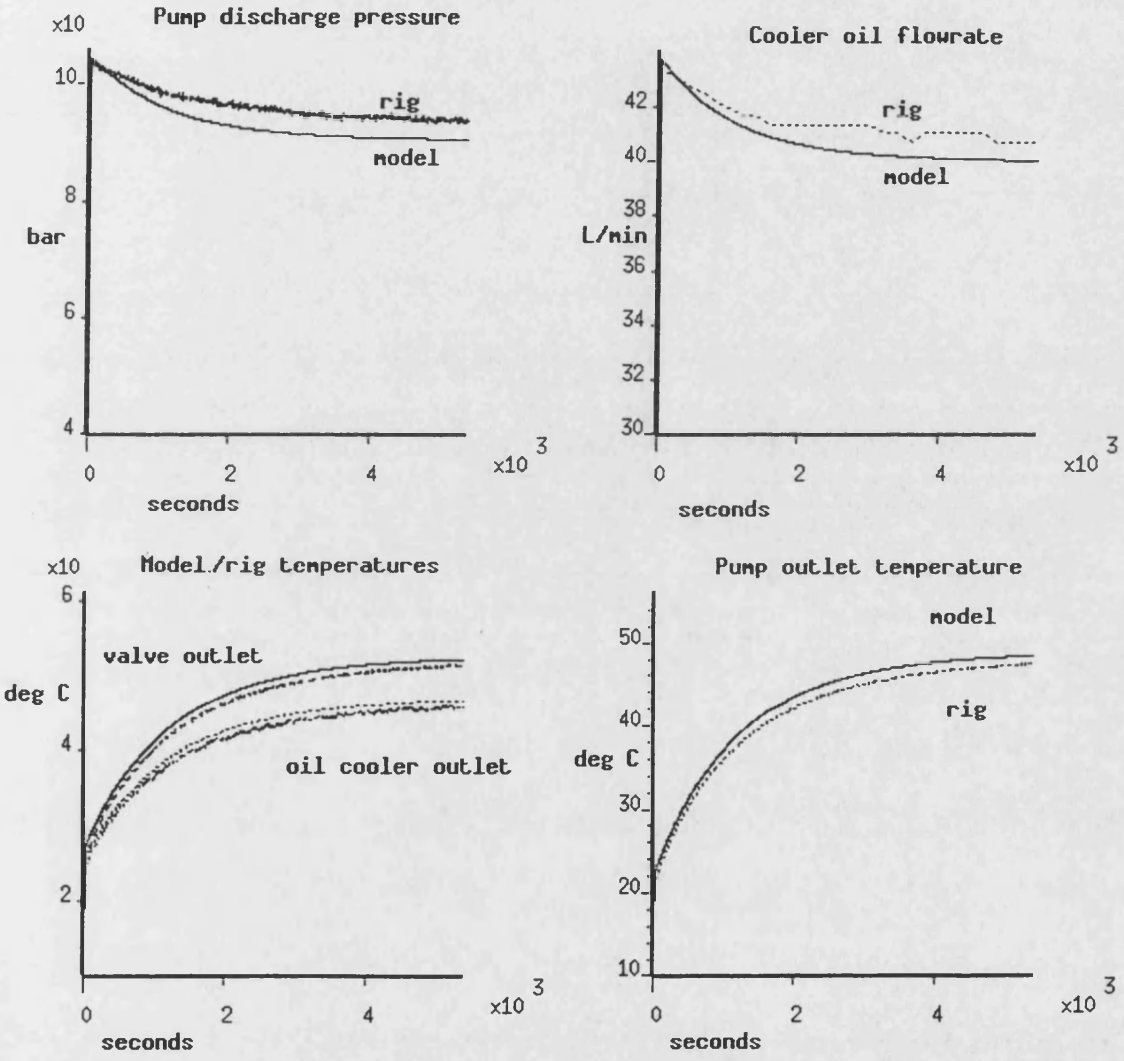

MODEL / RIG RESPONSE TO STEP CHANGE IN VALVE DIFFERENTIAL PRESSURE

FIGURE 6.1

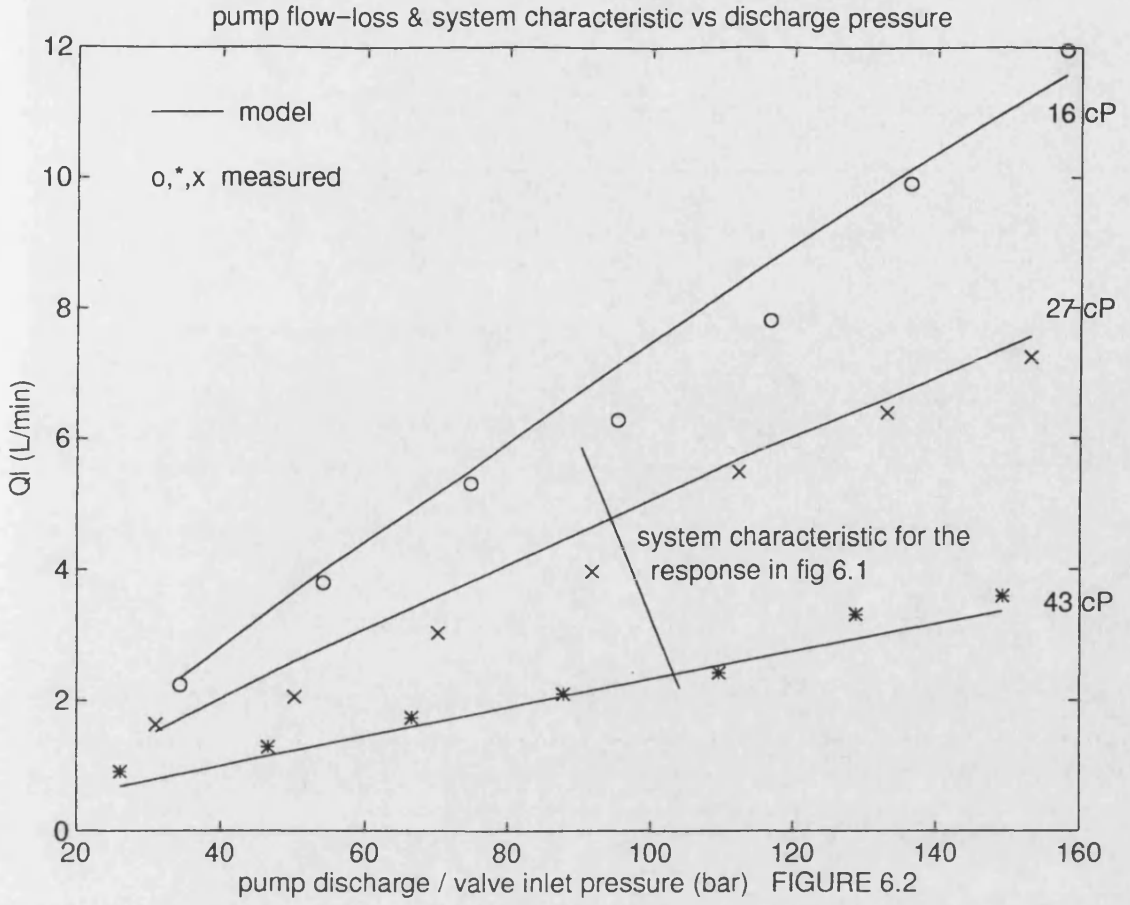

FIGURE 6.2

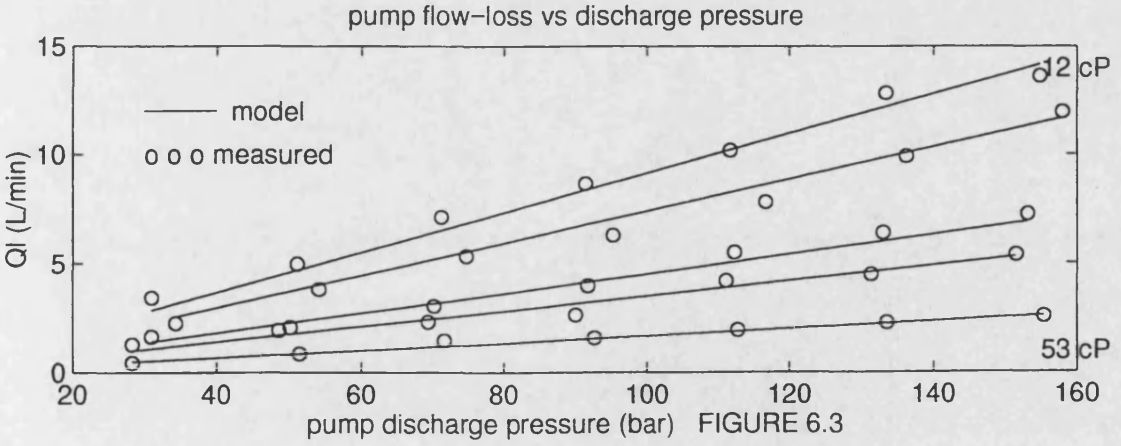

FIGURE 6.3

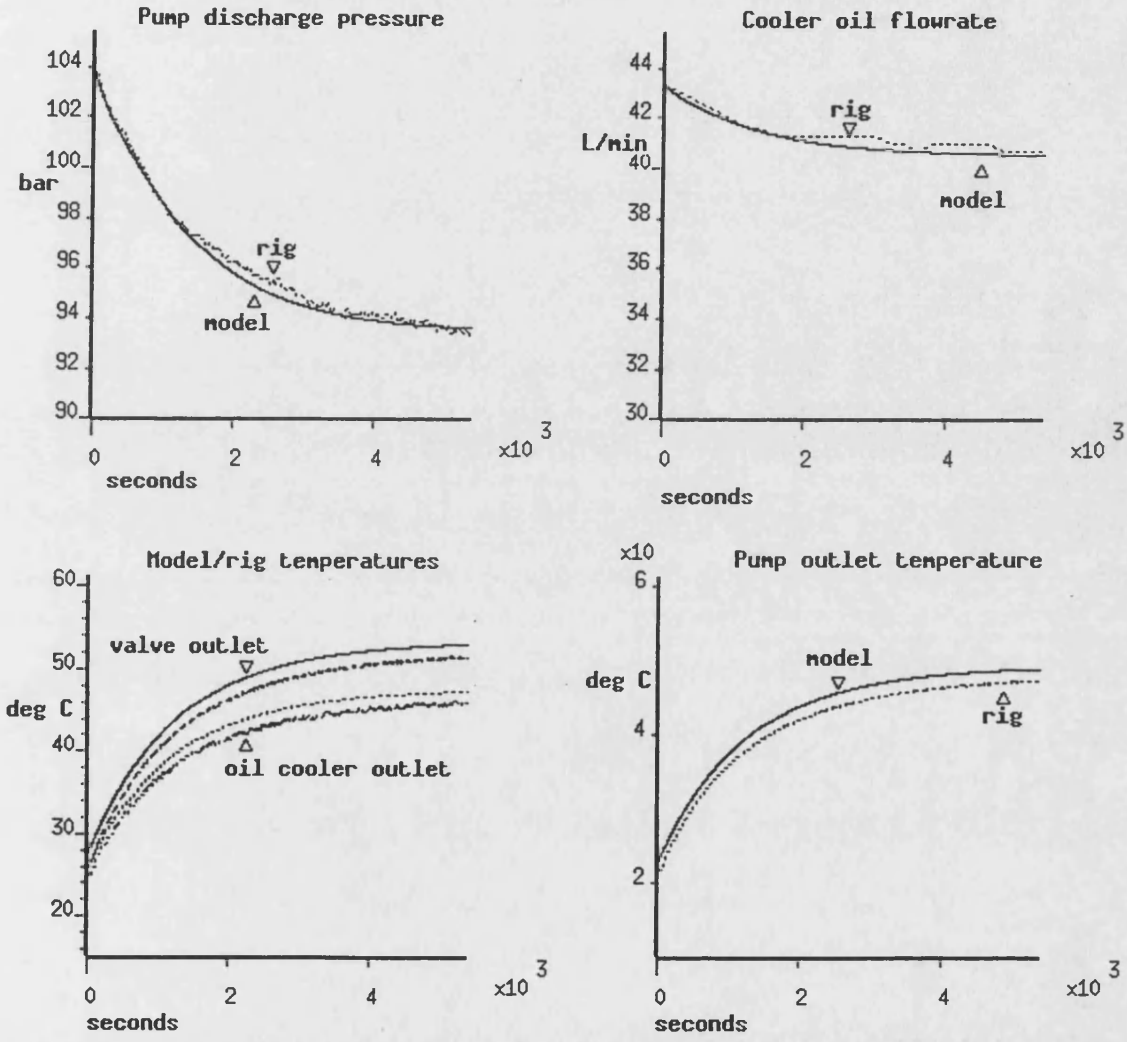

IMPROVED MODEL / RIG RESPONSE FIGURE 6.4

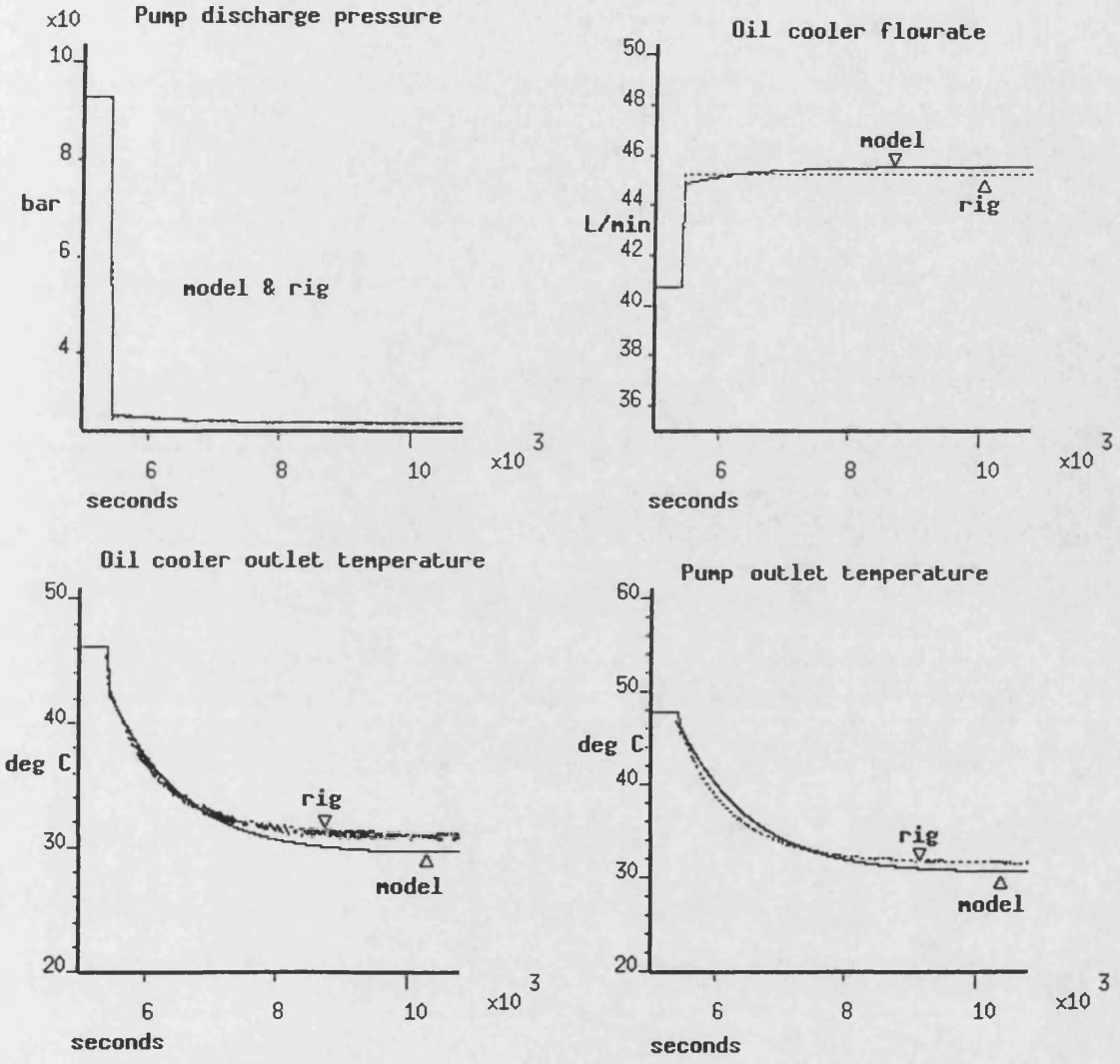

MODEL / RIG RESPONSE TO A REDUCTION IN VALVE DIFFERENTIAL PRESSURE

FIGURE 6.5

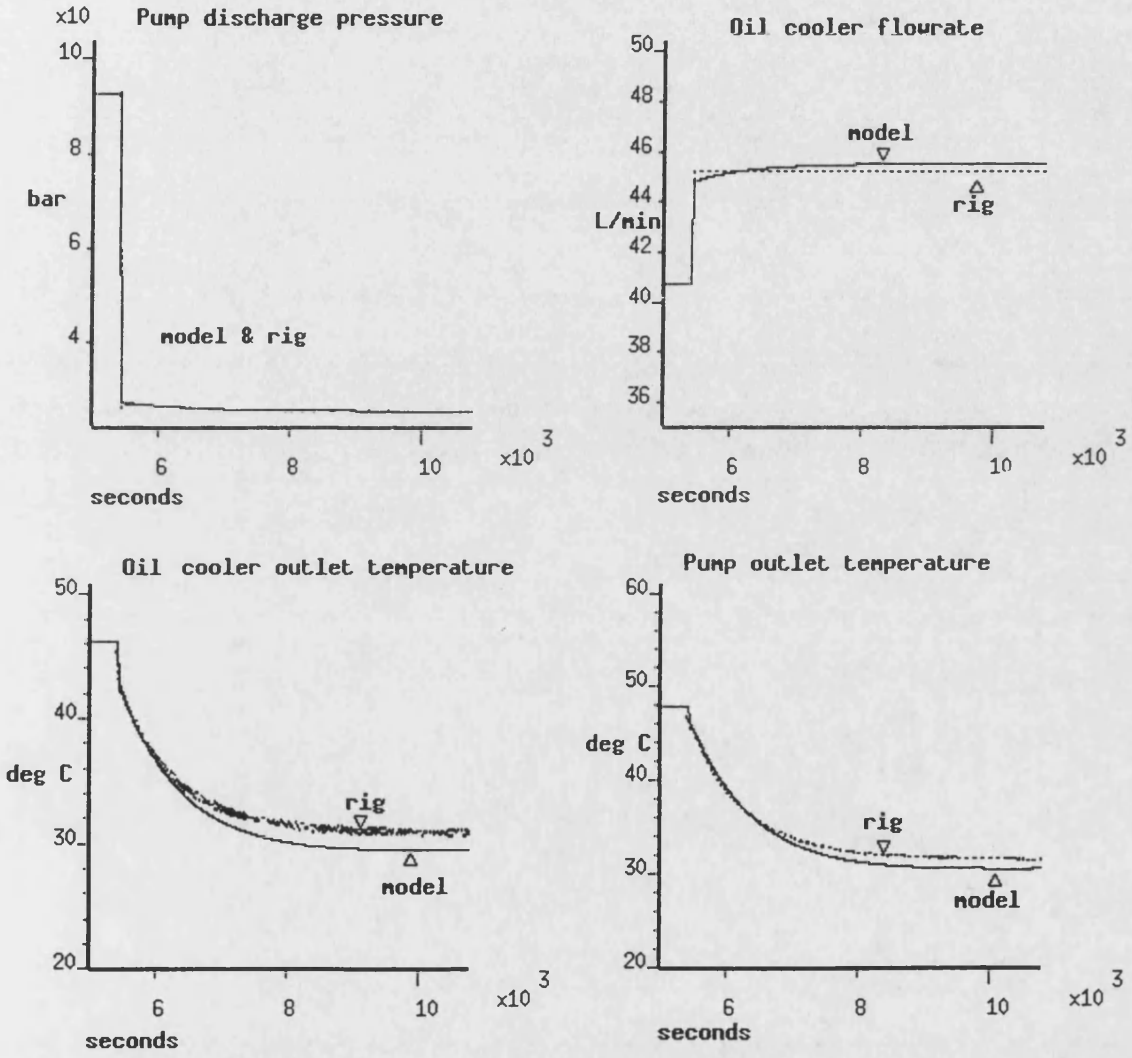

REVISED MODEL / RIG RESPONSE FIGURE 6.6

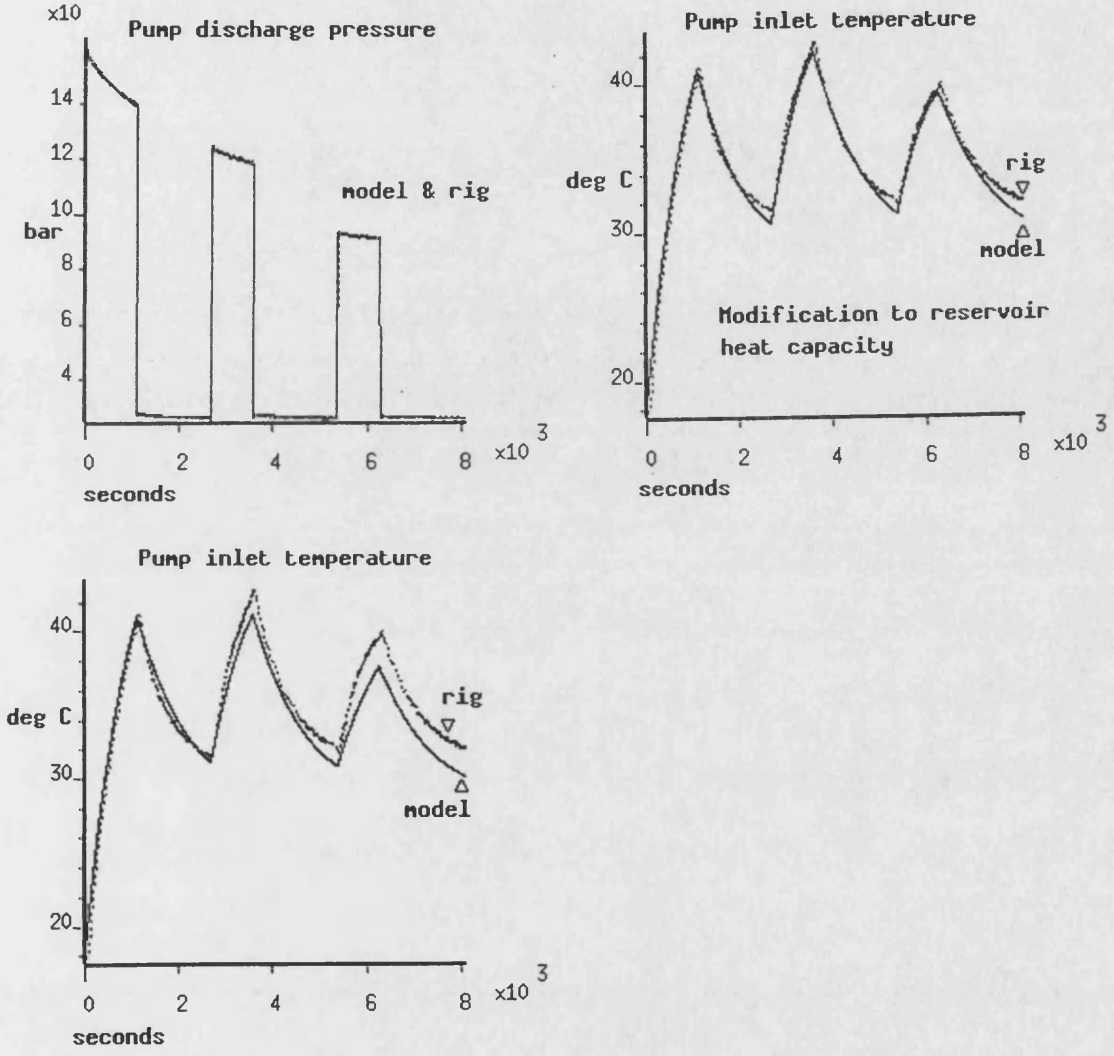

MODEL / RIG RESPONSE TO REPEATED CYCLING VALVE DIFFERENTIAL PRESSURE

FIGURE 6.7

CHAPTER 7

VEHICLE COOLING SYSTEMS

7.1 INTRODUCTION

The purpose of this Chapter is to apply the theoretical approach developed in Chapter 2 to simulate vehicle cooling systems. In many respects the process of model development for the vehicle cooling system components is very similar to that used for the hydraulic fluid power component models described in Chapter 5. This is due to the information required concerning the hydraulic characterisation of the components, and in particular how the hydraulic performance of components is affected by temperature variation. Contrasting this with the fundamental characteristics of the LP feed train described in Chapter 3 is interesting. Hydraulic characterisation of the LP feed train components is less important when compared with either the hydraulic fluid power or vehicle cooling systems. This is because the LP feed train condensate flow rate is ultimately determined by the rate of condensing heat transfer in the main condensers. Any change in condenser level is compensated for by the level control valves that provide a variable resistance in the circuit. The vehicle cooling system flow rate however is determined only by the hydraulic characteristics of the circuit.

Model development and simulation of the vehicle cooling system have been performed using the Bath*fp* simulation package. Experimental data have been used to characterise individual component models for the circuit.

7.2 VEHICLE COOLING SYSTEM DESCRIPTION

A vehicle cooling circuit was constructed to provide experimental data concerning individual components, and the whole circuit performance. This has evolved around a 1.8 litre internal combustion diesel engine and cooling system components. The cooling system components

comprised coolant pump, cabin heater, radiator, oil cooler, thermostat, deaeration header tank, hoses and junctions. An outline of the system is shown in Figure 7.1. Unfortunately, running the engine to provide experimental data was not possible, so an external heat source was constructed for this purpose and added to the test rig. This consisted of two electrical immersion heaters of 3 KW capacity, arranged in series within a conduit, with connections at each end for the coolant. Each heater could be thermostatically controlled. The heater assembly is positioned between the cabin heater inlet and radiator inlet and could be isolated from the system if so desired. Similarly an alternative power source for the coolant pump in the form of a variable speed electric motor is included in the test rig. The electric motor can provide the coolant pump with a speed range of between 0 and 5000 revs.min^{-1}.

At the engine coolant outlet (Figure 7.1) several connections distribute coolant to various parts of the circuit. Coolant is supplied to the thermostat inlet that is mounted directly onto the engine block. Depending on the coolant temperature, the coolant either passes directly back to the coolant pump inlet, or passes through the thermostat outlet valve onto the radiator. Typically under normal operating temperature conditions, a proportion of coolant will pass through the bypass and the remainder through the thermostat to the radiator. The thermostat can shut off the bypass flow at highly elevated temperatures. Coolant is supplied to the cabin heater via a hose from the engine coolant outlet. This again passes back to the coolant pump inlet. The remaining engine coolant outlet hoses, which are significantly smaller than the main coolant flow path routes, provide a deaeration function that discharge into the deaeration header tank. The deaeration flow paths contain restrictors designed to limit the flow rate to 5% of the pump flow rate.

A coolant pump is physically mounted on the engine block and provides the coolant flow into the block and through the head of the engine where it is distributed through the previously

described outlet connections.

7.3 COMPONENT MODEL DESCRIPTION

Lumped parameter models have been developed for each cooling system component using the Bath*fp* simulation package. The following section details the model development phase and discusses the assumptions made in each case.

7.3.1 Engine Component Model

The engine model has been developed to provide a representation of the thermal hydraulic characteristics of the coolant path ways within the block and cylinder head, and to incorporate the thermal inertia of the engine material for heat transfer purposes.

Due to the number of input and output coolant flow paths, the model has a dynamic continuity equation at the engine inlet and outlet based on equation (2.7) derived in Chapter 2, which includes the effects of temperature. This uses a core engine flow rate calculation based on experimental data for frictional resistance between the engine inlet and the thermostat inlet. Figure 7.2 shows the engine core hydraulic characteristic, tested over a range of flow rates using a 50/50 water/glycol coolant mixture. It may be seen that the pressure/flow rate relationship is to a first approximation linear. The effects of temperature could not be seen experimentally for a range of coolant temperatures between 20 and 80 °C. The engine core flow path is split into four sections that comprise one block section and three cylinder head sections in series. Heat transfer coefficients (htc) are calculated for each section using a Nusselt number relationship for typical pipe flow and using an equivalent diameter based on cross sectional area. This approach is based on the work of Tomlinson and Burrows[1994]. The individual htc's for each section are used to calculate an overall htc for the engine.

Conservation of energy is performed for the block and cylinder head by using a lumped parameter engine material temperature which balances the heat generated by the engine (a function of torque, speed and engine efficiency) and the convective heat loss to the coolant and atmosphere. Radiation heat transfer is included to the surroundings. Researchers such as Shayler *et al.*[1993] and Veshagh and Chen[1993] have found that a significant quantity of the heat generated by the engine is lost to the exhaust system and the sump lubricating oil. Tomlinson and Burrows[1994] realised this and assumed that 45% of the total heat generated was lost through these mechanisms. The figure of 45% for heat loss has been adopted for this research, although, it should be noted that the engine heat generation term is not important insofar that the experimental rig uses an external heat source. The engine heat generation term is used however in generating the transient responses in Chapter 8 to show the flexibility of the simulation from a fundamental design perspective.

The engine has coolant inlet and outlet dynamic energy equations based on equation (2.23) derived in Chapter 2. The pressure derivative term has been ignored because its effect on temperature is insignificant in this application. The engine inlet node balances the fluid energy transfer between the pump inlet, core and deaeration paths; no heat transfer is assumed for this node. The outlet dynamic energy equation caters for the energy balance between the engine coolant outlet and the heater, thermostat and final deaeration paths and represents the engine coolant outlet temperature. This node also includes the heat pick up through the engine core. The engine model is capable of reverse flow computation for both energy and continuity calculations. Provision is made for cavitation/air release effects by suitably adjusting the coolant bulk modulus to reflect this condition. The cavitation model is due to McCloy[1969] and the air release model is based on Perry *et al.*[1984]. The provision for cavitation /air release effects is already a facility built into the Bath*fp* model library and this feature is used in many models developed to represent the vehicle cooling system. A full description of modelling this cavitation

condition is given by Richards[1993a].

The nodal coolant dynamic energy equation is represented as follows:

$$\frac{dT}{dt} = \frac{\upsilon}{C_p V} \sum w_i C_p(T_i - T) + q \qquad (7.1)$$

where the ith component of mass flow rate w_i is entering the node.

Similarly the dynamic continuity equation is implemented as follows:

$$\frac{dp}{dt} = \frac{B_m w_{nett}}{\rho V} + B_m \beta \frac{dT}{dt} \qquad (7.2)$$

It should be noted that equation (7.2) differs from that generally used in hydraulic applications, which usually does not include the temperature derivative term. This is important due to the change in coolant temperature over the working range, however, the overall change in pressure will be attenuated significantly by the compressible air volume in the deaerator header tank. There will also be some reduction in circuit pressure due to the compliance of the coolant hoses. It may be shown that the absence of the temperature derivative term would result in the change in circuit static pressure (non running coolant pump) being attenuated by approximately half its final value (the change in pressure being attributed solely to that of the air in the deaeration header tank).

The circuit static working pressure may be deduced quite simply by considering the coolant and the air in the system to expand within a constant volume. Considering the system initial conditions to be atmospheric pressure and temperature, the engine coolant achieves a normal working temperature at the engine outlet of approximately 90 °C. To all intents and purposes the change in circuit pressure will have little effect on the expansion of the coolant over the working temperature range (the system relief valve pressure is typically around 1 bar above atmospheric pressure depending on the design, and therefore the change in pressure will have little effect on the specific volume of the coolant). Therefore, the expansion of the coolant can

be attributed to the change in temperature alone for the purpose of this calculation. The change in coolant specific volume is 0.41 * $10^{-4} m^3.kg^{-1}$ for a temperature change between 20 and 90 °C, the data has been extracted from the PPDS software. Table 7.1 details the system parameters necessary to determine the overall change in circuit static pressure.

Table 7.1 Air and Coolant Data

Initial coolant volume (20 °C, 1 bara)	6.75 L
Initial air volume (20 °C, 1 bara)	1.5 L
Mass of coolant	7.11 kg
Mass of air	$1.8*10^{-3}$ kg
Change in coolant volume (20 - 90 °C)	$+ 2.91*10^{-1}$ L
Change in air volume (20 - 90 °C)	$- 2.91*10^{-1}$ L
Final air volume	1.209 L
Gas constant for air	287 $J.kg^{-1}.K^{-1}$
Final air density	1.489 $kg.m^{-3}$
Final air pressure based on equation of state $p = \rho RT$	1.55 bara

It may be seen from Table 7.1 that the predicted circuit static working pressure is 1.55 bara (bar absolute). The circuit working pressure (deaeration header tank air pressure) may also be predicted from the equation of state alone, assuming no expansion of the coolant (a consequence of neglecting the temperature derivative term in equation (7.2)) which gives a working pressure of 1.25 bara. It can be seen that inclusion of the temperature derivative term in equation (7.2) is a prerequisite for accurate system pressure prediction. This point has been overlooked by Tomlinson and Burrows[1994] because of an incomplete thermal hydraulic analysis of the system.

It should be noted that the circuit dynamic pressures (coolant pump running) will vary for

different parts of the circuit, depending on the pressure losses involved. The dynamic pressure should not be confused with the previously calculated static pressure, however, the magnitude of static pressure will be reflected in the dynamic pressures in the circuit.

7.3.2 Pump Component Model

This is a radial impeller rotodynamic pump model. The model uses pressure boundary conditions to determine the volumetric flow rate of the coolant pump. Experimental data has been used to formulate a non-dimensional head/flow characteristic based on rotodynamic machine theory so that only one function is required to determine the operating point. The non-dimensional flow coefficient is a function of head coefficient as follows:

$$\frac{Q}{N} = f\left(\frac{H}{N^2}\right) \tag{7.3}$$

Figure 7.3 shows experimental data for the coolant pump for three different speeds. The maximum flow rate obtainable is limited to approximately 2 $L.sec^{-1}$ at 4500 $rev.min^{-1}$. The limitation was due to the rig configuration for the test that imposed a particularly high restriction to flow, since all but one of the engine outlet paths were open. The non-dimensional pump characteristic is shown in Figure 7.4. To obtain a reasonable polynomial fit, both head and flow coefficients have been scaled appropriately. Hydraulic tests involving matching corresponding points (fixed system resistance) confirmed the suitability of this approach. Figure 7.4 illustrates both model and experimental data that required a 4th order polynomial function for flow coefficient in terms of head coefficient.

The pump shaft torque is represented simply as follows:

$$Tr = \frac{Q\,\Delta p}{\eta\, N} \tag{7.4}$$

where the pump overall efficiency is a user defined parameter.

The pump coolant outlet temperature is represented in steady state form and includes losses due to pump inefficiency, and a term (β, cubical expansivity) which accounts for the change in fluid enthalpy due to pressure. In practically all situations with vehicle cooling systems this term will have little effect on temperature because of the very small circuit pressure differences, however it is included for completeness. It is interesting to compare this aspect with hydraulic fluid power systems examined in Chapters 5 and 6. The vehicle coolant pump is subject to a maximum differential pressure of 2.5 bar for a zero flow condition at maximum speed. In contrast, the hydraulic pump examined previously was subjected to differential pressures exceeding 150 bar. At this pressure differential, the temperature difference across the hydraulic pump is in the order of 3 °C. Because pump pressure differential is proportional to the pump fluid temperature difference, it may be inferred that the coolant temperature difference either side of the vehicle coolant pump would be approximately two orders of magnitude smaller. This level of temperature difference is less than an order of magnitude smaller than the accuracy of the E-type thermocouples used to record circuit temperatures, and therefore could not be verified by experimentation.

The pump outlet temperature is based on conservation of energy and is represented in steady state form as follows:

$$T_o = T_i + \frac{\Delta p}{\rho C_p} \left(\frac{1}{\eta} + \beta T - 1 \right) \tag{7.5}$$

At the pump inlet the adjacent model, here a hose, will expect to receive a temperature due to its ability to cater for reverse flow conditions. This variable has been set up as a first order lag of the current inlet temperature supplied from the hose. As the pump is not set up for reverse flow computation, this variable has been introduced purely to satisfy the port linking procedure within Bath*fp*.

7.3.3 Thermostat Component Model

This model has been written to satisfy the requirements concerning the thermal hydraulic characteristics of the thermostat and bypass coolant paths. A cross section of the thermostat and associated flow paths are shown in Figure 7.5.There are several approaches that may be made to represent the thermostat and bypass in Bath*fp*. Previous developments by Tomlinson and Burrows[1994] have included a dynamic momentum equation for the thermostat plunger incorporating friction, wax and spring force to provide position. However these models are qualitative insofar that estimates of friction and wax force have not been substantiated experimentally and therefore can be subject to large errors. Estimation of the wax force used in the Tomlinson model is an empirical nonlinear expression that requires estimated coefficients (this function was acquired from the Robertshaw Controls Company) which can introduce errors. The aforementioned details can all lead to unrepresentative model transient and steady state conditions. Coupled with this is the estimation of the thermostat hydraulic characteristic which previously had no experimental verification. This is not the case for the current model which includes characteristics based on experimental data.

The thermostat model used for this whole circuit simulation has dispensed with the dynamic calculation for position and relies on experimental temperature/position characteristics, however, a dynamic model incorporating many nonlinear physical attributes, which is based on a rigorous theoretical approach is discussed in Section 7.6.

The current thermostat wax temperature is implemented using a first order lag of coolant temperature from which thermostat stem position is calculated. The model makes provision for hysteresis such that the position verses temperature may be offset between the heating and cooling cycle. This hysteresis effect is well known in wax pellet type thermostats and is thought to be caused by the phase change in the wax. The hysteresis effect has been implemented by

tracking the wax temperature during both heat and cooling phases. Should the wax reverse its temperature in either phase, the model will automatically revert to a dead zone region where the temperature used to determine position remains fixed. The normal heating and cooling phase regions are reached should the wax temperature traverse the temperature hysteresis dead zone. The mean position/temperature characteristics for the thermostat are shown in Figure 7.6. The data was supplied from the Ford Motor Company. This data has been changed at the higher temperature condition with respect to the maximum opening. Measurement of the thermostat stem and cage suggests that the maximum travel available is 11mm. This gives a maximum opening for a mean wax temperature of 107°C.

The thermostat hydraulic characteristics which comprise volumetric flow rate for a given differential pressure and position, have been supplied by Ford and are based on experimental data. Initial attempts at modelling this relationship with the standard orifice flow equation proved to be inaccurate over the range of thermostat positions. Although the flow/pressure relationship proved to be adequate, close correspondence could only be maintained for a limited range of positions. Therefore, the standard orifice flow equation was modified to give a nonlinear relationship between position and flow rate. The relationship used for the thermostat flow rate in terms of pressure and position is as follows:

$$Q = \sqrt{\Delta p \; (\; 2.22e4 \; - \; 1.437e4 \; x \; + \; 2.699e3 \; x^2)} \qquad (7.6)$$

The coefficients for the above function were determined using multiple regression analysis. The above relationship is used for $3mm \leq x \leq 9mm$. Above and below this positional range the flow is scaled linearly based on the function boundary values. The model fit is compared with experimental data in Figure 7.7. It can be seen that the model compares well in most areas except the small pressure differential regions (≤ 0.1 bar). Further improvement could be made in this region with a function of greater complexity, however the present function is thought to be

adequate for most of the range and is the relationship currently used by the thermostat model. The bypass hydraulic characteristic is implemented using a typical pressure - flow rate relationship:

$$Q = x_b \, Cr \sqrt{\Delta p} \tag{7.7}$$

where x_b represents the fractional bypass opening parameter dependent on the thermostat position. Measurement of the thermostat housing suggests that when the thermostat position reaches 6mm open, the bypass coolant flow path fully closes. This is the relationship used by the thermostat model. The loss coefficient Cr is a user defined parameter, and a default value has been deduced from experimentation (100 $L.min^{-1}.bar^{-0.5}$)when the thermostat is shut.

The hydraulic characteristics for both the thermostat and bypass coolant paths assume that the flow enters the inlet and passes to either the bypass or the bypass and thermostat providing it is open. In this respect a common upstream pressure is assumed for the thermostat housing which feeds both the radiator and bypass coolant flow paths. No intermediate calculations are made for the flow path between the bypass, and the thermostat outlet to the radiator.

The model although being capable of reverse flow computation, will produce inaccurate thermal effects in this condition. It is assumed for thermal effects that the flow is always from the engine outlet and to the bypass and radiator. Therefore the incoming coolant temperature is equated directly to the thermostat and bypass coolant outlet temperatures. Future developments will consider correct computation under reverse flow conditions.

Future development of the thermostat model should consider first a dynamic position calculation, and secondly a detailed wax temperature model based on the heat transfer

characteristics of the thermostat. Both these areas are considered in Section 7.6.

7.3.4 Radiator Component Model

This model is designed for generic application of the study of the radiator thermal hydraulic performance.The model hydraulic performance is based on pressure boundary conditions from which the flow rate is determined. The volumetric flow rate is calculated using the standard orifice flow - pressure relationship with the inclusion of gravitational head. Experimental data from both the rig at Bath and Ford supplied data was used to deduce the restriction coefficient for the model, see Figure 7.8. It can be seen that both sets of data correspond well where the test range overlaps. Additionally, the model features 'potential head' outputs to adjacent models (hoses) that allow for gravitational effects.

The thermal performance of the radiator can be examined in a number of ways ranging from complex polynomial expressions to the more basic Number of Transfer Units (NTU) method. Of these the NTU method was chosen due to its generality and easy of implementation. To predict the rate of heat transfer with this method, all that is required are the inlet fluid conditions and effectiveness. Radiator effectiveness has been deduced from data supplied from Ford at three test conditions (Table 7.2), and an average value is used for the default in the model parameter selection list.

The rate of heat transfer is calculated using the NTU method as follows:

$$q = \epsilon \, Cmin \, (T_{hot(i)} - T_{cold(i)}) \qquad (7.8)$$

From the data supplied the following table details the level of effectiveness for each condition, for a coolant flow rate of 1.2 $L.s^{-1}$.

Table 7.2 - Radiator Effectiveness

Inlet air temperature °C	Outlet air temperature °C	Air velocity m/s	Inlet coolant temperature °C	Outlet coolant temperature °C	Radiator effectiveness ϵ
2.13	28.96	5.17	57.46	50.18	0.485
1.82	20.87	10.2	58.17	49.09	0.338
2.37	17.22	15.21	57.8	46.05	0.268

The incoming air velocity is supplied by an adjoining model that accounts for vehicle speed and cooling fan operation. The model is capable of correct computation under coolant reverse flow conditions. A dynamic energy equation is used at both inlet and outlet ports. Under normal operating conditions the outlet temperature derivative is formulated as follows.

$$\frac{dT}{dt} = \frac{\upsilon}{C_p V} [\, w_i C_p(T_i - T) + q_h \,] \qquad (7.9)$$

where 'q_h' the rate of heat transfer is calculated from the previously defined NTU method. If the mass flow rate falls below 0.001 kg.sec^{-1} then the inlet and outlet radiator coolant temperatures follow the adjacent hose model boundary coolant temperatures. This provision has been made because of lack of information about heat transfer from the radiator under low coolant flow conditions.

7.3.5 Cabin Heater and Oil Cooler Component Models

These models are designed for generic application of the study of the cabin heater and oil cooler thermal and hydraulic performance.The modelling approach for the cabin heater is similar to that of the radiator with identical inlet and outlet port variables. As no heat transfer performance data has been gathered, the default effectiveness value for the radiator is used as the default for the heater ($\epsilon = 0.4$).Figure 7.9 shows the heater hydraulic performance for a range of coolant temperatures. This suggests that the hydraulic performance is to some degree viscosity

dependent and future development of this model should include this effect. Another component in the heater coolant flow path is the oil cooler. The oil cooler hydraulic performance is shown in Figure 7.10. It can be seen that the hydraulic performance is again viscosity dependent. The oil cooler model is represented as a resistance only, however, for detailed studies it would be prudent to include the heat transfer from the sump oil.

7.3.6 Pressurised Deaerating Header Tank Component Model

This model performs the deaeration of the coolant by taking a small bleed flow from the main coolant circuit. The model is an extension to that detailed by Tomlinson and Burrows[1994] but has been enhanced to include more detailed physical phenomena. Additionally, the model features 'potential head' outputs to adjacent models (hoses) to allow for gravitational effects. Heat transfer from the tank walls is also included. The inlet pressure (air void) is determined from the equation of state as follows:

$$PV_a = M_a R T \tag{7.10}$$

Therefore the inlet pressure can be represented as:

$$\frac{dp_i}{dt} = \frac{M_a R}{V_a}\frac{dT}{dt} - \frac{M_a R T}{V_a^2}\frac{dV_a}{dt} \tag{7.11}$$

This assumes that the mass of air remains constant during a transient calculation. The height of the coolant in the tank is determined dynamically. If one considers first the tank coolant volume to be a function of mass and density:

$$V_c = \frac{M_c}{\rho_c} \tag{7.12}$$

Therefore the coolant volume derivative becomes:

$$\frac{dV_c}{dt} = \frac{1}{\rho_c}\frac{dM_c}{dt} - \frac{M_c}{\rho_c^2}\frac{d\rho_c}{dt} \tag{7.13}$$

Since the pressure variation is small the coolant density can be equated to a function of temperature only and therefore:

$$\frac{d\rho_c}{dt} = \frac{d\rho_c}{dT}\frac{dT}{dt} \tag{7.14}$$

The rate of change of density with respect to temperature is proportional to the coefficient of cubical expansion so equation (7.14) may be represented as follows:

$$\frac{d\rho_c}{dt} = -\rho_c \beta \frac{dT}{dt} \tag{7.15}$$

Because the coolant height is directly related to the coolant volume and cross sectional area (A) of the tank, the coolant height derivative may be formulated as follows, using equations (7.13) and (7.15):

$$\frac{dh}{dt} = \frac{Q_i - Q_o}{A} + \beta h \frac{dT}{dt} \tag{7.16}$$

The air volume derivative then becomes:

$$\frac{dV_a}{dt} = -A\frac{dh}{dt} \tag{7.17}$$

The outlet pressure is formulated as a state variable, the derivative is represented as follows:

$$\frac{dp}{dt} = \rho g \frac{dh}{dt} + \frac{dp_i}{dt} \tag{7.18}$$

Provision has been made for the inlet pressure to be confined to the cap relief valve pressure (default set at 1.4 barg (bar gauge)). Should this condition arise, correct computation will only

resume providing the nett flow rate into the tank becomes negative.

7.3.7 Three Port Flow Junction Component Model

This model represents a constant volume thermal hydraulic junction with three ports. It has been created effectively to link hose models together at specific junctions in the cooling circuit; for example the header tank outlet to the main coolant and the engine deaeration lines to the header tank inlet. The structure of the model is such that each port is represented as a friction orifice and a central node that represents junction coolant pressure and temperature dynamically.

Port flow rates are determined with knowledge of the pressure boundary conditions, the central node pressure and the port restriction coefficients. The port restriction coefficients are dimensionless user supplied data items. The losses at each port are expressed as follows:

$$h_f = k_r \frac{u^2}{2g} \tag{7.19}$$

where k_r is the port restriction coefficient.

From equation (7.19) the coolant velocity and therefore mass flow rate of each port can be determined. The true nature of the losses due to friction and separation will primarily be due to the motion of the coolant as it changes its flow path direction at the central node.

Both the continuity and energy equations are solved dynamically at the junction central node and provision is made for cavitation/air release effects by suitably adjusting the coolant bulk modulus to reflect this condition. The dynamic energy equation is represented in terms of temperature and considers the three port flows as follows:

$$\frac{dT}{dt} = \frac{\upsilon}{C_p V} \sum_1^3 w_i C_p (T_i - T) \tag{7.20}$$

Where 'i' represents the individual contribution from each port providing the flow is entering the central node. Heat transfer is assumed to be negligible from the junction model and is not included. Incoming and exit coolant temperatures are modified to maintain the isenthalpic condition across each port restriction, however because of the small pressure losses this effect could be ignored and is only included for completeness. In this respect the junction model is generally applicable to situations covering a wide range of flow rates and pressures.

The central node continuity equation is typically represented as follows:

$$\frac{dp}{dt} = \frac{B_m \, w_{nett}}{\rho V_n} + B_m \beta \frac{dT}{dt} \qquad (7.21)$$

The model is capable of reverse flow computation for thermal hydraulic effects in all flow paths. Additionally, the model outputs a value for potential head in relation to a datum height (thermostat outlet) to account for gravitational effects determined in the hose models.

7.4 HOSE MODEL DESCRIPTION

Chapter 5 described the development of a hydraulic pipe model that was used as the starting point for the hose models detailed in this section. The modelling has been extended to a considerable extent so that satisfactory thermal hydraulic simulations are possible. Including thermal effects may be accomplished in a number of ways regarding the physical representation of energy accumulation and heat transfer within a hose. Associated with the change in coolant temperature is the variation in coolant thermodynamic and transport properties that have been made available for both pure water and a 50/50 mix of water and ethylene glycol. This has caused a number of numerical problems particularly for the calculation of hose friction that essentially produces very long execution times, however, an effective solution has been

developed and is described later in Section 7.5. During the model development phase, a variety of hose formulations were tested in an attempt to improve simulation times or resolve numerical difficulties. These are detailed in the following model descriptions. All the variations of hose models take account of gravitational effects and receive boundary height values from adjacent component models.

All the hose models use both the dynamic energy and continuity equations derived in Chapter 2. In general terms these may be stated as follows:

$$\frac{dp}{dt} = \frac{B_m(w_i - w)}{\rho V} + B_m \beta \frac{dT}{dt} \tag{7.22}$$

$$\frac{dT}{dt} = \frac{v}{Cp\ V}\left[w_i[(v - \beta T v)(p_i - p) + Cp(T_i - T)] + q_h - W_s \right] + \frac{v\beta T}{Cp}\frac{dp}{dt} \tag{7.23}$$

Although the other component model formulations usually require at least one of these conservation equations with suitable assumptions applied, it is relevant at this point to expand on the origin and assumptions used when dealing with the hose models since they require both conservation equations.

The assumptions are that the hose volume remains constant and no work is done on or by the fluid. Therefore only heat transfer to or from the surroundings and the thermodynamic conditions of the fluid at entry to the hose are responsible for changing the coolant temperature. Equations (7.22) and (7.23) are generally required to be solved simultaneously at any particular time step. The implicit relationship may be removed by substitution that yields a modified coolant temperature derivative. In this instance however both equations are assumed to be decoupled, if one considers the pressure derivative term in equation (7.23) to be insignificant to the physical dynamics of the vehicle cooling system. Modification to the temperature

derivative has been made to overcome duplication of pressure at the connecting ports (a measure required with the hydraulic pipe models). This has arisen because the difference in fluid enthalpy is represented as a function of both pressure and temperature difference between adjacent models and the hose model. Therefore to solve the energy equation (7.23) it is necessary to pass both pressure and temperature between adjacent component and hose models. This is clearly an unwanted feature. For example, a hose receiving both flow rate and coolant temperature from a component does not require inlet pressure as this is already a boundary condition calculated by the hose. Therefore, the difference in coolant enthalpy between component and hose can be entirely represented by temperature alone. This analogy can be extended to the case for hose models that solve the momentum equation if the outlet coolant temperature from the hose is suitably modified to account for the isenthalpic temperature rise due to frictional losses. As previously mentioned in the description of other component models, the pressure differences within vehicle cooling systems has an almost negligible effect on enthalpy and therefore temperature, however, it is included for completeness.

The above assumptions have been used for both conservation equations within the hose models that are represented as follows:

$$\frac{dp}{dt} = \frac{B_m \, w_{nett}}{\rho V} + B_m \beta \frac{dT}{dt} \tag{7.24}$$

$$\frac{dT}{dt} = \frac{\upsilon}{C_p \, V} \left[w_i \, C_p (T_i - T) + q_h \right] \tag{7.25}$$

The modified exit temperature leaving the hose, accounting for the isenthalpic temperature rise due to frictional losses is:

$$T_{exit} = T + \frac{(v - \beta T v)(p - p_{exit})}{Cp} \qquad (7.26)$$

Similarly, under reverse flow conditions, The incoming temperature from an adjacent model is modified to reflect the isenthalpic temperature rise across the resistive element of the hose model.

All hoses incorporate heat transfer to or from the surroundings due to convection and radiation from the hose material surface. The hose wall is considered to be at a uniform temperature which allows heat transfer calculations from both the coolant to the inner hose wall and from the outer hose wall to the surroundings. A lumped hose wall temperature does imply that the wall thickness is small compared to the diameter, which is not necessarily the case for all coolant hoses. In cases where the wall thickness is significant compared to the diameter the error incurred should be compared with the overall level of heat transfer from the circuit.

The heat transfer between the coolant and the hose wall is based on convective heat transfer relationships. The model checks whether the flow is laminar or turbulent and suitably adjusts the heat transfer coefficient. The heat transfer coefficient is calculated using the Nusselt number. For laminar flow a precise solution exists for the Nusselt number in pipes (Nus = 3.65). For turbulent flow, an empirical relationship has been used, which is based on Reynold's and Prandtl number, Eastop and McConkey[1978]:

$$Nus = 0.243\ Re^{0.8}\ Pr^{0.4} \qquad (7.27)$$

In practice the Nusselt number is smoothed in the region $Re_{crit} < Re < 1.5Re_{crit}$ to avoid the sudden discontinuity at the Re_{crit} condition.

The heat transfer coefficient is deduced from:

$$h_{fw} = \frac{Nus\ k}{d} \tag{7.28}$$

The calculation of heat transfer from the hose wall to the surroundings includes natural convection and radiation components. The heat transfer coefficient is based on the representation found in Rogers and Meyhew[1980c]:

$$h_{ws} = 1.32\ [\ \frac{\theta_{ws}}{d}\ ]^{0.25} \tag{7.29}$$

The rate of heat transfer between coolant and hose becomes:

$$q_{fw} = h_{fw}\ A_i\ \theta_{fw} \tag{7.30}$$

And the rate of heat transfer between the hose wall and the surroundings becomes:

$$q_{ws} = h_{ws}\ A_o\ \theta_{ws} + \sigma \in A_o\ [T_m^4 - T_s^4] \tag{7.31}$$

The rate of change of hose material temperature can be calculated with knowledge of the hose material specific heat capacity as follows:

$$\frac{dT_m}{dt} = \frac{q_{fw} - q_{ws}}{M\ Cp} \tag{7.32}$$

A common feature with all hose models is the restriction to two ports, i.e. one exit and one entry port. This is a departure from the pipe model developed in Chapter 5 where ports that solve the continuity equation in general can have multiple source input flow rates. This has arisen due to the convention for satisfying the momentum equation with gravitational effects. The convention adopted requires all component models to supply height to adjacent models (usually hoses). The restrictions are such that each hose model must have a component model at each of its two ports. This eliminates any confusion caused by associating a gravitational head to each hose directly and therefore introducing the possibility of an incorrect sign into the calculations.

The following subsections detail each specific hose model and their accompanying assumptions in addition to the modelling details that are common to all hoses given in Section 7.4.

7.4.1 Hose Model A

This model uses steady state momentum. Flow rate is determined for a given inlet and exit pressure using incompressible flow theory and includes friction, gravitational head and additional losses if required. Friction is represented by Darcy's equation, with a turbulent friction factor model based on the Haaland[1983] formulation, which is a function of Re and relative roughness. The laminar flow region is also represented. The procedure for calculating Re_{crit} and coolant velocity was originally similar to that described by Richards[1993b] with the exception of a different turbulent friction factor model for calculating flow velocity and the inclusion of gravitational effects. Numerical difficulties arose however using this technique. One problem was found to occur at the discontinuity point between laminar and turbulent transition, and was also compounded by low coolant viscosities (high temperatures). For this reason a fixed Re_{crit} has been used ($Re_{crit} = 5000$) which allows the computation to overcome the discontinuity at the laminar - turbulent transition. Because of the implicit relationships between flow velocity, Re and friction factor in the turbulent flow region, an algebraic loop solver is used to determine friction factor, and this is described by Richards[1993b].

The Haaland turbulent friction factor model is represented as follows:

$$\frac{1}{\sqrt{4f}} = -1.8\log_{10}\left(\frac{6.9}{Re} + \left(\frac{rr}{3.7}\right)^{1.11}\right) \qquad (7.33)$$

The critical Reynolds number would normally be calculated by equating the relationship for friction factor assuming a laminar flow condition to the Haaland friction formula. The resulting function that follows is solved by the Newton - Raphson method:

$$\sqrt{Re_{crit}} + 14.4\log_{10}\left(\frac{6.9}{\sqrt{Re_{crit}}} + \left(\frac{rr}{3.7}\right)^{1.11}\right) = 0 \tag{7.34}$$

For this hose model however Re_{crit} is set to 5000 to overcome computation difficulties, as mentioned above.

The laminar flow velocity becomes:

$$u = \frac{d^2}{32\ \mu\ l}\ (\Delta p + \rho\ g\ \Delta z) \tag{7.35}$$

The laminar flow velocity with additional losses due to fittings becomes:

$$u = -\frac{32\ \upsilon_{kin}\ l}{1000\ k_f\ d^2} + \sqrt{\left(\frac{32\ \upsilon_{kin}\ l}{1000\ k_f\ d^2}\right)^2 + \frac{2}{k_f}\left(g\Delta z + \frac{\Delta p}{\rho}\right)} \tag{7.36}$$

The turbulent flow velocity becomes:

$$u = \sqrt{\frac{\rho\ g\ \Delta z + \Delta p}{\frac{2\ f\ \rho\ l}{d} + \frac{k_f\ \rho}{2}}} \tag{7.37}$$

Throughout the development of this hose model, it became clear that the performance would be unacceptable in terms of very long execution times with the current integration techniques and the algebraic loop solution for friction factor available. The execution time also increased significantly at elevated coolant temperatures. Because of the numerical difficulties associated with the friction factor calculation (algebraic loop solution dependent on iteration), it was decided to pursue investigations further in this area. This work led to the development of two further hose models described below.

7.4.2 Hose Model B

To improve the simulation execution times an explicit expression for friction factor for fully established turbulent flow based on the formulation by Nikuradse, see Douglas *et al.*[1981]. The friction factor is a function of hose wall relative roughness only. A laminar flow region is not included. This model will give accurate flow rate predictions for fully established turbulent flow conditions, but the consequence of using a constant friction factor will clearly affect the prediction at low Re.

The fully developed turbulent flow friction factor by Nikuradse is represented as follows:

$$\frac{1}{\sqrt{f}} = 4 \log \left(\frac{1}{rr}\right) + 2.28 \qquad (7.38)$$

The flow velocity is calculated using equation (7.37).

While hose model B gave quite acceptable executions times (up too three times as fast when compared with hose model A, depending on the transient of concern), the accuracy falls below a Re of 10^6 (fully developed turbulent flow exists when $Re > 10^6$) which corresponds to a hose wall relative roughness of 10^{-4}. Since all hose coolant flow rates tended to exist in the transition region between laminar and fully established turbulent flow ($Re < 10^6$), then hose model B would consistently under estimate the pressure loss due to friction. This point is not as onerous as it first suggests since the components in the circuit contribute much larger pressure losses than the hoses. It can be concluded that there will be little loss in accuracy for the circuit flow rate predictions when using hose model B. The thermal hydraulic performance of hose models A and B are discussed in greater detail in Chapter 8.

To overcome the numerical difficulties presented by hose model A, and the inaccuracies introduced with hose model B, a different approach to the solution of the hose hydraulic

performance was considered. This is discussed in the following subsection.

7.4.3 Hose Model C

Flow rate is determined for a given inlet and exit pressure and includes friction, gravitational head and additional losses if required. Friction is accounted for using Darcy's equation, with a turbulent friction factor model based on the Haaland formulation, which is an identical approach to that used for hose model A. The model is capable of computation under laminar flow conditions. The significant difference is the use of a dynamic momentum solution to determine flow rate.

The use of the Haaland friction model coupled with the dynamic momentum solution removes the implicit relationships between friction and flow rate, and therefore removes the need for an algebraic loop solver to resolve the computation (which is required by hose model A). Unfortunately, this model did increase computation times compared with either of the steady state momentum hose models (A or B). However if computation time is not an issue, then this model will give precise flow rate calculations in all regions and at elevated coolant temperatures.

The dynamic momentum equation in terms of volumetric flow rate becomes:

$$\frac{dQ}{dt} = \frac{(A\ \Delta p - Fw + A\ \rho\ g\ \Delta z)}{\rho l} \tag{7.39}$$

Equation (7.39) consists of the forces due to pressure, gravitation and viscous friction. The viscous friction term Fw accounts for both laminar and turbulent flow conditions and includes a term for additional losses if required.

Both the energy and continuity equations are solved at the inlet port in an identical way to that of hose models A and B. Heat transfer is also represented. Re_{crit} is computed correctly using

equation (7.34).

7.5 COOLANT THERMODYNAMIC AND TRANSPORT PROPERTIES

During both component and hose model development there existed the requirement to incorporate variation in coolant properties. Variation in coolant properties can affect the hydraulic characteristics significantly. This is primarily due to the large variation in coolant viscosity caused by the change in operating temperature of the cooling system over the working range. If one considers extreme coolant temperatures in the range -35 to 120°C then the corresponding coolant viscosity assuming a 50/50 water/ethylene glycol mixture would be 70 to 0.5 Centipoise. This variation exceeds two orders of magnitude and will clearly affect pressure loss in the system. In general the coolant properties are affected by the variation in temperature to a much greater degree than pressure. Additionally, the circuit pressures are contained within a small range and therefore the coolant property information has been extracted at the 2 bar gauge pressure conditions. There also existed the need to represent both water and water/ethylene glycol mixtures during the experimental/development work and this has been implemented.

The coolant properties implemented and set up as functions of temperature, are: specific volume, specific heat capacity, bulk modulus, coefficient of cubical expansion, dynamic viscosity and thermal conductivity. These data have been extracted from Union Carbide and PPDS.The data is set up in subroutines using corresponding data pairs and linear interpolation is used for intermediate positions.

In Section 7.4, problems associated with the computation of friction factor were discussed in relation to the hydraulic performance of hose models. Alternative formulations were considered which resulted in three alternative hose models being developed. The development of different

hose models have all resulted as a consequence of the difficulties encountered with the method of friction factor calculation. It should be noted however that this is a tried and tested approach when using hydraulic oils. The conclusions drawn from this are as follows:

There are two fundamental differences between hydraulic fluids and vehicle coolants that could have influenced the efficiency of computation for the current circuit. First, the viscosity of the vehicle coolant is more than one order of magnitude smaller compared with hydraulic oil. Secondly, the variation of vehicle coolant viscosity over the working range is generally larger, due in part to the large variation in temperature.

To assist the computation within the hose models, two different methods of coolant property update were implemented as follows:

(a) At each converged integration step.

(b) At a user defined coolant temperature change.

Of the above two methods, (b) will generally allow the simulation to run at a significantly faster rate when using hose model A, and in the limit lets the user hold the coolant properties constant if so desired. It should be noted however that updating the coolant properties using a discrete approach such as (b) will produce small step changes in the hydraulic characteristic of the hoses (and any other component model who's hydraulic characteristic is a function of viscosity) which will be evident when inspecting the transient response. This effect can be attenuated by selecting a smaller temperature change before property update is performed, at the cost of increasing the execution time. The effects of using method (b) to update coolant properties are not considered detrimental to the quantitative prediction of the overall transient response of the system, and is

the method most suitable for use with hose model A.

The use of either method (a) or (b) to update the coolant properties will significantly increase the speed of computation. It should be noted that the alternative, which is normally used, is to allow the coolant properties to vary continuously between each integration step.

7.6 PROPOSED THERMOSTAT MODEL DEVELOPMENT

Attempts at modelling wax pellet thermostats have in the main been accomplished by describing the physical behaviour empirically. This may be seen in the work of Tomlinson & Burrows [1993], Chiang & Keller [1990] and Nelson & Robichaux [1997]. Nelson's empirical model is essential pseudo linear in form. The model is a second order transfer function with hysteresis and a nonlinear gain function. Nelson has adopted this approach on the basis that an analytical model would be difficult to generate because of unknowns such as the properties of the wax, the complexities of establishing the friction coefficients and hysteresis, and representing the phase change in the wax. However with a well considered methodical approach, these problems can be overcome.

Tomlinson & Burrows [1993] went part way to describing an analytical model insofar that they have considered the physical processes of heat transfer to the wax, the thermal inertia of the wax, and have introduced a dynamic momentum equation to provide for stem position. However, the relationship between the generated wax force and wax temperature is still empirical.

The development of an analytical model is possible, although, there are some unknowns such as wax properties, which will need to be resolved in due course. In the development of a proposed thermostat model, it has been assumed that the wax is a homogeneous liquid and that the expansion of the wax is conducted in this single phase. This implies that there is no phase

change in the wax for the proposed model, when above the initial melt point temperature.There is some ambiguity in this assumption on the basis that other researchers have referred to the wax expansion as a continuous phase change in the wax. It is possible that if this were the case, then the wax could be a colloid of substances with individual phase changes at different temperatures. It is known that the wax is a mixture of substances and expermentation is required to deduce its behaviour.

As a precursor to developing a theoretical model for a wax pellet thermostat the following assumptions are stated. The wax is a homogeneous liquid after it has melted, and its liquid state may be considered to behave as follows:

1 the state will change only by the influence of heat or mechanical work

2 two-independent properties are sufficient to define the state of the wax

3 No chemical reactions are taking place.

To derive a theoretical model of the thermostat it is convenient to consider the wax operating as an internally reversible process. Consider the entropy of the wax expressed as a function of both temperature and pressure:

$$ds = \frac{\partial s}{\partial T}\Big|_p dT + \frac{\partial s}{\partial P}\Big|_T dp \qquad (7.40)$$

The partial properties of equation (7.40) can be represented as follows:

$$\frac{\partial s}{\partial T}\Big|_p = \frac{Cp}{T}, \quad \frac{\partial s}{\partial P}\Big|_T = -\beta\upsilon \qquad (7.41)$$

If the relationships in equation (7.41) are substituted into equation (7.40), noting that:

$$T.ds = \frac{dQ}{M} \qquad (7.42)$$

where Q is the total heat transferred, then the rate of change of wax temperature may be

expressed as:

$$\frac{T_w}{dt} = \frac{q}{M\ Cp} + \frac{\upsilon\beta T_w}{Cp}\frac{dp}{dt} \tag{7.43}$$

where q is the rate of heat transfer into the wax.

Considering pressure as an independent property is useful, as it is needed to define the force generated by the wax on the thermostat stem. Because pressure is a property of the wax, we may consider it a function of two other independent properties. The previously defined wax temperature is available. The wax density is also known because it is a linear function of stem position (the wax mass being constant). Therefore if wax pressure is defined as a function of temperature and density in differential form, this gives:

$$\frac{dp_w}{dt} = \frac{\partial p_w}{\partial \rho_w}\Big|_T \frac{d\rho_w}{dt} + \frac{\partial P_w}{\partial T_w}\Big|_\rho \frac{dT_w}{dt} \tag{7.44}$$

Because the wax mass is constant, the rate of change of wax density may be represented as:

$$\frac{d\rho_w}{dt} = -\frac{M}{V^2}\frac{dV}{dt} \tag{7.45}$$

It has been shown that the partial property $\partial p/\partial T\,|_\rho$ equates to Bm.β, Sidders *et al.*[1996]. The isothermal bulk modulus is defined as $Bm = \rho\ \partial p/\partial \rho\,|_T$. Using these relationships and equation (7.45), then the rate of change of wax pressure may be expressed as:

$$\frac{dp_w}{dt} = Bm\ (\beta\frac{dT_w}{dt} - \frac{1}{V}\frac{dV}{dt}) \tag{7.46}$$

The rate of change of wax volume may be determined from the dynamic momentum equation, using a similar expression to that of Tomlinson and Burrows [1993]. Tomlinson considers the sum of the forces on the thermostat stem as follows:

$$M_s \frac{d^2x}{dt^2} = \sum F \tag{7.47}$$

where x is the stem position.

The summation of forces should include the following influences: wax, coolant pressure drop, stiction, coulomb friction (probably responsible for the hysteresis effect), viscous friction and spring force.

It is convenient to represent the wax volume as a state variable. It is related to the stem position as follows:

$$\frac{dV}{dt} = \frac{\Pi d_s^2}{4} \frac{dx}{dt} \tag{7.48}$$

where d_s is the stem diameter.

The wax is contained in a cylindrical brass sleeve. The geometry of the sleeve (thin wall section of 1.5mm) suggests that it could by modelled as one element in lumped parameter form. The validity of this may be tested with respect to the value for Biot number, which is a measure of the resistance to heat flow inside the solid to that of an adjacent fluid. If the Biot number is small, typically less than 0.1, then the surface convection resistance is large compared with the solid conduction resistance. It can then be deduced that the temperature distribution within the solid is reasonably uniform and suitable for modelling in lumped parameter form.

The Biot number is defined as:

$$Bi = \frac{htc\ vol}{K\ area} \tag{7.49}$$

Taking the thermal conductivity of brass to be 70 $W.m^{-1}.K^{-1}$, the limiting heat transfer coefficient

can be deduced, assuming the limiting Biot number = 0.1.

Volume of sleeve = $2.\Pi rm.\Delta r.\Delta z$

area = $4\ \Pi.rm.\Delta z$

where rm = 7 mm mean radius, Δr = 1.5mm wall thickness, Δz = 18mm length

The above data provides a limiting htc of 9.3 $KW.m^{-2}.K^{-1}$.If the htc were larger than this, then having a uniform wall temperature would not be appropriate. It is very unlikely that the external htc would get to the limiting value since 10 $KW.m^{-2}.K^{-1}$ is the upper limit for liquids under forced convection conditions. It is suspected that the coolant flow pattern across the sleeve to range from being cross flow (thermostat closed) to near axial flow (bypass closed), depending on the thermostat stem position. Some useful Nusselt number and therefore htc relationships for both the external htc (forced convection, coolant to sleeve), and internal htc (free convection, sleeve to wax) may be found in Holman[1992b] and could be used in the first instance.

The lumped parameter sleeve material temperature can be represented as:

$$\frac{dT_{sl}}{dt} = \frac{\sum q}{M_{sl}\, Cp_{sl}} \tag{7.50}$$

To remove the implicit relationship between wax temperature and pressure, substitute equation (7.46) into (7.43). This gives a wax temperature derivative as follows:

$$\frac{dT_w}{dt} = \frac{\frac{q}{M} - \frac{\upsilon\, \beta\, Bm\, T_w}{V}\frac{dV}{dt}}{Cp - \upsilon\, \beta^2\, Bm\, T_w} \tag{7.51}$$

One difficulty as Nelson[1997] has pointed out is the estimation of the thermodynamic

properties of the wax such as bulk modulus (Bm), coefficient of cubical expansion (β), and the specific heat at constant pressure. What is required is a set of experiments to establish the partial properties. This would require the design of a receptacle for the wax such that it could be subject to varying pressures and temperatures, with the provision for determining the change in volume. Ideally, a characteristic equation (see Rogers & Meyhew[1980d]) could then be determined, which would be of the form:

$$\frac{p_w}{\rho_w} = a + b\rho_w + c\rho_w^2 + d\rho_w^3 \ldots \qquad (7.52)$$

where the coefficients are functions of temperature. It would be possible to deduce both the coefficient of cubical expansion and the bulk modulus of the wax from equation (7.52). More advanced experimentation would be needed however to determine the specific heat capacity of the wax.

7.7 CLOSURE

A suite of vehicle cooling system models have been developed which have been compared with experimental rig data. A variety of techniques have been established to determine hose friction with low viscosity coolants, primarily because of convergence difficulties with the current algebraic loop solution. It is the author's opinion that because the vehicle cooling circuit configuration remains fixed, the computation of circuit pressures and flow rates should be examined by iteration alone at each integration time step, leaving the deaeration header tank air pressure as a state variable. This would not affect the dynamic response of the circuit as the header tank air pressure dominates the pressure transient response. This would have the benefit of reducing the number of state variables, which could lead to improvements in computation time. It would also be a useful test for the interaction between the algebraic loop friction factor calculation and the coolant pressure. If the coolant pressure nodes are algebraic instead of state

variables, then any potential instabilities caused by the circuit pressure states would be removed.

A library of coolant thermodynamic and transport properties has been established for water, and water / ethylene glycol coolant concentrations. These may be used to assess the sensitivity of different coolant concentrations on circuit performance.

A proposed thermostat model has been discussed in Section 7.6, based on rigorous theoretical techniques. Future developments of the vehicle cooling circuit should consider implementation of this model.

Future developments should also include the viscosity dependence on the hydraulic performance of components to a greater degree. Detailed testing of the coolant pump such that torque and hence efficiency can be assessed is seen as a prerequisite for future work.

Chapter 8 discusses the steady state and transient response of the vehicle cooling circuit model when subject to a number of forcing functions, including comparison with rig data. The sensitivity of the steady state momentum hose models is assessed and a simulated drive cycle involving component change is examined to show the flexibility of the model from a design perspective.

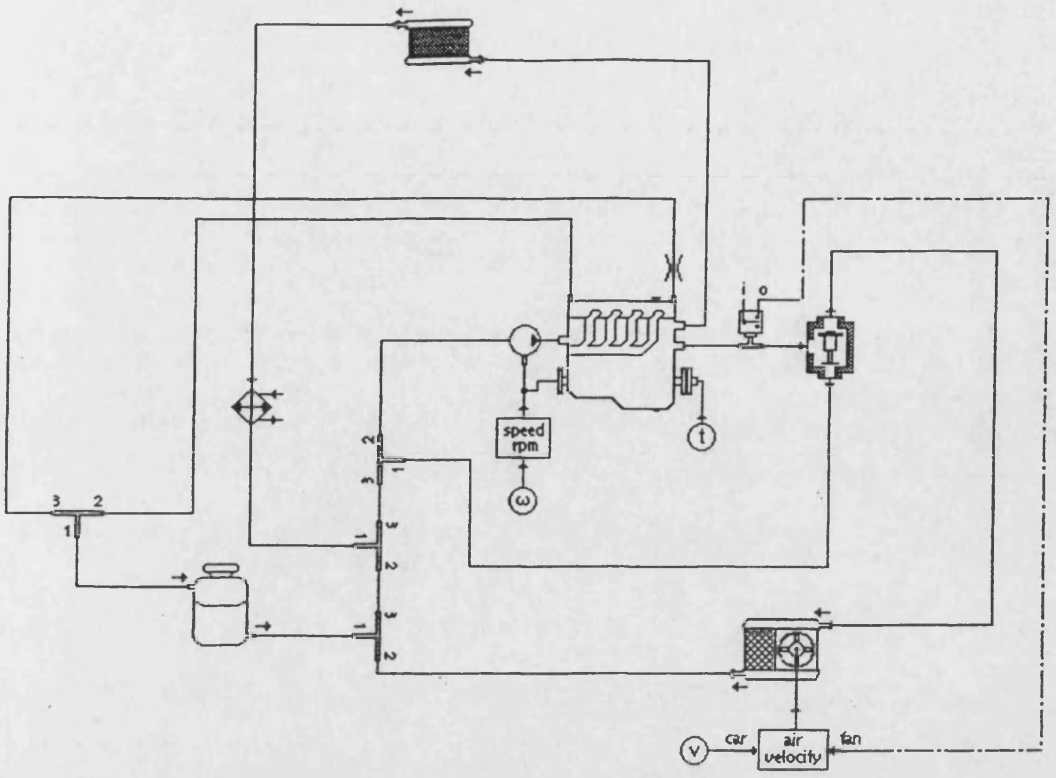

Vehicle Cooling System FIGURE 7.1

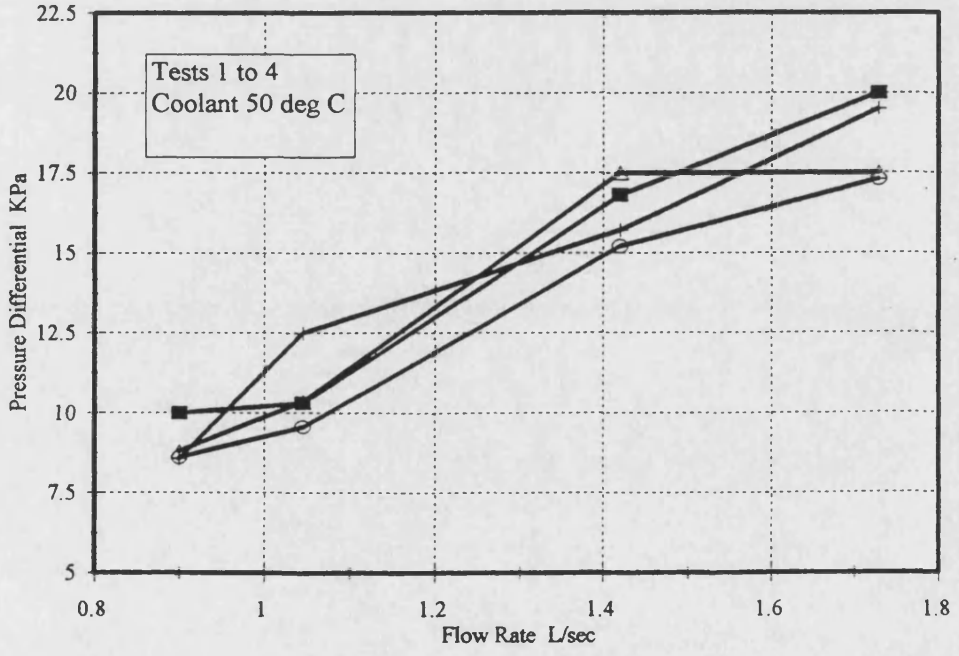

Engine Core Hydraulic Characteristic FIGURE 7.2

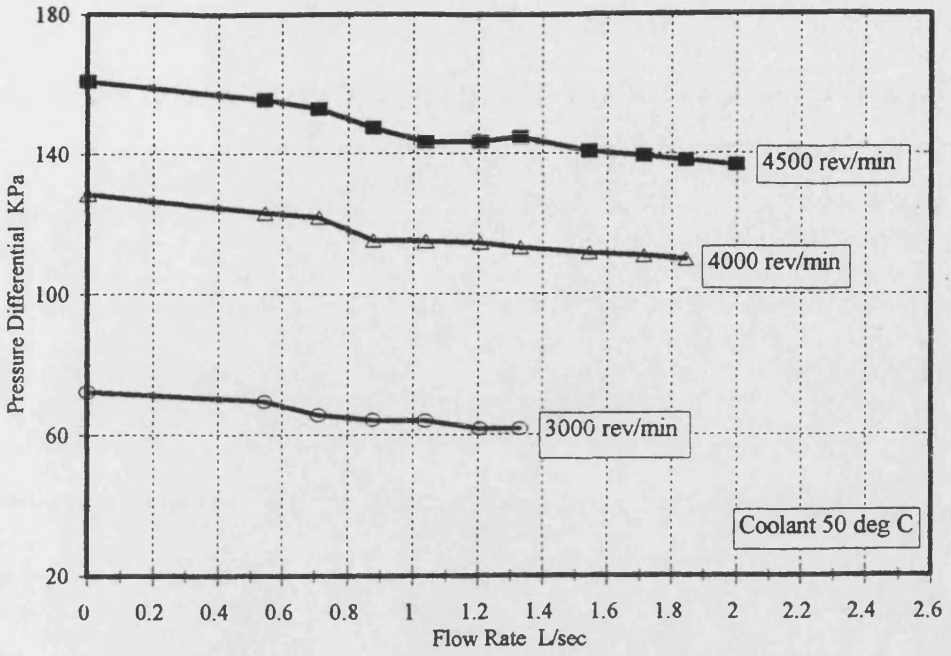

Coolant Pump Hydraulic Characteristic FIGURE 7.3

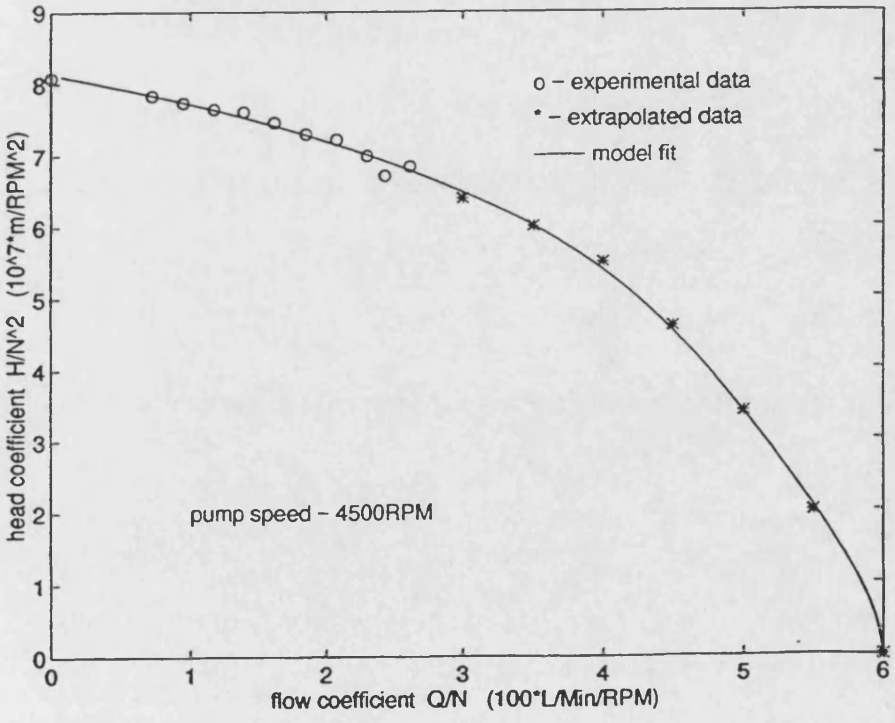

Non-Dimensional Pump Characteristic FIGURE 7.4

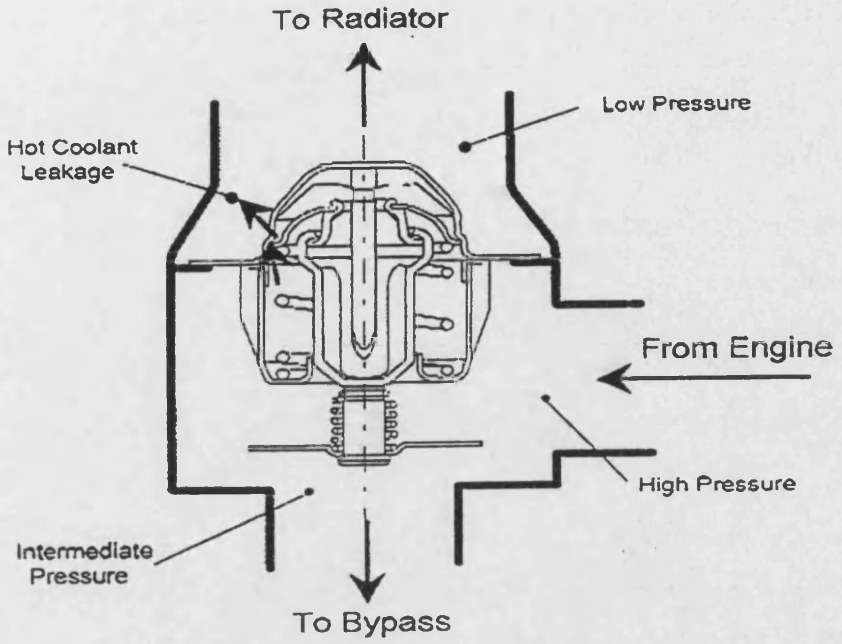

Wax Pellet Thermostat and Flow Paths FIGURE 7.5

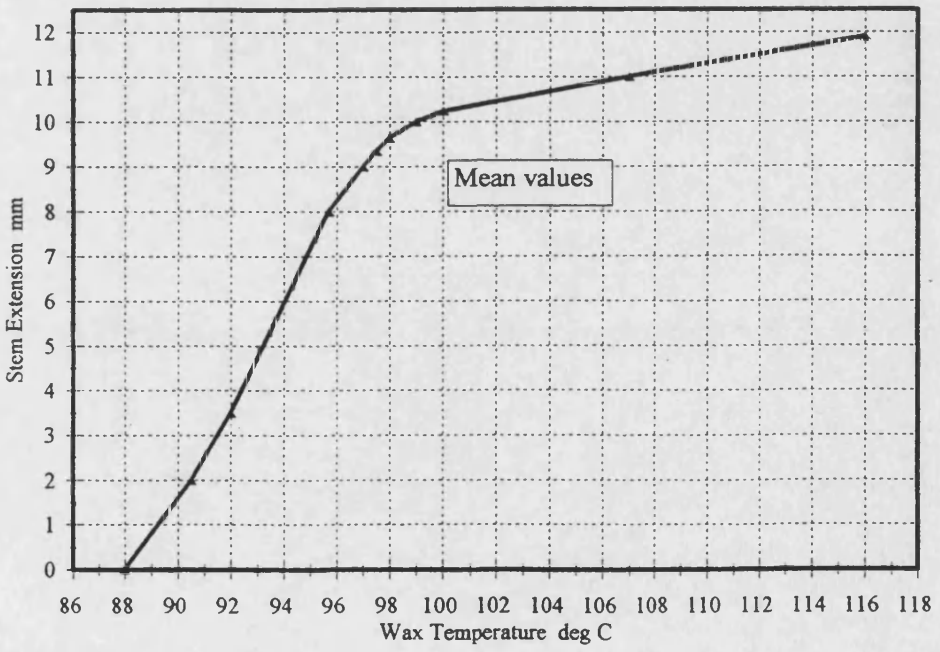

Thermostat Pos - Temp Characteristic FIGURE 7.6

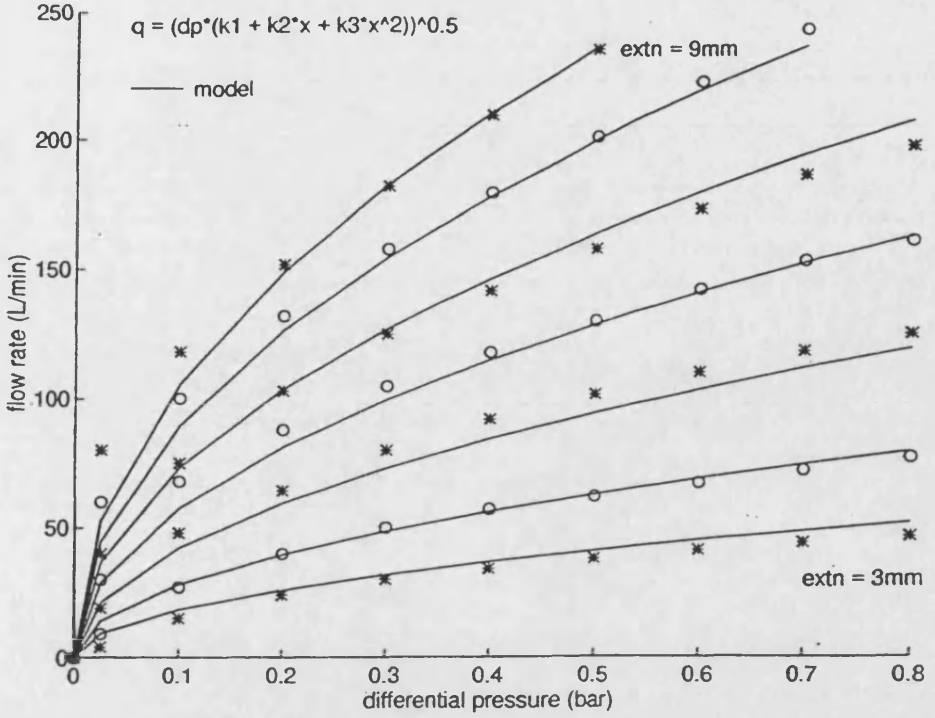

Wax Pellet Thermostat Hydraulic Characteristic FIGURE 7.7

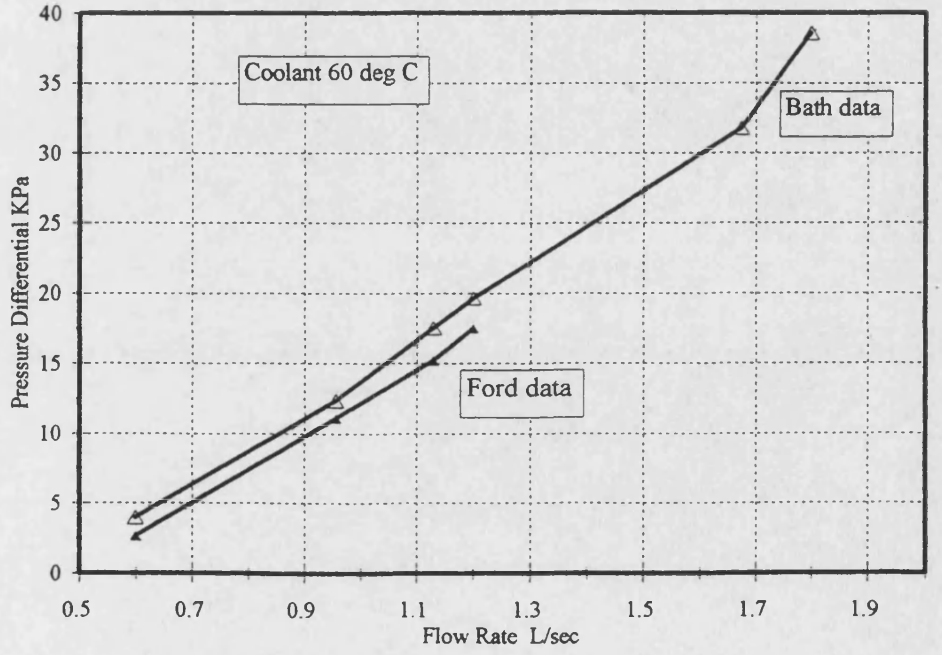

Radiator Hydraulic Characteristic FIGURE 7.8

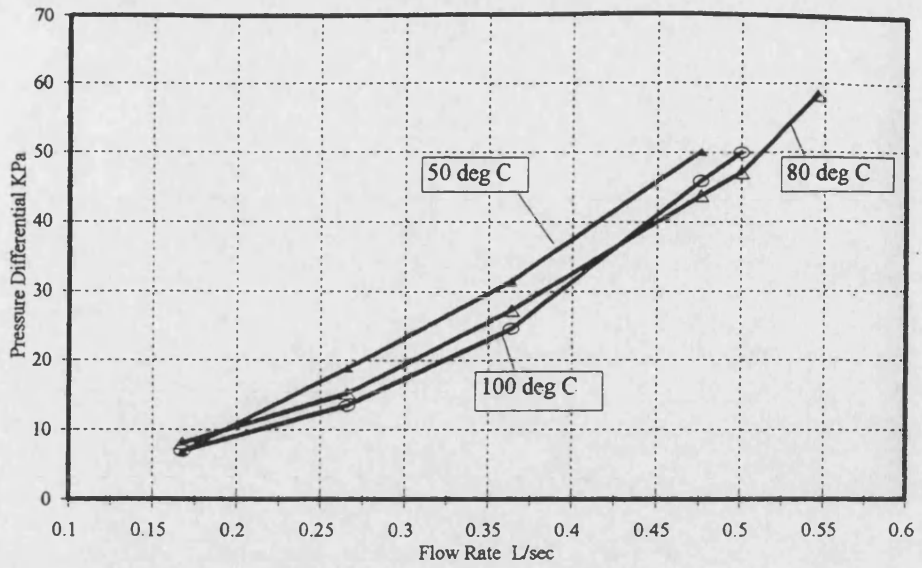

Cabin Heater Hydraulic Characteristic — FIGURE 7.9

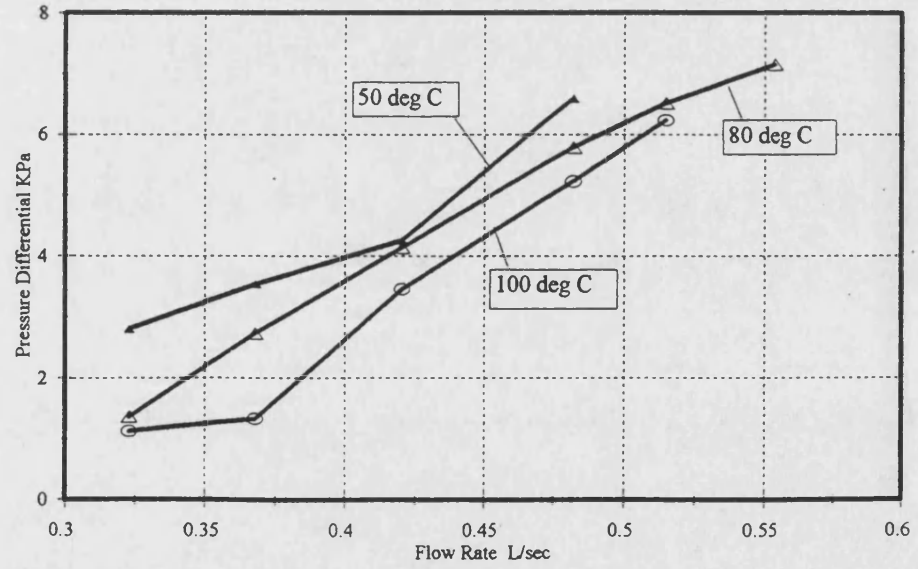

Oil Cooler Hydraulic Characteristic — FIGURE 7.10

CHAPTER 8

VEHICLE COOLING SYSTEMS - INSTRUMENTATION AND MODEL ASSESSMENT

8.1 INTRODUCTION

The purpose of this Chapter is to describe the experimental rig instrumentation and assess the vehicle cooling circuit model developed in Chapter 7 with respect to its steady state and dynamic performance prediction. The circuit performance is assessed by simulations that are split into three sections as follows:

A Initial circuit simulation that includes comparison of hose models A and B discussed in the previous Chapter.

B Circuit comparison with experimental data at coolant pump speeds of 2100, 3100 and 4500 revs.min^{-1}.

C Simulated drive cycle with component variation that shows the flexibility of the model from a design perspective.

8.2 EXPERIMENTAL RIG INSTRUMENTATION

Circuit temperatures and pressures were gathered on a purpose built 'Thermo Electric' data logger capable of storing and processing in excess of 20 temperature measurements and 5 pressure measurements. This equipment was supplied by the Ford Motor Company. The data logger was electronically configured to interface with 'K' type thermocouples which have an accuracy of ± 1.5 °C. Unfortunately, these thermocouples are inferior to the 'T' type used for the hydraulic fluid power system studies described in chapters 5 and 6 since their accuracy is 3 times poorer. Nevertheless these thermocouples gave very good repeatability and uniformity when coolant temperatures were measured in a thermally flat circuit (no heat input). Throughout

the experimental work, deviations in excess of 0 .5 °C between thermocouple readings were not observed with the circuit in this condition. Pressure was measured at several points in the circuit using transducers with a measurement range of -15 to +36 PSIG (pounds per square inch gauge) with an accuracy of 1% of full scale deflection (FSD). Coolant pump speed was adjusted via the directly coupled variable speed electric motor with a speed range of 0 to 5000 rev.min^{-1}. Hydac turbine flow meters were used to monitor coolant flow rate with an accuracy of ± 1.5% of measured value. However, because of the large temperature and hence viscosity changes in the system, somewhat larger errors than this must be expected from these flow measurement devices.

8.3 INITIAL SIMULATION AND HOSE COMPARISON

The Bath*fp* vehicle cooling system circuit is shown in Figure 8.1. This shows the previously defined component and hose models assembled into a standard configuration. The initial simulation contains the following attributes and forcing functions:

Hose model B (constant friction factor).

Coolant - 50/50 water-ethylene gylcol.

Coolant properties updated every integration step.

Coolant pump speed set constant at 4500 rev.min^{-1}.

Vehicle speed set constant at 10 m.s^{-1}

Heat exchanger effectiveness 0.34

The engine load torque is linearly applied from 5 to 135 Nm over 30 seconds. The torque is then held constant for 350 seconds. A step reduction in torque is then applied with the torque set to 5 Nm for 100 seconds. Finally the torque is raised back to 135 Nm for the remainder of the simulation, see Figure 8.2.

This simulation forces the engine to heat the coolant from ambient conditions to its normal operating temperature. The torque reduction allows the coolant to fall in temperature thus initiating a closure of the thermostat. Finally on reinstatement of the load torque the system is returned to its normal operating temperature.

Figures 8.3 to 8.9 show the dynamic response of the cooling system when subject to the above boundary conditions. It can be seen that when the coolant temperature exceeds the thermostat cracking temperature of 88 °C, the thermostat opens and finds a pseudo steady state at approximately 1 mm open (the thermostat hysteresis is set at 0.5 °C). This also corresponds to a rate of heat removal from the radiator of approximately 23 KW (Figure 8.8). At a load torque of 135 Nm and speed of 4500 rev.min^{-1}, there is a corresponding coolant temperature rise across the engine of approximately 3.2 °C, see Figure 8.4. During the transient the coolant pump flow rate is approximately 125 kg.min^{-1} although variations occurred due to the change in circuit resistance caused by the transient variation in thermostat thrust rod position.

For comparison purposes, an identical transient was performed, with the inclusion of hose model A (laminar and turbulent friction factor included, with steady state momentum solution). Figure 8.10 shows a comparison of the mass flow rates from the coolant pump, bypass and radiator for both simulations. This suggests that little error in flow rate has occurred when using the constant friction factor hose model B. This is a strong argument for adopting this model in simulations of the cooling system due to the reduction in simulation times.

It can be seen in Figure 8.10 that the circuit with the more accurate friction hose models (hose model A) produces slightly less mass flow rate compared with the constant friction case. This is expected as any hose model whose Reynolds number is less than the fully established turbulent flow value (Re = 10^6 fully establish turbulent flow, for a relative roughness = 0.001)

will have a friction factor which is greater than the fully established turbulent flow value, and hence produce a greater pressure drop for a given flow rate.

The flow rates in a vehicle cooling circuit change considerably. The factors affecting flow rate are associated with engine speed, load and system/ambient temperatures. In this respect high speed and load situations will be accommodated more easily with hose model B simulations since the expected flow rates should be above the laminar - turbulent transition region. In the limit, simulations with hoses models A and B will be identical provided fully developed turbulent flow is established.

8.4 CIRCUIT COMPARISON WITH EXPERIMENTAL DATA

As a precursor to using the whole circuit simulation to predict the cooling system performance with component variation (Section 8.5), a set of transients were performed and compared with experimental data to ensure confidence in the simulated predictions. The circuit simulation was set up to provide a map of the thermal hydraulic performance at three different speeds, 2100, 3100 and 4500 revs.min^{-1}. Figures 8.11 to 8.13 show pump inlet / outlet and engine outlet pressure for variations in coolant temperature between 20 and 80 °C. It can be seen that there is a good correspondence between simulated and experimental results. Figures 8.11 to 8.13 show that circuit pressures rise with increasing coolant temperature which is expected when heating a closed volume of coolant and air.

It should be noted that if the coolant temperatures were allowed to increase past the thermostat cracking temperature and therefore allow coolant to flow through the radiator, a step change in pressures would occur due to the marked change in circuit resistance.

8.5 DRIVE CYCLE WITH COMPONENT VARIATION

To demonstrate the change in component parameters on cooling system performance, a drive cycle was simulated which assumed a vehicle towing a load, initially at a low torque steady state condition. After 1000 seconds, the vehicle negotiates a steep hill where the vehicle speed is reduced from 25 to 5 $m.s^{-1}$and the engine torque increased from 50 to 110 Nm. This mode of operation continues for 500 seconds. There after the vehicle is brought to rest with the engine speed set to idle at 850 $revs.min^{-1}$. Three simulations were performed for the previously described drive cycle, which demonstrate the cooling system performance when different components are used. These are stated as follows:

A Standard cooling system.

B The cooling system with an undersized coolant pump. This has been achieved by running the coolant pump at half normal speed.

C The cooling system with both an undersized coolant pump and radiator. The radiator cross sectional area has been reduced by half the standard size.

The air inlet temperature is 25 °C for all three cases. Figures 8.14 and 8.15 show engine coolant outlet temperature and thermostat stem displacement during the drive cycle. It can be seen that both the standard cooling system and the system with the undersized pump, control coolant temperature adequately. Coolant temperature rises slightly when the vehicle negotiates the hill. When the vehicle stops there is a small rise in coolant temperature due to the thermal inertia of the system. This is compensated by the thermostat opening, see Figure 8.15. There after coolant temperatures rise slowly because the engine heat generated at the idling condition is dissipated by natural convection and radiation from component surfaces (vehicle stopped). This condition would eventually result in the cooling fan engaging for these cases. It can be seen that the undersized pump and radiator configuration cannot dissipate sufficient heat on the hill climb,

which results in the cooling fan engaging twice before the vehicle comes to rest. This results in peak coolant temperatures being limited to 95 °C. Figure 8.16 shows the air velocity through the radiator for this configuration where it can be seen that the fan contributes an additional 5 $m.s^{-1}$ to the air velocity passing through the radiator. This is responsible for engine outlet temperature being reduced below that achieved for the correct component configuration, after the vehicle has stopped.

It is interesting to note that the hysteresis of the thermostat (Figure 8.15) is evident for the undersized pump and radiator configuration and is indicated by the thermostat stem displacement at 1300 and 1500 seconds respectively.

Further inspection reveals insight into the cooling system behaviour, see Figures 8.17 to 8.19. These Figures show the temperature difference from engine inlet to outlet. Throughout the course of this simulation, all three configurations have to remove very similar amounts of heat generated by the engine drive cycle. This is verified by the small temperature rise in the correct component configuration, see Figure 8.17. It can be seen that because the coolant pump is undersized in both the other configurations, the engine coolant temperature rise has approximately doubled. This would indicate that the mass flow rate has halved. The effects of the fan engagement for the undersized pump and radiator is evident in Figure 8.19. It can be seen that this additional cooling has significantly reduced the engine coolant inlet temperature which has resulted in the low coolant temperatures after the vehicle has stopped.

8.6 CLOSURE

Comparison of the model and experimental data showed a close correspondence for a number of circuit pressure and temperatures, at three coolant pump speeds. This has provided confidence and a degree of validation for the circuit model. Ideally the circuit model should be compared

with experimental data for a wide range of conditions, thereby increasing confidence in the model predictions, and this should be considered for future work.

The differences in hose model friction calculations have been shown to have a negligible effect on circuit coolant flow rates. This is primarily attributable to the component pressure losses being much larger in magnitude when compared with the hoses. This however does not alleviate the need for further work to improve the hydraulic performance of the hose models. A course of development for hose model pressure - flow calculations has been suggested in Chapter 7, based on iteration of the flow network at each integration time step. Although this could improve the accuracy and speed of the whole circuit model, it could reduce the flexibility from a design perspective. The merits of purpose built flow network solver operating in a Bath*fp* simulation environment would have to be offset against the ability to change the circuit configuration with ease (at present a desirable feature of Bath*fp*).

The accuracy of model prediction should be of a similar order of magnitude to that considered for the hydraulic fluid power system in Chapter 6. The basis of the physical relationships describing the thermal hydraulic characteristics is to all intents and purposes identical. Fundamental differences that would have affected accuracy include the quality of the measurement transducers, some of which were inferior to those used in Chapter 6. However more precise information was obtainable concerning the coolant properties (PPDS software) which should have enhanced the model prediction. One of the main experimental concerns was the removal of air from a freshly filled coolant circuit, a procedure that was completed several times during the course of this research. Air in the coolant circuit can cause inaccurate flow measurement calculations. Unfortunately changes to the circuit configuration were necessary to characterise individual components and circuit flow paths.

The accuracy of the flow measurement could have been impeded when considering the temperature and hence viscosity change over the operating range. In some instances the turbine flow meters were used at their limits of their range (≥ 90 °C).This not only affects accuracy, but also the integrity and robustness of the flow meter could be challenged if used for extended periods at these temperatures. In this respect future research should attempt to improve on both the accuracy and robustness of transducers.

Cooling system design embodies many issues, and it has been shown that some of these may be addressed by the circuit model demonstrated in this Chapter. The nature of the Bath*fp* simulation environment allows component sensitivity and different design configurations to be assessed easily. A typical example would be the merits of placing the thermostat at the engine inlet or outlet. This type of study relies on the ability to predict transient information concerning circuit fluid and engine material temperatures, as one of the key factors is the minimisation of thermal shock. Another factor is the dynamic stability of the thermostat and therefore the risk of coolant temperature oscillations. This analysis requires whole circuit modelling with transient performance prediction, which is not possible with the type of techniques used by Blumcke and Nefischer[1995] as stated in Chapter 1.

The simulations of Section 8.5 have shown the flexibility to assess component sensitivity and changes in system configuration from a design perspective. This approach will aid the process of cooling system design and optimisation.

It is considered that further research would improve the model prediction, and would embrace the following issues:

1 Discretising of the engine block, head and sump into components such that smaller

lumped heat capacity elements may be modelled. This would clearly improve the dynamic response of the engine material temperature since at present it is determined by one heat capacity node. A similar approach has been taken by researchers such as Shayler *et al.*[1993]. If the combustion process were to be modelled, this would be seen as a prerequisite since temperature differences across the cylinder wall can be very large. Clearly one thermal node would be inappropriate for this condition, considering the thermal gradients involved. In this respect it would be appropriate to continue the research with a running engine. This would also improve the quality of data since the engine could be tested over the complete operating range.

2 The theoretical wax pellet thermostat model described in Chapter 7 Section 7.6 should be implemented once it has been proved to give robust results. This is seen as a fundamental step in further research since other studies have relied on describing the physical behaviour empirically. This may be seen in the work of Tomlinson & Burrows[1993], Chiang & Keller[1990] and Nelson & Robichaux[1997]. The wax pellet thermostat is typically highly nonlinear and exhibits hysteresis such that empirical models become cumbersome. As such empirical models are rarely able to provide accurate dynamic performance predictions because of the complexities involved.

3 Improvements to the radiator model could be made in that experimental results should be taken in a controlled environment, preferably with a running engine. This would allow the complete operating range to be embraced. Improvements could also be made to the physical model such as including buoyancy effects (a known phenomenon where coolant stagnation pockets can occur).

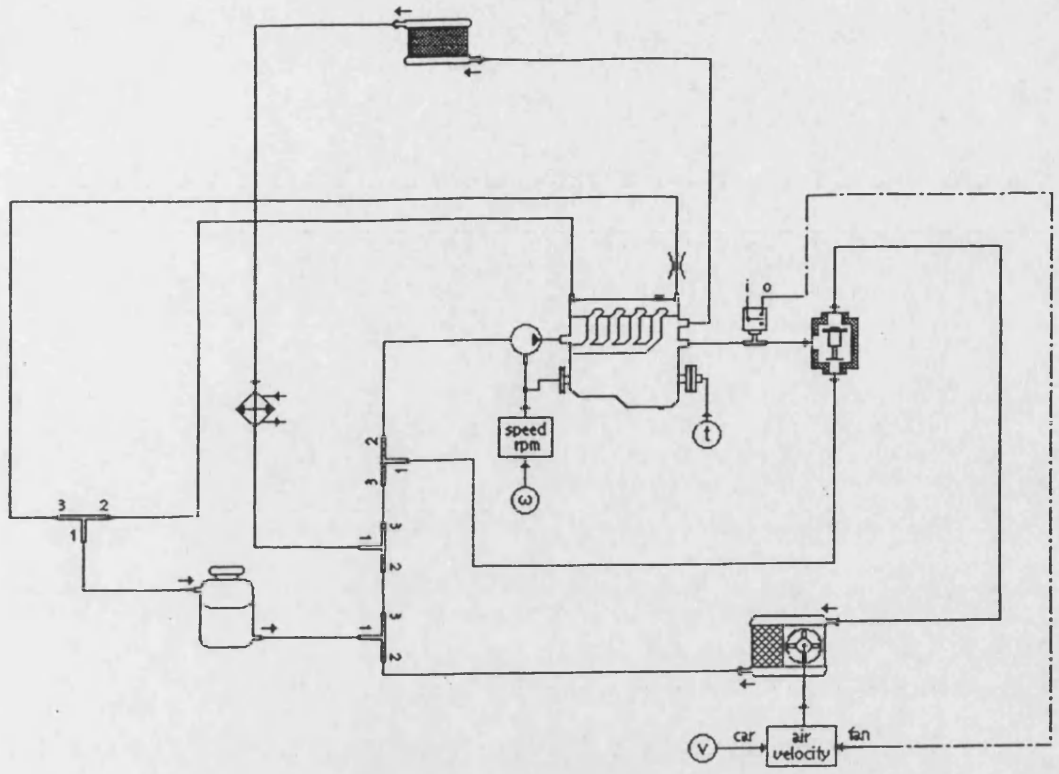

Vehicle Cooling System FIGURE 8.1

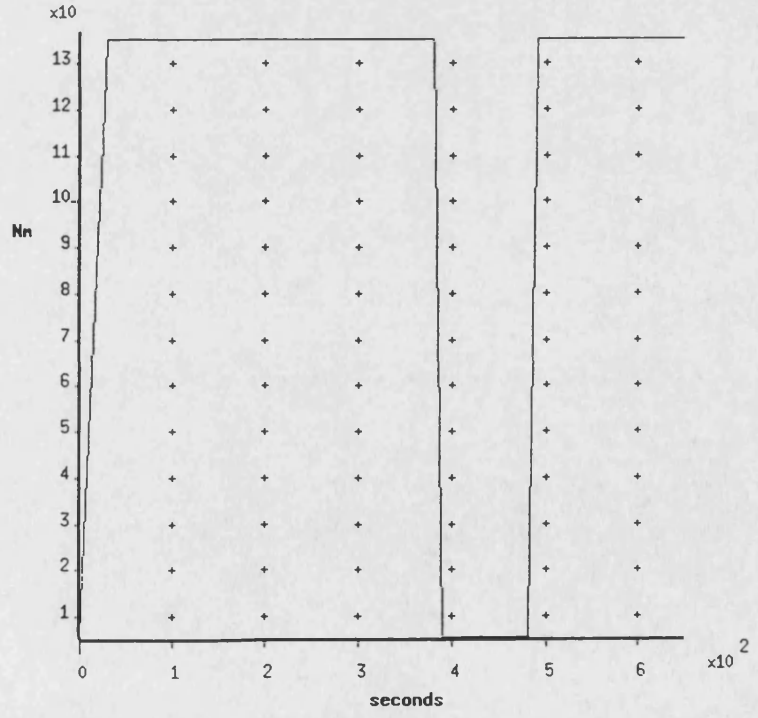

Engine Load Torque FIGURE 8.2

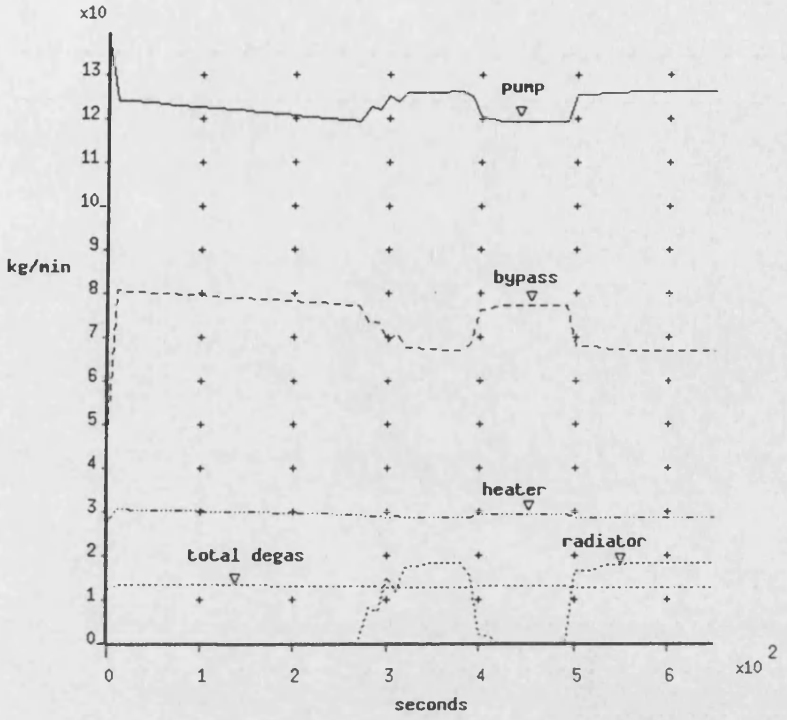

Vehicle Cooling Circuit Mass Flow Rates FIGURE 8.3

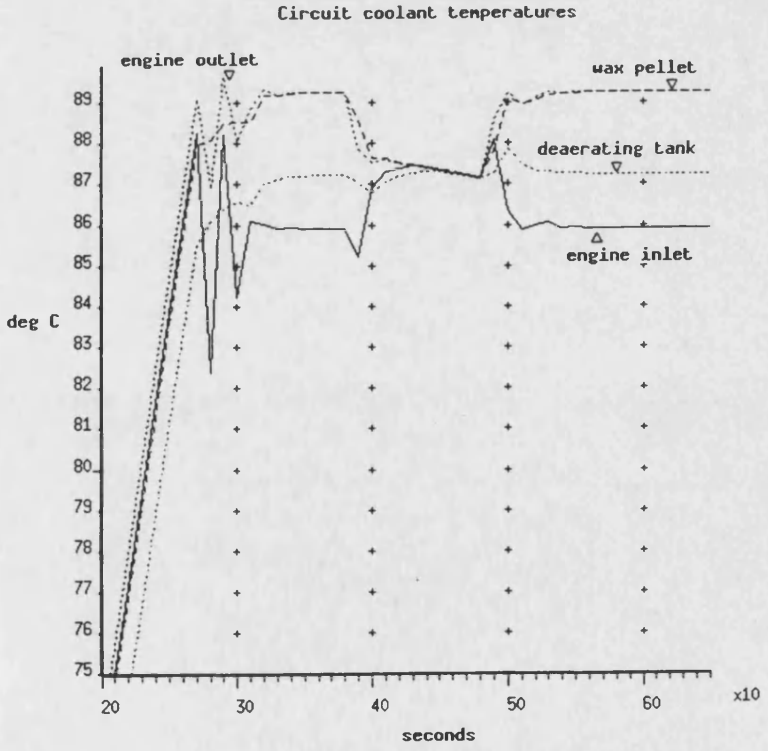

Vehicle Cooling Circuit Temperatures FIGURE 8.4

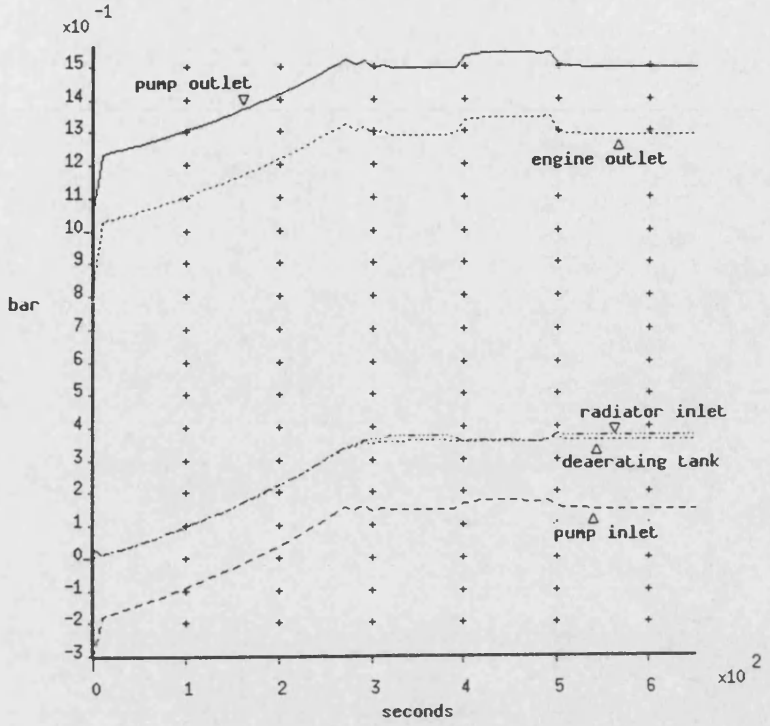

Vehicle Cooling Circuit Pressures FIGURE 8.5

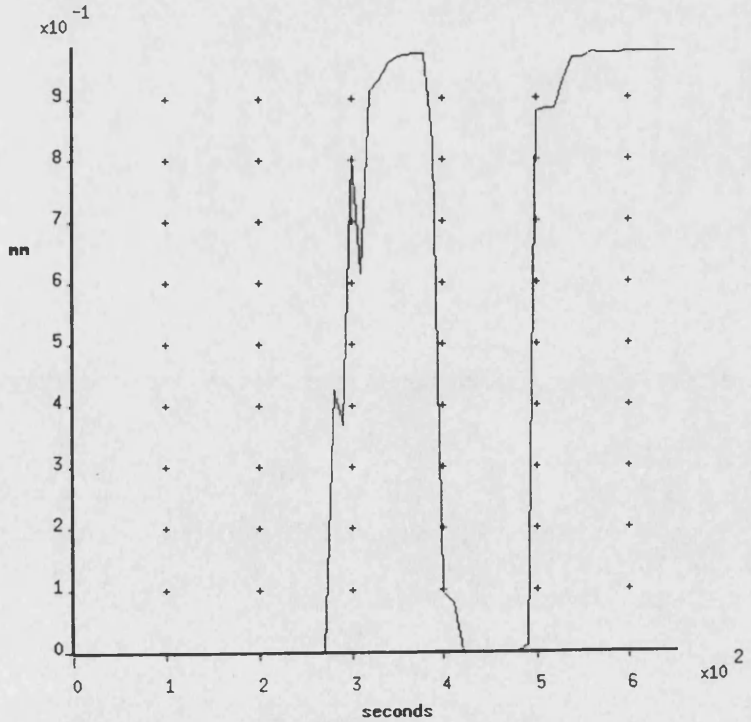

Thermostat Stem Displacement FIGURE 8.6

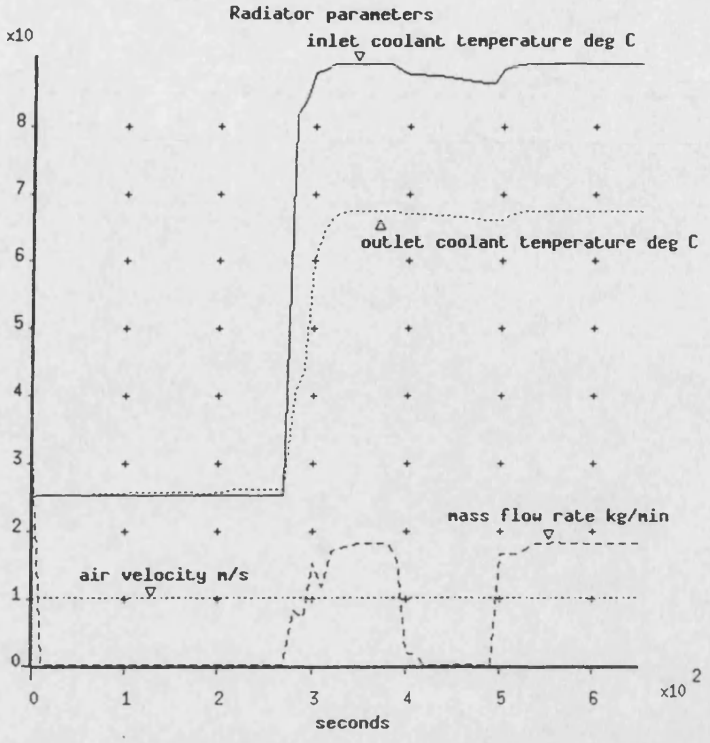

Radiator Coolant and Air Conditions FIGURE 8.7

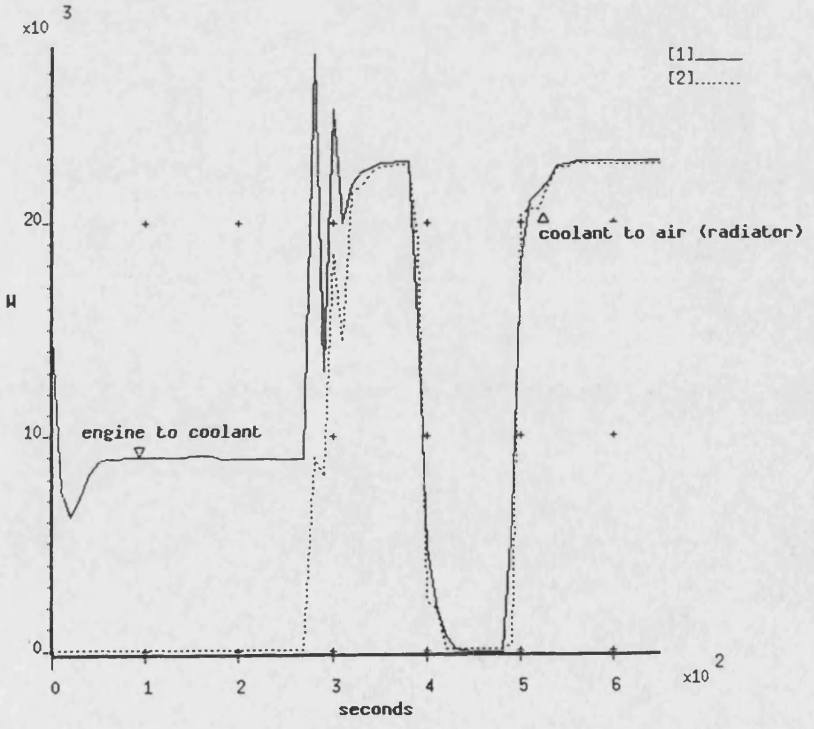

Vehicle Cooling Circuit - Rate of Heat Transfer FIGURE 8.8

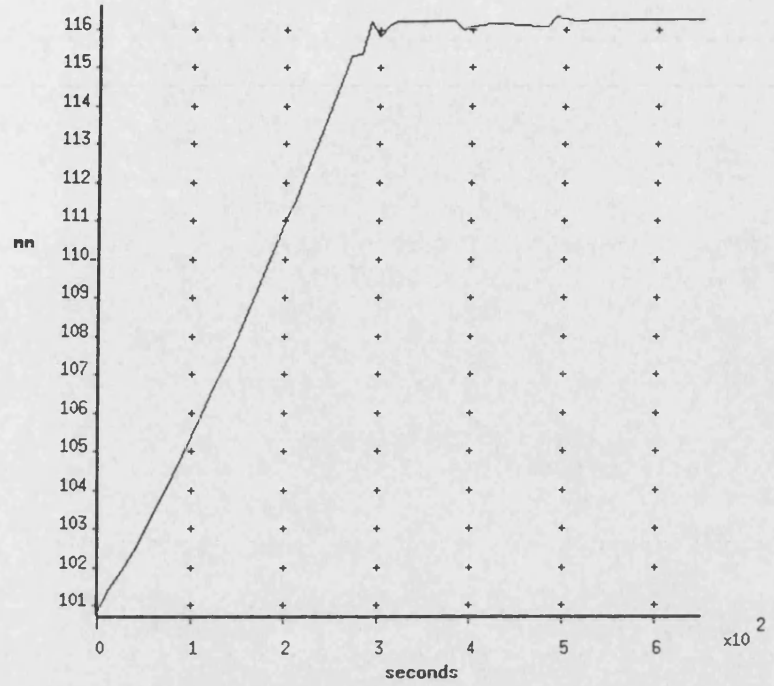

Deaeration Header Tank Coolant Level FIGURE 8.9

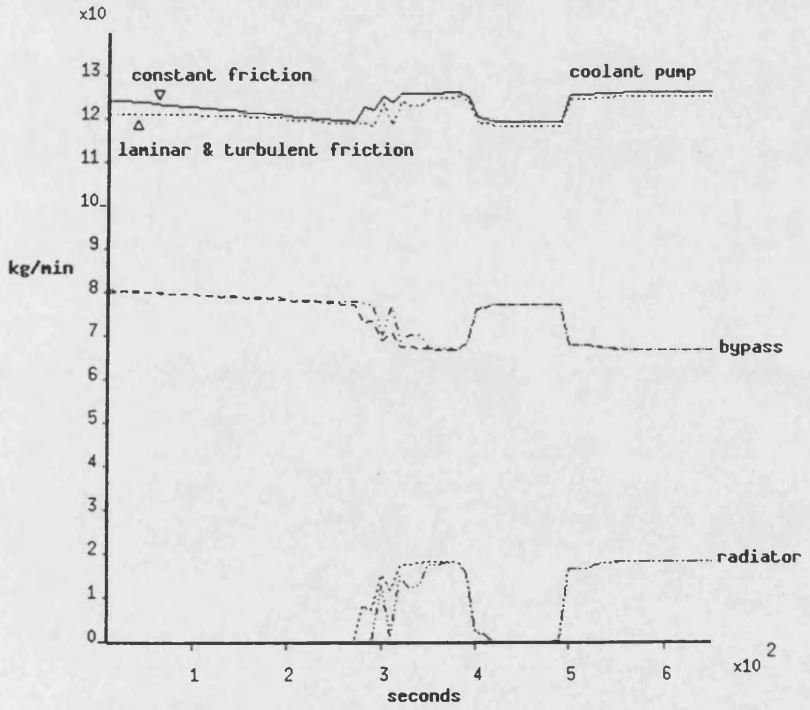

Circuit Mass Flow Rate Comparisons - Hose models A & B FIGURE 8.10

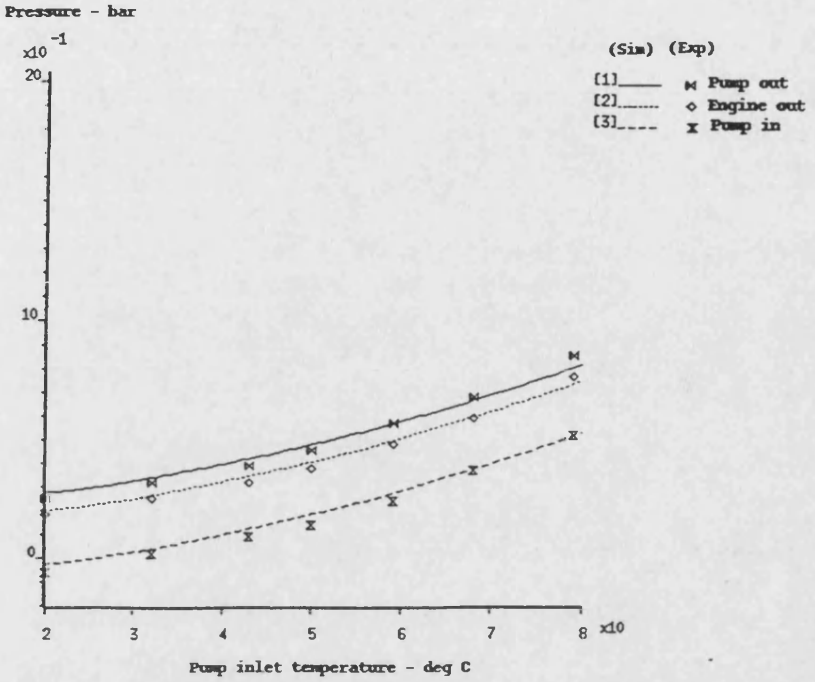

Circuit Thermal Hydraulic Performance at 2100 rev.min^{-1} FIGURE 8.11

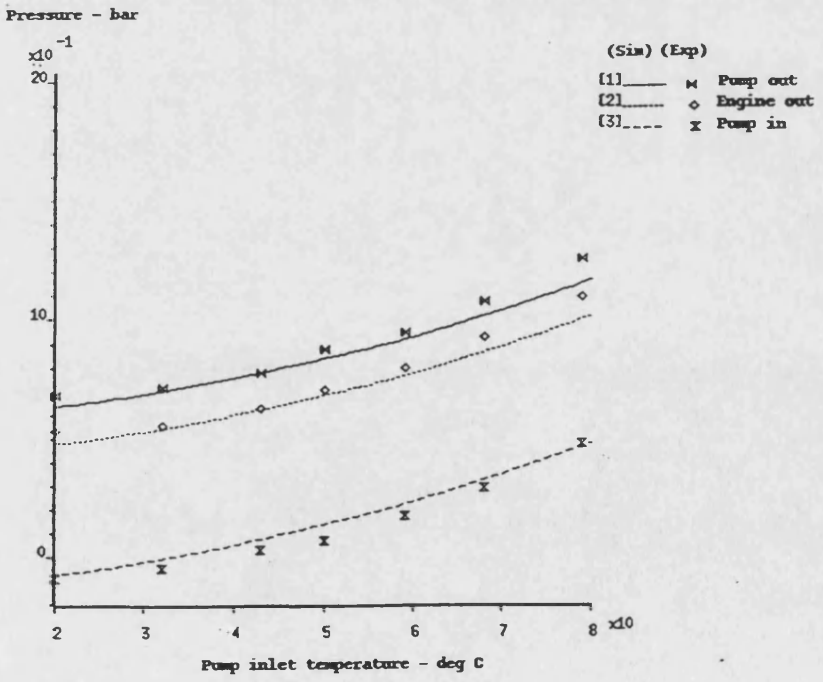

Circuit Thermal Hydraulic Performance at 3100 rev.min^{-1} FIGURE 8.12

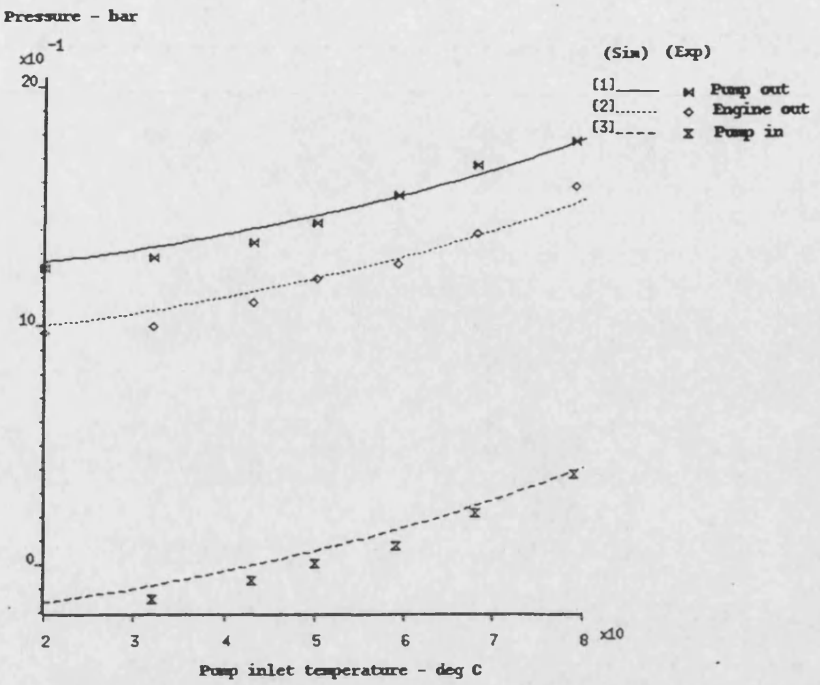

Circuit Thermal Hydraulic Performance at 4500 rev.min^{-1} FIGURE 8.13

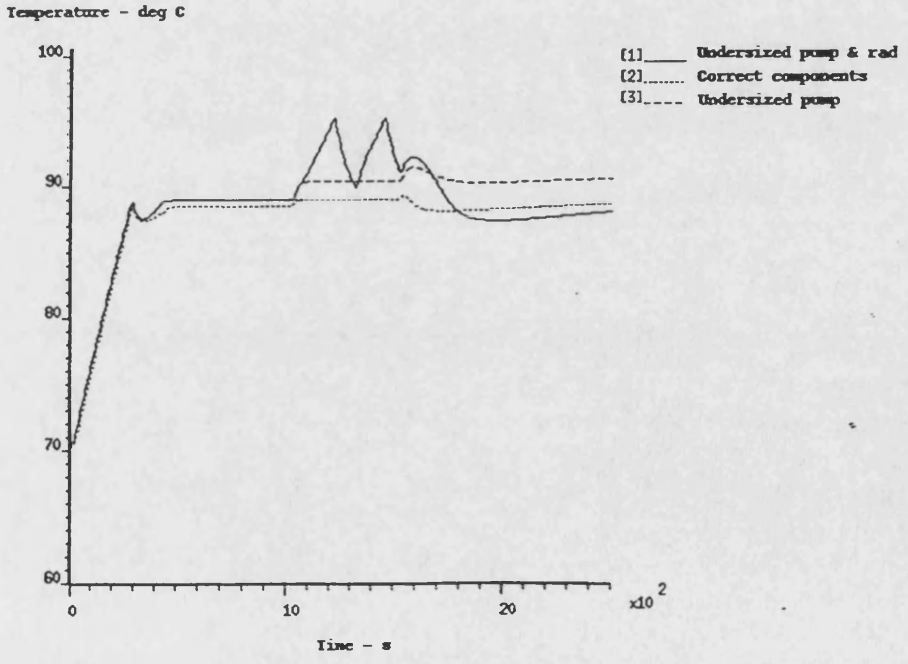

Drive Cycle Engine Coolant Outlet Temperatures FIGURE 8.14

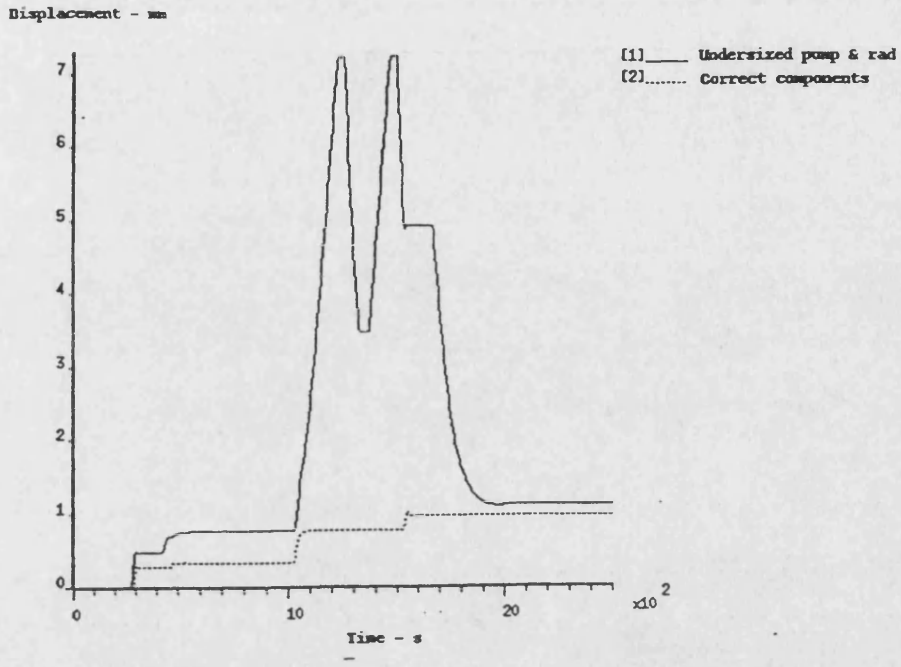

Drive Cycle Thermostat Stem Displacement FIGURE 8.15

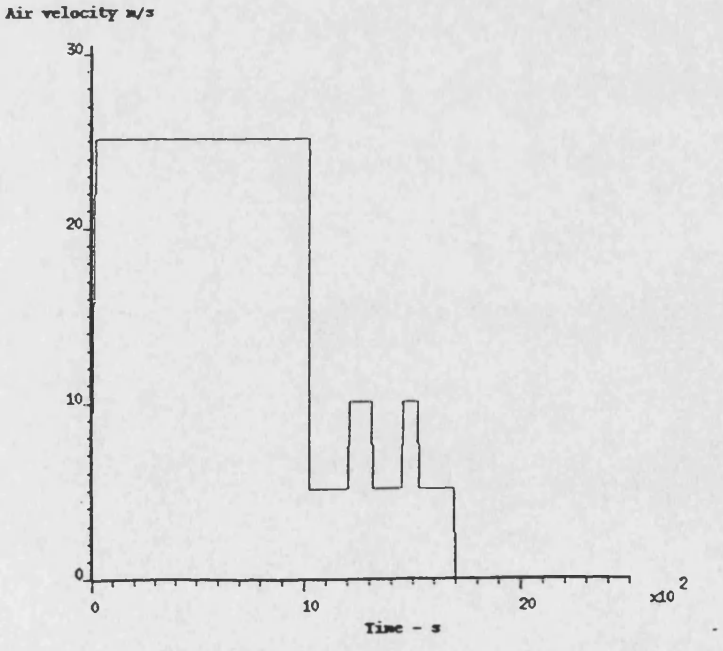

Drive Cycle Air Velocity FIGURE 8.16

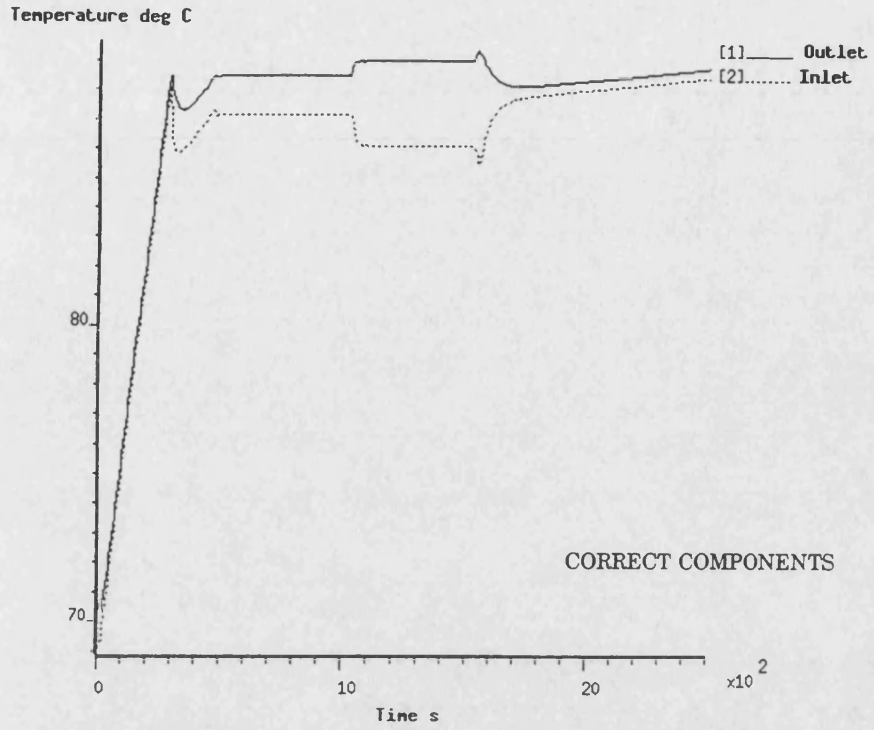

Drive Cycle Engine Coolant Temperatures FIGURE 8.17

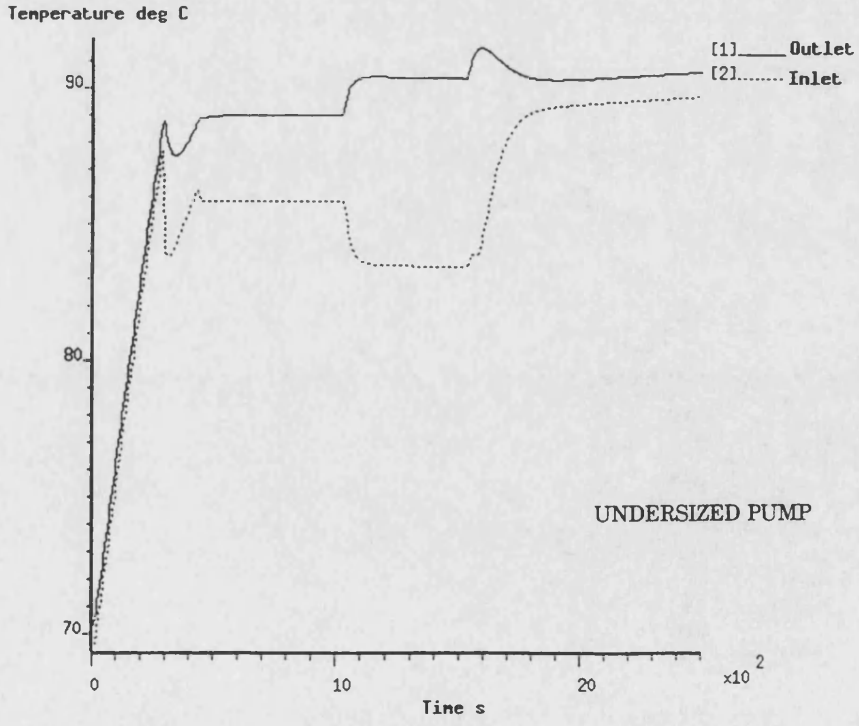

Drive Cycle Engine Coolant Temperatures FIGURE 8.18

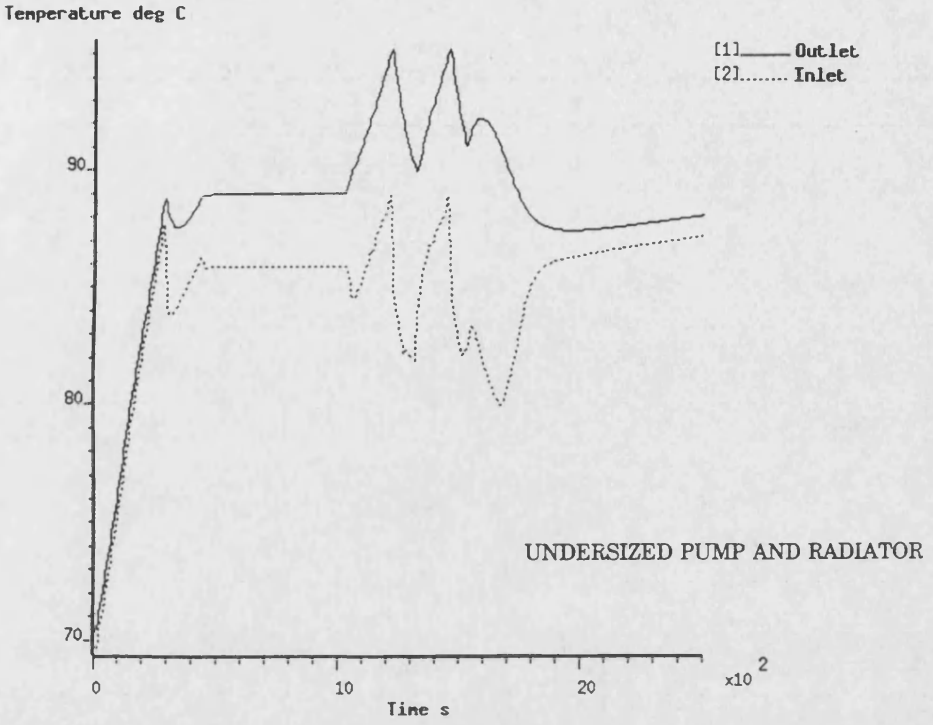

Drive Cycle Engine Coolant Temperatures FIGURE 8.19

CHAPTER 9

CONCLUSIONS AND FURTHER WORK

The research undertaken has focused on the application of lumped parameter modelling techniques to aid the design and analysis of thermal hydraulic systems. The aim of this research has been to extend the range and sophistication of the modelling approach which will lead to increased flexibility at the design and analysis phase. The efficacy of the thermal hydraulic systems design process should therefore be improved.

Chapter 2 demonstrated that the fundamental conservation equations for fluid mass and energy are prerequisites for modelling the transient behaviour of thermal hydraulic systems. The basic advances in representation compared with the formulation of Harris[1990] for hydraulic systems can be summarised as follows:

A The dynamic continuity and energy equations are coupled and form a set of simultaneous differential equations. This means that there is a mode of transient response where pressure and temperature dynamics occur at the same frequency.

B By virtue of condition A above, the continuity equation now includes the effect of temperature.

C Explicit in the formulation is the consideration of moving boundaries.

D The method of derivation caters for a non flat intensive property profile across the control volume since no implicit assumptions have been made about the intensive properties, other than values will change in the direction of the flow path; and that the

inlet and outlet conditions are related to a mean value within the control volume. This flexibility is conceptually more satisfying and allows more representative sets of models for application.

Additionally, the representation of mass and energy in terms of pressure and temperature allows a variety of fluids to be investigated. This is primarily due to the availability of data relating to properties such as bulk modulus and the coefficient of cubical expansion, which both happen to be functions of the partial derivatives of the conservation equations derived in Chapter 2. This allowed the analysis of both hydraulic oils and vehicle coolants, and could be extended to include a variety of fluids providing the above properties are available. If however a complete set of thermodynamic properties for a fluid is available, this does make the modelling somewhat easier. Energy can then be represented in terms of enthalpy which avoids the duplication of pressure at connecting ports using a simulation language such as Bath*fp*, as explained in Chapter 5. This is caused by representing conservation of energy in terms of a temperature state variable, whereas energy in fact is a function of both temperature and one other thermodynamic property.

The analytical tools derived in Chapter 2 were used to investigate the behaviour of the LP feed system of Heysham 2 power station. Most of the effort has been directed towards development of a suitable LP heater model, that is capable of showing the dynamic response to the automatic frequency regulation mode of operation (AFRO). This has required a detailed examination of conservation of mass and energy for vessels containing a two phase water/steam mixture. Of particular importance is the necessity to represent a two phase drains flow. Without this, the cascaded heater/flash vessel system is unstable when standard single phase liquid pressure / flow models are used.

Comparison of both the steady state and dynamic performance of the LP feed train model against plant data in Chapter 4 has indicated a close correspondence for most model variables. The model is clearly suitable for analysing a variety of situations that the plant could be subjected to, including the AFRO mode of operation for which it has been specifically developed.

Comparison of the quadrant trip event could have been significantly improved if the Boiler Feed Pump Turbine (BFPT) steam flow to the Deaerator (DA) had been recorded. This would avoid a qualitative assessment of the mass and energy levels received by the DA and thus define the DA model boundary explicitly. The changes made to the DA boundary conditions have been justified on the basis of an assessment of DA, BFPT exhaust and Intermediate/Low pressure (IP/LP) crossover steam pressures, and their effects upon the bled steam flow in the initial period following the quadrant trip.

Refinements to the LP feed train model should be investigated with respect to the heat transfer correlations used. Using more exacting heat transfer correlations for condensing heat transfer could well find improvements to the steady state mappings discussed in Section 4.2.1, Chapter 4.

Further examination of the apparent hunting exhibited throughout the plant condenser/feedheating system, which is evident in the condenser level and control valve position (WC-244) would improve the correspondence between model and plant. This behaviour could possibly be due to incorrect control system data or nonlinearities in the control system hardware that is not reproduced in the model.

The analytical approach of Chapter 2 was again used to analyse the transient and steady state

thermal hydraulic performance of a hydraulic fluid power circuit. For the circuit studied, a good thermal correspondence is achieved between model and rig, when taking into account the possible systematic and random errors involved (Appendix B). It has been shown that this level of correspondence requires accurate hydraulic performance models that include the effects of temperature and therefore viscosity. This is demonstrated by the pump flow loss model and the loading valve hydraulic performance model. The circuit has provided a useful test bed for validation of the theoretical approach for typical components used in fluid power systems.

The thermal response of the hydraulic circuit studied in Chapters 5 and 6 is dominated by the heat capacity of the reservoir and the dynamic cross coupling effect between pressure and temperature will have negligible impact on the overall transient response. The dynamic cross coupling effect between pressure and temperature will be more noticeable in systems where large pressure fluctuations occur for a sustained period (such as the LP feed train examined in Chapters 3 and 4), and where the heat capacity of the system is small. An example of this could include systems where cyclical loading occurs via a hydraulic actuator. To successfully study and predict the dynamic response of these systems, would require improvement in thermocouple dynamic response, such that it is comparable with the pressure transducer dynamic response.

The dominance of the system heat capacity in the thermal transient response, suggests that it is acceptable to base estimations of the response time on the thermal inertia of the system. In this respect, the modelling approach of Harris[1990] could be used without significant loss of accuracy being incurred. It has been shown that providing there is an accurate thermal hydraulic characteristic for each component, then the steady state performance is also predicted with confidence.

Further investigations should be undertaken to refine the reservoir model. The thermal

performance during the cooldown period was shown to suffer from the effects of thermal stratification that effectively reduces the heat capacity of the reservoir oil. Harris[1990] has shown that for this type of reservoir, a reduction of oil inlet temperature on the cooling phase can induced buoyancy effects in the reservoir oil such that a layer of unmixed fluid is maintained at the free surface. This accounts for the apparent reduction in oil heat capacity and so a reduction in thermal response time for the system. Model refinements should consider the buoyancy effects caused by differences if oil temperature. It is the author's view that this would involve a significant amount of research, since the phenomena of heat and mass transfer within a single phase fluid would need to be established.

Improvements could also be made by introducing and enhancing heat transfer correlations for component models other than the oil cooler. This would have a second order effect but nevertheless improve the model prediction at all operating conditions. To access the heat transfer in detail from each component would require thermocouples with improved accuracy compared with that currently used for this study. This is due to the temperature rise across most components being typically less than a few °C.

Chapters 7 and 8 employed similar techniques to examine the performance of a vehicle cooling system. Comparison of the model and experimental data showed a close correspondence for most circuit pressure and temperatures, at three coolant pump speeds. This has provided confidence and a degree of validation for the circuit model. Ideally the circuit model should be compared with experimental data for a wide range of conditions, thereby increasing confidence in the model predictions, and this should be considered for future work.

The differences in hose model friction calculations have been shown to have a negligible effect

on circuit coolant flow rates. This is primarily attributable to the component pressure losses being much larger in magnitude when compared with the hoses. This however does not alleviate the need for further work to improve the hydraulic performance of the hose models. A course of development for hose model pressure - flow calculations have been suggested in Chapter 7, based on iteration of the flow network at each integration time step. Although this could improve the accuracy and speed of the whole circuit model, it could reduce the flexibility from a design perspective. The merits of purpose built flow network solver operating in a Bath*fp* simulation environment would have to be offset against the ability to change the circuit configuration with ease (at present a desirable feature of Bath*fp*).

The simulations of Section 8.4 have shown the flexibility to assess component sensitivity and changes in system configuration from a design perspective. This will aid the designer in optimising vehicle cooling systems.

A proposed vehicle cooling system wax pellet thermostat model was discussed in Section 7.6, based on a rigorous theoretical approach. Future developments of the vehicle cooling circuit should consider implementation of this model. Further investigations are required to determine the properties of the wax before a robust model can be developed.

Future developments should also include the viscosity dependence on the hydraulic performance of components to a greater degree. This aspect was shown to be important for the hydraulic circuit in Chapters 5 and 6. Detailed testing of the coolant pump such that torque and so efficiency can be assessed, is seen as a prerequisite for future work.

Further consideration should also be given to the following research and development:

Discretising of the engine block, head and sump into components such that smaller lumped heat capacity elements may be modelled. This would clearly improve the dynamic response of the engine material temperature since at present it is determined by one heat capacity node. If the combustion process were to be modelled, this would be seen as a prerequisite since temperature differences across the cylinder wall can be very large. Clearly one thermal node would be inappropriate for this condition, considering the thermal gradients involved. In this respect it would be appropriate to continue the research with a running engine. This would also improve the quality of data since the engine could be tested over the complete operating range.

Improvements to the radiator model should be considered by enhancing the physical model such that buoyancy effects are included (a known phenomenon where coolant stagnation pockets can occur).

The modelling approach developed in Chapter 2 has shown that it is possible to predict the performance of a range of thermal hydraulic systems using the fundamental conservation equations for mass and energy, coupled with the knowledge of the hydraulic characteristics and heat transfer of the system in question. It has been shown that explicit details such as the dynamic cross coupling effect between pressure and temperature, are not always required to successfully predict the system performance. However, with the advance of computing engines, there is no reason a rigorous approach to modelling these systems cannot be adopted on a generic basis. This will avoid instances where the designer has to decide the degree of model sophistication for acceptable and confident performance prediction.

This research has extended the range and sophistication of modelling techniques that will allow the engineer greater flexibility in design and analysis of thermal hydraulic systems.

REFERENCES

Bauer, W., Ehrenreich, H and Reister, H., May 1995

Design of Cooling Systems with Computer Simulation and Underhood Flow Analysis using CFD. *Vehicle Thermal Management systems Conference Proceedings*, pg 499 - 512.

Blumcke, E. and Nefischer, P., May 1995

Improved Engine Cooling Systems using Calculation Methods, *Vehicle Thermal Management Systems Conference Proceedings*, pg 347 - 356.

Buckingham, J., 1986

Computer Simulation of Temperature Effects in Hydraulic systems, MSc Thesis, School of Mechanical Engineering, University of Bath.

Chiang & Keller, 1990

The thermostat characteristics and its effect on low-flow engine cooling system performance, *SAE paper* 900904

Deacon, D.R, (a)

A compilation of notes describing the behaviour of steam through a turbine, CEGB.

Douglas, J.F., Gasiorek, J.M., & Swaffield, J.A., 1981

Fluid Mechanics, p265, Pitman.

Eastop, T. D. and McConkey, A., 1978

Applied Thermodynamics for Engineering Technologists, pg 664 - 668, Longman.

Ford internal report, 1996

Cooling System Hydraulic Design Process guide.

Haaland, S.E., March 1983

Simple and Explicit Formulas for the Friction Factor in turbulent pipe flow, *ASME Journal of Fluids Engineering*, Vol 105.

Harris, R. M., 1990

The Modelling and Simulation of Temperature Effects in Hydraulic Systems, PhD Thesis, University of Bath UK.

Holman, J.P. 1992a

Heat Transfer, pg 282, McGraw-Hill.

Holman, J.P. 1992b

Heat Transfer, McGraw-Hill.

Kjolle, A., August 1978

Thermodynamic Methods for Determining Losses in Hydraulic Components - A Survey. NEL Report No: 657.

Lewitt, E.H., 1953

Thermodynamics Applied to Heat engines, pg294, Pitman.

Lin, Z.H., Zhao, J.Y., Wang, D., 1992

Pressure Losses of Gas-Liquid Two-Phase Flow Passing Through Orifices. *International Journal of Engineering Fluid Mechanics,* 5 (4), 501-515

Liu, Y., Chen, T. and Chen, X., 1988

Steam-Water Two-Phase Flow Measurements with Sharp-Edged Orifices

McAdams, 1954

Heat transmission, pg 352, McGraw-Hill

McCandlish, D. and Dorey, R.E., 1984

The Mathematical Modelling of Hydrostatic Pumps and Motors. *Proc. Instn Mech. Engrs,* 198B(10).

McCloy, D., 1969

Cavity Formulation in Valve Controlled Hydraulic Cylinders, *Proc.I.Mech.E.*, Vol. 184, No. 52, pp969-982.

NEI Parsons Ltd, 1989

Heysham 2 Power Station Unit 7, Report on Official Acceptance tests, No: 90.314.2383

Nelson & Robichaux, 1997

A model to simulate the behaviour automotive thermostat , *Proc Vehicle Thermal Management Systems,* SAE International Conference 1997.

NNC Ltd, 1994

Sibdym Steam Turbine Module Reference version, SXB - IP - 0951481.

Perry, R. H., Green, D.W., & Maloney J.O., 1984

Chemical Engineers Handbook', 6th Ed., McGraw-Hill, Singapore, Section 4.

PMSP

The Plant Modelling System Programme. Nuclear Electric Ltd.

PPDS

Physical Property Data Service, Fluids and Process Technologies Division, National Engineering Laboratory.

Richards, C.W., September 1993a

Bathfp Manual Volume 2 The Bathfp Model Reference Guide, Submodel description 'prdyn0', Fluid Power Centre report, University of Bath.

Richards, C.W., September 1993b

Bathfp Manual Volume 2 The Bathfp Model Reference Guide, Submodel description 'hpfrsm', Fluid Power Centre report, University of Bath.

Richards, C. W. and Tilley, D. G., March-April 1991

System Analysis with Bath*fp*. *Fluid Po*wer, 3, 50-53.

Rogers & Meyhew., 1980a

Engineering Thermodynamics Work & Heat Transfer, pg 89, Longman.

Rogers & Meyhew., 1980b

Engineering Thermodynamics Work & Heat Transfer, pg 525 - 549, Longman.

Rogers and Meyhew., 1980c

Engineering Thermodynamics Work & Heat Transfer, pg 556, Fig 22.17, Longman.

Rogers & Meyhew., 1980d

Engineering Thermodynamics Work & Heat Transfer, pg 87, Longman.

Ronney, D.H., Chisholm, D., and Cornwell, R.S., 1973

Flow of Steam - Water mixtures through Sharp-Edged Orifices. *Proc Instn Mech Engrs, 3.*

Shayler, P.J., Christian, S.J., and Ma, T., March - April 1993

A Model for the Investigation of Temperature, Heat Flow and Friction Characteristics During engine Warm-up, pg 667-676, *Proc Vehicle Thermal Management Systems,* SAE International Conference, Columbus Ohio USA.

Sidders, J.A., 1989

ANYDYM - A Fossil Fired Total Plant Mathematical Model, No: PKR/SE/255 CEGB Report.

Sidders, J. A., Tilley, D. G. and Chapple, P. J., 1996

Thermal-Hydraulic Performance Prediction in Fluid Power Systems, *Proceedings of the Institute of Mechanical Engineers*, Journal of Systems and Control Engineering part I, vol 210, No 4.

Sidders, J. A. and Tilley, D. G., May 1997

Optimising Cooling System Performance Using Computer Simulation, *Vehicle Thermal Management systems Conference Proceedings*, No 971802.

Stachowski, D., May 1993

The Combined Cycle Gas Turbine Total Plant Model CCGTDYM, Nuclear Electric Report ITD/SYSENG/CCGTDYM/001

Tomlinson, S.P. 1987

The Hydraulic Automatic Simulation Package - HASP, Modelling and Simulation Aspects, PhD Thesis, School of Mechanical Engineering, University of Bath.

Tomlinson, S.P. & Burrows, C.R., 1994

Computer Simulation of Vehicle Cooling Systems, *ASME/WAM*, Chicargo, Illinois.

Union Carbide reference data on glycols.

Veshagh, A. and Chen, C., March - April 1993

A Computer Model for Thermofluid Analysis of Engine Warm-Up Process, pg 677-687, *Proc Vehicle Thermal Management Systems*, SAE International Conference, Columbus Ohio USA.

Whitmarsh-Everiss, M.J., June 1990

Automatic Frequency Responsive Operation of Gas Cooled Reactor Plant, Nuclear Electric report TD/SPB/REP/0072.

Whitmarsh-Everiss, M.J., March/April 1993

The Mathematical Modelling Of Plant Behaviour: An Evolutionary History and Forward Projection Part3, *The Nuclear Engineer, Journal Of The Institution Of Nuclear Engineers*, Volume 32, No2.

Wilson, W.E., 1946

Rotary Pump Theory. *Trans. ASME*, 68, 371.

Wilson, W.E., 1948

Performance Criteria for Positive Displacement Pumps and Fluid Motors. *ASME Semi-annual Meeting*, paper 48-SA-14.

Yang, H., 1987

Some Problems in Hydraulic Circuit Design, PhD Thesis, School of Mechanical Engineering, University of Bath.

APPENDIX A

CONSERVATION OF FLUID MASS AND ENERGY FOR LUMPED PARAMETER SYSTEMS

To develop the necessary equations that describe the behaviour of fluid in a control volume, general thermodynamic relationships are developed by applying suitable assumptions to the partial differential conservation equations to leave a set of ordinary differential equations. The desired result will be to produce a set of equations which have been integrated over the control volume to produce finite length nodes thereby reducing the distributed effects to equivalent lumped parameters. It is also assumed that the distributed effects exist and are time dependant in one direction only. Therefore, the direction subscript used in the following equations represent the direction parallel to the flow path and normal to the control volume surface. The development of these relationships from partial differential equations allows a greater theoretical insight into the formulation, although the final set of equations are derivable starting from a control volume basis. The author was first made aware of a similar theoretical approach by Babcock and Wilcox[1983] during his employment within the Electricity Supply Industry.

Equation Development

Hughes and Brighten[1967a] considers the control volume, the conservation of mass equation or continuity equation in differential form as follows:

Conservation of Mass

$$\frac{\partial \rho}{\partial t} + \frac{\partial}{\partial x_i}(\rho \forall_i) = 0 \qquad \text{(A1)}$$

Note that the above equation describes a point in the flow path

where

ρ = fluid density

$\forall_i$ = fluid velocity vector

x_i = direction vector

Assumptions: Mass is neither created nor destroyed within the control volume

Hughes and Brighten[1967b] considers the control volume, the energy equation in differential form as follows:

Conservation of Energy

$$\frac{\partial}{\partial t}(\rho e) + \frac{\partial}{\partial x_i}(\rho e \forall_i) + \frac{\partial}{\partial x_i} q_i + q''' + \frac{\partial}{\partial x_i}(p \forall_i) - \frac{\partial}{\partial x_i}(\forall_i \sigma_s) = 0 \qquad \text{(A2)}$$

Note that the above equation describes a point in the flow path

where

p = Fluid pressure

e = Energy per unit mass (internal energy + kinetic energy + potential energy)

q''' = Internal heat generation rate per unit volume

σ = Viscous shear stress

q_i = Rate of heat transfer per unit volume

Assumptions: No chemical reactions occur within the control volume

The term q''' is negligible in hydraulics applications and will be omitted

No energy is created or destroyed within the control volume

The previous equations represent the basic conservation laws for mass and energy in differential form. It should be noted that the momentum equation has not been derived but will need to be used to complete the equation set. The requirement now is to establish a set of solvable ordinary differential equations that parameterise the distributed properties into finite sections. These

equations will represent the extensive thermodynamic properties. To achieve a solvable set of equations however, the intensive properties (per unit mass) will be required. This requires additional assumptions which will be established later.

For example the conservation of mass equation will need to be integrated across the control volume and as such will take on a form as follows:

$$\int_v \frac{\partial \rho}{\partial t}\, dV = - \int_v \frac{\partial}{\partial x_i}(\rho \forall_i)\, dV \qquad \text{(A3)}$$

The first integral represents the rate of change of mass within the control volume and can be assigned to the total rate of change of mass in the control volume if the control boundary remains fixed in space and the control surface remains fixed with time. In other words the integration over the control volume removes the spacial dependence on density within the control volume. This condition can be represented as follows:

$$\frac{\partial}{\partial t} \int_v \rho\, dV \rightarrow \frac{d}{dt} \int_v \rho\, dV \qquad \text{(A4)}$$

This however is not always the case since the control surface (CS) or bounding surface to the control volume can move with time.

To accommodate control volume boundaries that move with time, for example actuator cylinder volumes, it is necessary in the development of the ordinary differential equations to integrate over moving integration limits. To accommodate this, reference is made to Jeffery[1984] where integral limits may be a function of a parameter and the function to be integrated is also a function of this parameter. In this instance the parameter is time. Jeffery states a general

mathematical relationship for this condition as follows:

$$\frac{d}{d\alpha}\int_{\phi(\alpha)}^{\psi(\alpha)} f(\alpha, x)\, dx = \frac{d\psi}{d\alpha} f(\psi, \alpha) - \frac{d\phi}{d\alpha} f(\phi, \alpha) + \int_{\phi(\alpha)}^{\psi(\alpha)} \frac{\partial f}{\partial \alpha}\, dx \qquad \text{(A5)}$$

This does look somewhat cumbersome, however, if equation (A3) is used as an example, the result simplifies to yield a general relation for integration of a thermodynamic property across a control volume with moving boundaries. If the left hand side of equation (A3) is put into the form of equation (A5) making the appropriate substitutions for the various parameters, gives:

$$\frac{d}{dt}\int_{V_e(t)}^{V_f(t)} \rho\, dV = \frac{dV_l}{dt}\rho_l - \frac{dV_e}{dt}\rho_e + \int_{V_e(t)}^{V_f(t)} \frac{\partial \rho}{\partial t}\, dV \qquad \text{(A6)}$$

The volume derivatives in equation (A6) take account of the control surface movement with time. The change in volume with time can be equated to the product of control surface velocity parallel to the flow path and cross sectional area perpendicular to the flow path. For example:

$$\frac{dV}{dt} = \forall_s A \qquad \text{(A7)}$$

It follows therefore that the first two terms on the right hand side of equation (A6) can then be equated to the surface integral of the thermodynamic extensive property per unit volume around the control volume. Thus:

$$\oint_s \rho \forall_s .dA = \frac{dV_l}{dt}\rho_l - \frac{dV_e}{dt}\rho_e \qquad \text{(A8)}$$

The following general relationship may be inferred from equations (A6,7, and 8)

$$\int_v \frac{\partial B}{\partial t}\, dV = \frac{d}{dt}\int_v B\, dV - \oint_s B \forall_s .dA \qquad \text{(A9)}$$

where:

B = any extensive property per unit volume

$\forall_s$ = surface velocity vector of the control boundary

dA = is an incremental area normal to the control surface and positive when outward from the control volume

The first integral term reflects the time rate of change of B within a finite size control volume with fixed boundaries. The second integral term reflects the time rate of change of B within a finite size control volume with moving boundaries. The last integral term represents the nett difference of the rate of B crossing the control surface due to movement in the control surface.

In integrating the thermodynamic parameters over the control volume to produce a finite sized node, the following assumptions apply:

The velocity vectors are normal to the control volume surface

The flow within the control volume is one dimensional

Changes in the potential and kinetic energy of the control volume are negligible

The inlet and outlet surface areas of the control volume are time invariant

Heat conduction along the flow path is negligible

Conservation of mass

Converting the left hand integral of equation (A3) into the form of equation (A9) and equating to the right hand side of equation (A3) gives:

$$\frac{d}{dt}\int_v \rho\, dV - \oint_s \rho \forall_s .dA = -\int_v \frac{\partial}{\partial x_i}(\rho \forall_i)\, dV \qquad \text{(A10)}$$

The right hand side of equation (A10) can be converted into a surface integral using the

divergence theorem thereby removing the partial derivative of the spacial coordinate:

$$\int_v \frac{\partial}{\partial x_i} (\rho \forall_i)\, dV = \oint_s \rho \forall_i \, .dA \tag{A11}$$

Substituting equation (A11) into (A10) and re-arranging the surface integrals onto the right side of the equation gives:

$$\frac{d}{dt} \int_v \rho \, dV = \oint_s \rho \forall_s \, .dA - \oint_s \rho \forall_i \, .dA \tag{A12}$$

It should be clear that the term on the left hand side of equation (A12) represents the rate of change of mass within the control volume:

$$\frac{d}{dt} \int_v \rho \, dV = \frac{dM}{dt} \tag{A13}$$

where

M = the instantaneous mass with the control volume

Integrating the surface integrals across the boundary of the control volume gives

$$\oint_s \rho \forall_s \, .dA = + A_l \rho_l \forall_{sl} - A_e \rho_e \forall_{se} \tag{A14}$$

where

$\forall_{se}$ = velocity of the control boundary at entry of the control volume

$\forall_{sl}$ = velocity of the control boundary at the exit of the control volume

*** note:**

It should be explained that integration of the surface integral is completed around the entire

(closed) control volume surface. Since the fluid volume is bounded by a pipe, 3 surface integrals are required to complete the integration across the surface. These are for the 2 ends and the outer diameter. Therefore, a number of assumptions have been made. Firstly it is assumed that the velocity of the fluid and the intensive property across the control surface do not vary. Any variation in properties takes place normal to the control surface in the direction of fluid flow. Clearly a real fluid will have a variation in velocity from the pipe surface ($\forall = 0$) to the centre of the pipe ($\forall = \forall_{max}$). However for the purposes of calculation $\forall = \forall_{mean}$ is used which simplifies the integration. Secondly, implicit in formulating the surface integrals is the assumption that each term is multiplied by a unit vector 'n' normal to the control surface and positive when outwards from the surface. Therefore, when evaluating the surface integral at the entry surface, the normal vector is parallel but opposite in direction to that of the direction vector x_i. Therefore this integral must have a negative sign assigned to it. Thirdly, The surface integral of the outer diameter of the control volume = 0 since $\forall = 0$ at this surface. See figure A1 for a schematic of the control volume.

Similarly

$$\oint_s \rho \forall_i \, .dA = + A_l \rho_l \forall_l - A_e \rho_e \forall_e \qquad \text{(A15)}$$

At this point it is useful to define the quantity 'mass flow' in order to group the above terms. If the mass flow is defined relative to the control surface gives:

$$w = A\rho(\forall_i - \forall_s) \qquad \text{(A16)}$$

It should be noted that this becomes absolute mass flow relative to an inertial reference if the control surface is stationary.

With the definition described in equation (A16) the continuity equation becomes:

$$\frac{dM}{dt} = w_e - w_l \qquad \text{(A17)}$$

The Energy Equation

Integrating the energy equation (A2) over the control volume, with a term included for shaft work (e.g. pump work) gives:

$$\int_v \frac{\partial}{\partial t}(\rho e)\, dV = \int_v \left[- \frac{\partial}{\partial x_i}(\rho e \forall_i) - \frac{\partial}{\partial x_i} q_i - \frac{\partial}{\partial x_i}(p \forall_i) + \frac{\partial}{\partial x_i}(\forall_i \sigma_s) - W \right] dV \qquad \text{(A18)}$$

The terms in the energy equation are as follows. The integral of $\partial/\partial t\ (\rho e)$ represents the rate of change of energy with time within the control volume. The integral $\partial/\partial x_i\ (\rho e \forall_i)$ represents the energy crossing the control boundary due to mass flow. The integral $\partial/\partial x_i (q_i)$ represents the heat transfer out of the control volume. For the sake of clarity, the sign will be changed in future reference to heat flow with the following convention: heat flow (q) out of the control volume will be regarded as negative which will change the sign in the above equation. It should be noted that the shear stress term is usually small in comparison to the other terms (Hughes & Brighten[1967c]) for normal pipe nodes and will be neglected. The 'W' term represents the rate of work done by the fluid (shaft work) per unit volume. The integral $\partial/\partial x_i (p \forall_i)$ is the flow work term.

Using the result expressed in equation (A9) to overcome control surface movement, the left hand side integral of equation (A18) can be converted to:

$$\int_v \frac{\partial}{\partial t}(\rho e)\, dV = \frac{d}{dt} \int_v (\rho e)\, dV - \oint_s \rho e \forall_s \, .dA \qquad \text{(A19)}$$

In keeping with the previous assumption that changes in kinetic and potential energy are negligible, it can be recognised that the first term on the right hand side of equation (A19)

represents the rate of change of internal energy for the control volume which is an extensive property:

$$\frac{d}{dt}\int_v (\rho e)\, dV \rightarrow \frac{d}{dt}\int_v (\rho u)\, dV = \frac{dU}{dt} \tag{A20}$$

where

u = internal energy of the fluid per unit mass (intensive)

U = internal energy of the fluid within the control volume (extensive)

The surface integral of equation (A19) is then integrated over the surface to give:

$$\oint_s \rho e \forall_s .dA = A_l \rho_l u_l \forall_{sl} - A_e \rho_e u_e \forall_{se} \tag{A21}$$

This then represents the rate of change of internal energy due to the control surface movement.

Converting the flow work term and the energy crossing the control boundary into surface integrals using the divergence theorem and evaluating, gives:

$$\int_v \frac{\partial}{\partial x_i}(p\forall_i)\, dV = A_l p_l \forall_l - A_e p_e \forall_e \tag{A22}$$

$$\int_v \frac{\partial}{\partial x_i}(\rho e \forall_i)\, dV = A_l \rho_l u_l \forall_l - A_e \rho_e u_e \forall_e \tag{A23}$$

The volume integral of the rate of heat transfer can be left as a single term for now (q_b). This will be developed further when applying these equations to represent the different forms of heat transfer into a node. Similarly this also applies to the shaft work term which can be left as W_s.

Substituting equations (A20) to (A23) back into (A19) gives:

$$\frac{dU}{dt} = A_e p_e \forall_e - A_l p_l \forall_l + A_e \rho_e u_e (\forall_e - \forall_{se}) - A_l \rho_l u_l (\forall_l - \forall_{sl}) + q_h - W_s \qquad \text{(A24)}$$

Using the definition for mass flow crossing the control volume (equation (A16)), the 3rd and 4th terms on the right hand side of the above equation become '$w_e u_e$' and '$w_l u_l$' respectively. It should also be recognised that the first two terms on the right hand side are equivalent to the rate of flow work done by the fluid only as the velocity vectors are with respect to an inertial reference. In order to re-formulate the above energy equation in terms of mass flow crossing the boundary, the nett work done by movement of the control boundary can be related to the flow work by the following equation:

$$w_e p_e v_e - w_l p_l v_l = A_e p_e \forall_e - A_l p_l \forall_l + p\frac{dV}{dt} \qquad \text{(A25)}$$

i.e.

|rate of work done by fluid| = |rate of flow work + rate of work done by boundary motion|

| and boundary |

where

υ_e = specific volume at entry to the control volume

υ_l = specific volume at the exit of the control volume

dV/dt = rate of change of the control volume with time

p = average pressure within the control volume

The first two terms of equation (A24) can then be re-formulated using (A25). If this is substituted into equation (A24) along with the expressions $w_e u_e$ and $w_l u_l$ this will give the energy equation in terms of mass flow crossing the control boundary:

$$\frac{dU}{dt} = w_e (u_e + p_e v_e) - w_l (u_l + p_l v_l) - p \frac{dV}{dt} + q_h - W_s \qquad \text{(A26)}$$

Making the substitution for enthalpy in the above equation (h = u+pυ) gives :

$$\frac{dU}{dt} = w_e h_e - w_l h_l - p \frac{dV}{dt} + q_h - W_s \qquad \text{(A27)}$$

This brings to an end the formulation of both the continuity and energy equations in extensive form.

To make the above equation set into a usable set of equations, they need converting to thermodynamic properties which can be suitably measured. Also the relationship between the extensive properties within the control volume and the leaving properties (intensive) will be required. Finally, heat transfer and shaft work will also be required.

APPENDIX A REFERENCES

The Babcock & Wilcox Company and Bectel Group, March 1983
Modular Modeling System (MMS): A Code for the Dynamic Simulation of Fossil and Nuclear Power Plants No CS/NP-2989.

Hughes & Brighten, 1967a
Fluid Dynamics, Schaum's series, pg45, Mcgraw-Hill

Hughes & Brighten, 1967b
Fluid Dynamics, Schaum's series pg57, Mcgraw-Hill

Hughes & Brighten, 1967c
Fluid Dynamics, Schaum's series, pg54, Mcgraw-Hill

Jeffrey, A., 1984
Mathematics for Engineers and Scientists, second edition pg293, Van Nostrand Reinhold.

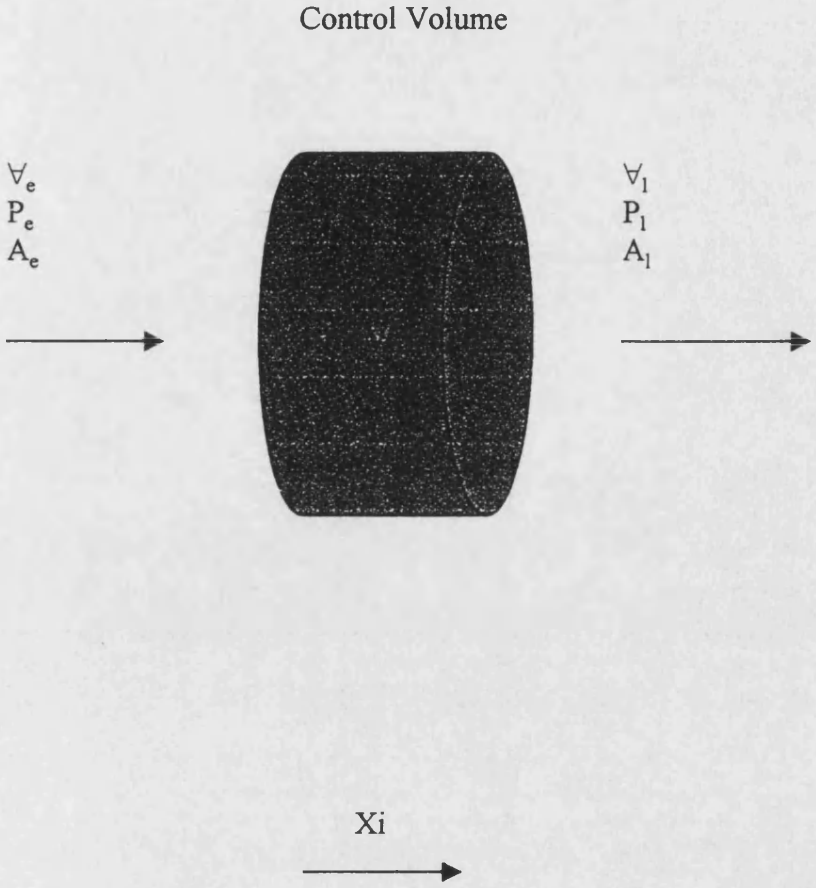

n = Unit vector outward normal

$$\oint_s f.n\ dA = \int_v \nabla.f\ dV$$

FIGURE A1

APPENDIX B

POWER GENERATING PLANT DATA AND CALCULATIONS

LP Heaters

The calculations for the heater coefficients are performed as follows. First determination of the secondary side heat transfer coefficient (htc) is deduced. The secondary side htc is determined from the application of the well known Dittus Boelter correlation:

$$Nu = 0.023\ Re^{0.8}\ Pr^{0.4} \tag{B1}$$

where Re - Reynolds Number

Pr - Prandtl Number

Nu - Nusselt Number

The secondary side htc can therefore be found from the relation:

$$htc_s = \frac{Nu\ k}{d} \tag{B2}$$

To determine the initial condition for the lumped tube temperature, use is made of rate of heat transfer (q_s) into the condensate from the tube material and the average condensate temperature ($Tcon_{ave}$) derived in Chapter 3. The initial condition tube temperature is:

$$T_t = \frac{q_s}{A_s\ htc_s} + Tcon_{ave} \tag{B3}$$

Because the tube material temperature is now known, the primary side heat transfer coefficient for water may be calculated. The primary side rate of heat transfer (q_p) into the tube bundle is derived in Chapter 3 and may be re-arranged to determine the htc_w:

$$htc_w = \frac{q_p}{(T_p - T_t)\ (A_w + 3A_c)} \tag{B4}$$

However the initial condition is derived on the basis that the drains water is at the bottom of the vessel. This implies that the area of tubing covered by water is zero ($A_w = 0$).

A specimen calculation for LP heater 4 follows:

Total number of tubes = 1100

Tube internal diameter = 17.22mm

Maximum continuous rating condensate flow rate = 481 $kg.s^{-1}$

Tube length = 18.228m

Total inner tube surface area (all tubes) = 1085 m^2

Total outer tube surface area (all tubes) = 1200 m^2

Mass flow rate per tube = 0.4373$kg.s^{-1}$

Condensate conditions: 8 bara, $Tcon_{ave}$ = 126.03 °C, ρ = 939 $kg.m^{-3}$,

$\mu = 222.27*10^{-6}$ $N.s.m^{-2}$, Pr = 1.38, Re = 145470, k = 0.684 (units).

Primary side saturation temperature Tp = 134.2 °C. From equation (B1) Nu = 353.1, therefore htc_s = 14.026 $Kw.m^{-2}.K^{-1}$

From equation (B3) the initial tube temperature T_t = 128.44 °C

The primary side heat transfer coefficient for water may now be determined from equation (B4), htc_w = 1.769 $KW.m^{-2}.K^{-1}$.The following Table summarises both primary and secondary htc's for all LP heaters, drains cooler and TMEC. The method of calculation being identical to that for LP heater 4

Table B1 Summary of heater htc's

LP heater 1	htc_w = 2.675 $KW.m^{-2}.K^{-1}$	htc_s = 10.04 $KW.m^{-2}.K^{-1}$
LP heater 2	htc_w = 1.446	htc_s = 11.4
LP heater 3	htc_w = 1.962	htc_s = 12.93
LP heater 4	htc_w = 1.769	htc_s = 14.03
Drains Cooler	htc_w = 4.017	htc_s = 10.45
TMEC	htc_w = 2.088	htc_s = 8.462

Main Condensers

There are three main condensers at Heysham 2 PS. Each condenser is an individual unit and can exist at a different thermodynamic condition with respect to the other two condensers. There is a common exit plenum which connects all three condensers and forms the condensate flow path to the deaerator (DA).

Data for the main condensers follow:

At 672 MW generated load (acceptance test data), NEI Parsons Ltd [1989]

Cooling Water (CW):

Inlet temperature = 7.12 °C, outlet temperature = 18.14 °C

Heat rate per condenser = 295.9 MW

Mean condenser pressure 35.29 mbara

CW flow rate = 19.65 $m^3.s^{-1}$

CW density = 1027.3 $kg.m^{-3}$, Pr = 8.694, k = 0.5874 (sea water)

CW specific heat = 3.991 $KJ.kg^{-1}.K^{-1}$, $\mu = 1211*10^{-6}$ $N.s.m^{-2}$

Condenser saturation pressure and temperature: 35.29 mbara; 26.87 °C

Tube bundle material = titanium

Tube number per condenser = 9756, ID = 24 mm, OD = 25.4 mm,

Length between tube plates = 14m

Internal volume per condenser = 845 m^3

Using the data above, the following information is determined for each condenser:

From Chapter 3, equation (3.15) the averaging coefficient Ac = 0.4327

From Chapter 3, equation (3.14) the average CW temperature

TCW_{ave} = 18.14 - 0.4327(11.02) = 13.37 °C

CW Reynolds no = 30214

From eqn (B1)

Nu = 209.7

Therefore the secondary side $htc_s = Nu.k/d_i = 5.132\ KW.m^{-2}.K^{-1}$

From equation (B3) the tube temperature T_t = 18.96 °C

The primary side heat transfer coefficient is determined from:

$$htc_p = \frac{q_p}{(T_p - T_t)\, A_o} \qquad \text{(B5)}$$

$htc_p = 295.2*10^3/((26.87 - 18.96)\ 10899) = 3.424\ KW.m^{-2}.K^{-1}$

This calculation differs from that used to determine the htc_p for the feed heaters insofar that there is no longer a requirement to compensate for water level. The condenser water level is controlled by condensate feed regulating valves. Even when subject to severe transient disturbances, the change in condenser water level is small due to the very large surface area (90 m^2 per condenser) of the water in the vessel.

CONDENSATE EXTRACTION PUMP

The condensate pump is a vertical spindle four stage caisson type which is driven by a constant speed motor, capable of providing 500 $kg.s^{-1}$ with a corresponding discharge pressure of 22 bara. The pump has been modelled using non-dimensional relationships determined from the data in Table B2.

Table B2 Condensate extraction pump performance data

Mass Flow Rate $kg.s^{-1}$	Head Rise m	Efficiency
0	264	0
100	254	22
200	248	50
300	245	67
400	237	76
500	225	82
600	206	84
700	182	83
750	170	81

LP TURBINES

The LP turbines have been detailed in Chapter 3, section 3.4.1. The resistance coefficients for the turbine ellipse law are determined by fitting to acceptance test data (NEI Parsons Ltd [1989]). The following example details the calculation of the resistance coefficient for LP turbine 1, first stage. The resistance coefficient is defined as follows:

$$KT_{1,1} = \frac{w_T}{\sqrt{\rho_1 p_1}\sqrt{1 - \left(\frac{p_2}{p_1}\right)^{\frac{m+1}{m}}}}$$

The following data has been used:

$p_1 = 5.625$ bara

$p_2 = 0.852$ bara

$\rho_1 = 2.18\ kg.m^3$

$WT = 159.38\ kg.s^{-1}$

$m = 1/(1 - \eta\,(\gamma - 1)/\gamma)$: stage efficiency $\eta = 0.89$;

ratio of specific heats for steam $\gamma = 1.3$

Which gives $KT_{1,1} = 47.966$

It should be noted that the bleed flows to the LP feed heaters are taken into account for calculation of the turbine stage resistances in stages 2, 3 and 4. This applies to all 3 LP turbines. The division of bled steam flows has been tabulated in Chapter 3 Table 3.1. LP turbine 1 provides steam for heater 1, 2 and the TMEC, while turbines 2 and 3 provide steam for heaters 1, 3, 4 and the TMEC. As such asymmetries exist such that there are small differences in the stages flows between turbines. This is also reflected in the differences in stage resistance coefficients items below.

Table B3 Turbine Stage Resistances

LP Turbine	Stage	Stage Resistance Coefficient
1	1	47.966
	2	250.61
	3	453.95
	4	1363.4
2	1	50.976
	2	111.53
	3	453.95
	4	1363.4
3	1	61.121
	2	68.05
	3	453.95
	4	1363.4

CONTROL VALVES

Chapter 3 describes the control valves in the LP feed system. The makeup and letdown valves transfer feed water both too and from the LP feed system. The main condenser level control valves are situated in parallel in the condensate feed path. The sum of all resistances, gravitational heads, makeup, letdown flow rates and the condensate extraction pump head/flow characteristic are used to determine condensate flow rate in the LP feed system. The condensate flow rate is represented by a loop breaking integrator and is used to satisfy conservation of mass in the system. All control valves are represented using a standard valve pressure - flow characteristic which includes a valve loss coefficient 'Cv'. However the valve relationship is used in a different way depending on the information required. The modelling requirements of both makeup and letdown valves is to determine flow rates entering and leaving the condensate system such that the valve relationship is used in the following way:

$$w_v = A_v C_v \sqrt{\rho \Delta p}$$

Condenser level control valves form part of the LP condensate feed system. Because feed flow is determined by a loop breaking integrator, the condenser level control valves are required to provide a differential pressure in the feed path based on the current condensate flow rate. The differential pressure is determined for the control valves in parallel using the following equation:

$$\Delta p = \frac{w_v}{(C_{v1} A_{v1} \sqrt{\rho} + C_{v2} A_{v2} \sqrt{\rho})^2}$$

APPENDIX B REFERENCES

NEI Parsons Ltd, 1989

Heysham 2 Power Station Unit 7, Report on Official Acceptance tests, No: 90.314.2383

APPENDIX C

ERROR ASSESSMENT IN MODEL PREDICTION FOR FLUID POWER SYSTEMS

Chapters 5 and 6 details experimental work and model prediction of thermal effects for a rig comprising a hydraulic pump, loading valve, heat exchanger, reservoir and hoses. In any assessment of this nature it is important to consider the effects of errors with respect to model prediction, as this will determine how representative the predictions are. Once this is done, conclusions can be drawn concerning predictions that fall outside the error tolerances. For instance, this could highlight problems with model uncertainty such as ignoring heat loss from a component model formulation. If the heat loss was significant then it is quite probable that the predicted temperature change would be significantly different from the measured change. An error assessment will provide a quantitative measure for the deviations of model prediction.

With the current system studied, one of the sources of error originates from the deviation of the predicted thermodynamic and transport properties of the mineral oil used from their true values. Typically the physical properties of mineral oil stem from empirical determination based on experimental data. Often these take the form of polynomial expressions where temperature and (or) pressure are the independent variables. These expressions will have associated with them errors based on the accuracy of fit. These errors are usually termed systematic errors.

In addition to the above errors, measurement (random) errors of both pressure and temperature will also effect the model prediction.

As an example of the determination of errors in the model prediction, the hydraulic pump will serve as a useful component. Consider the temperature change across the unit in the steady state as follows:

$$T_l - T_e = \frac{\upsilon}{Cp}\left(\frac{1}{\eta} + \beta T - 1\right)(p_l - p_e) \qquad \text{(C1)}$$

It is evident that the temperature change is dependent on the physical properties of the fluid as well as the pressure rise across the unit, and also the overall efficiency of the unit. The pump will in comparison to many of the other components be affected indirectly by measurement of shaft torque, volumetric flow rate and shaft speed, since these quantities are used to assess the efficiency at a given operating point. It is also worth considering how the efficiency calculation is performed within the pump model. Although torque and shaft speed measurements were used to determine the pump flow and torque losses over a range of pressures and temperatures, this data was subsequently fitted to polynomial expressions which are used by the model in the deduction of efficiency. In this sense due consideration should be given not only to the errors in fundamental parameters such as speed and flow rate, but also the errors in the expressions for torque and flow losses over the operating range. An example of this can be seen in the pump flow loss representation where the maximum error amounted to 0.5 $L.min^{-1}$. This should be seen in contrast to the perceived accuracy of the flow rate measurement of within ± 0.5% of measured value (± 0.25 $L.min^{-1}$ max) used to characterise the pump. The error in the efficiency will therefore include an estimation of the maximum error of both flow rate and shaft torque due to errors in polynomial expressions used in part to determine these quantities.

The errors in the pump temperature difference (ΔT) calculation can be summarised as follows:

Error Source	Influence on ΔT
Specific Volume	$\delta\Delta T_\upsilon = \partial\Delta T / \partial\upsilon \,.\delta\upsilon$
Coefficient of Cubical Expansion	$\delta\Delta T_\beta = \partial\Delta T / \partial\beta \,.\delta\beta$
Specific Heat	$\delta\Delta T_{Cp} = \partial\Delta T / \partial Cp \,.\delta Cp$

Error Source	Influence on ΔT

Pressure Measurement	$\delta\Delta T_p = \partial\Delta T / \partial p \,.\delta p$
Temperature Measurement	$\delta\Delta T_T = \partial\Delta T / \partial T \,.\delta T$
Unit Efficiency	$\delta\Delta T_\eta = \partial\Delta T / \partial \eta \,.\delta \eta$

To deduce a total error it is normal practice to find the square root of the sum of the errors squared as follows:

$$\delta\Delta T = \pm \sqrt{(\delta\Delta T_\upsilon^2 + \delta\Delta T_\beta^2 + \delta\Delta T_{Cp}^2 + \delta\Delta T_p^2 + \delta\Delta T_T^2 + \delta\Delta T_\eta^2)} \qquad \text{(C2)}$$

To arrive at expressions for the errors of the individual contributions as detailed above requires finding the partial derivative of equation C1 with respect to the source of error in question. The following relationships have been established for the above sources of error:

$$\delta\Delta T_\upsilon = \frac{\partial\Delta T}{\partial\upsilon} \,.\, \delta\upsilon = \frac{p_1 - p_e}{Cp} \left(\frac{1}{\eta} + \beta T - 1 \right) \,.\, \delta\upsilon$$

$$\delta\Delta T_\beta = \frac{\partial\Delta T}{\partial\beta} \,.\, \delta\beta = \frac{(p_1 - p_e)\,\upsilon T}{Cp} \,.\, \delta\beta$$

$$\delta\Delta T_{Cp} = \frac{\partial\Delta T}{\partial Cp} \,.\, \delta Cp = - \frac{(p_1 - p_e)\,\upsilon}{Cp^2} \left(\frac{1}{\eta} + \beta T - 1 \right) \,.\, \delta Cp$$

$$\delta\Delta T_p = \frac{\partial\Delta T}{\partial p} \,.\, \delta p = \frac{\upsilon}{Cp} \left(\frac{1}{\eta} + \beta T - 1 \right) \,.\, \delta p$$

$$\delta\Delta T_T = \frac{\partial\Delta T}{\partial T} \,.\, \delta T = \frac{(p_1 - p_e)\,\upsilon\beta}{Cp} \,.\, \delta T$$

$$\delta\Delta T_\eta = \frac{\partial\Delta T}{\partial\eta} \,.\, \delta\eta = \frac{(p_1 - p_e)\,\upsilon}{Cp\,\eta^2} \,.\, \delta\eta$$

The magnitudes of the sources of error need to be established before evaluation of the total error in pump temperature difference can be made. Further consideration of the pump efficiency must also be made in order to establish its error. The efficiency of the pump may be established from

the following relationship:

$$\eta = \frac{Q\,(p_l - p_e)}{Ts\;\omega}$$

The error in efficiency can be estimated using an identical procedure to that for assessing the error in pump temperature difference.

$$\delta\eta = \pm \sqrt{(\,\delta\eta_Q^2 + \delta\eta_p^2 + \delta\eta_{Ts}^2 + \delta\eta_\omega^2\,)} \qquad \text{(C3)}$$

Where:

$$\delta\eta_\omega = \frac{\partial\eta}{\partial\omega} \cdot \delta\omega = -\frac{Q(p_l - p_e)}{Ts\;\omega^2} \cdot \delta\omega$$

$$\delta\eta_{Ts} = \frac{\partial\eta}{\partial Ts} \cdot \delta Ts = -\frac{Q(p_l - p_e)}{Ts^2\;\omega} \cdot \delta Ts$$

$$\delta\eta_p = \frac{\partial\eta}{\partial p} \cdot \delta p = \frac{Q}{Ts\;\omega} \cdot \delta p$$

$$\delta\eta_Q = \frac{\partial\eta}{\partial Q} \cdot \delta Q = \frac{(p_l - p_e)}{Ts\;\omega} \cdot \delta Q$$

From manufacturers data the following accuracies for the measuring devices were deduced:

(a) Speed and Torque

$\delta\omega = \pm$ 1 RPM

δTs = ± 0.11% Full Scale Deflection for instrumentation which is ± 0.15 Nm but increased to ± 0.4 Nm due to error in polynomial expression for torque loss as a function of viscosity.

(b) Flow rate and Pressure

δQ = ± 0.5 L/min, error due to polynomial expression for flow loss as a function of pump differential pressure and viscosity.

$\delta p = \pm 0.21\%$ of full range : ± 0.735 bar

(c) Temperature

$\delta T = \pm 0.5$ °C ('T' type thermocouples)

The errors in the physical properties namely density or specific volume, specific heat and the coefficient of cubical expansion are established from the origins of the empirical relationships which may be found in numerous texts on rheology. The specific volume is determined from an empirical fit of density with temperature as the independent variable as follows, Davenport[1973]:

$$\rho = \rho_1 - 0.623(T - 15.6)$$

Where ρ_1 is the density at 15.6 °C. Davenport suggests that this expression is capable of predicting density to within $\pm 0.5\%$. Since the definition of the coefficient of cubical expansion (β) is determined from :

$$\beta = - \frac{1}{\rho} \frac{\partial \rho}{\partial T}$$

the error in β may be established from the error in density as follows:

$$\delta\beta = \frac{\partial \beta}{\partial \rho} . \delta\rho = - \frac{0.003115}{\rho}$$

The error in specific heat capacity constitutes the largest in magnitude compared with other physical properties. The empirical relationship used is as much as $\pm$ 5% in error, Cameron[1966]. For the mineral oil used, the following relationship was used to predict specific heat capacity:

$$Cp = \frac{4187(0.402 + 8.1*10^{-4} T)}{\sqrt{\rho /1000}}$$

With the above information it is now possible to tabulate the estimated error in pump

temperature difference over the operating range. In estimating the errors it is sensible to chose operating points over the complete range of experimental data that was gathered. For this reason four sets of data were used covering both low and high pressures and temperatures (Table C3). firstly the error in efficiency is established:

Table C1: Constituent errors in pump efficiency

Pump Δp bar	Pump inlet temperature °C	$\delta\eta_{Ts}$ p.u.	$\delta\eta_{p}$ p.u.	$\delta\eta_{Q}$ p.u.	$\delta\eta_{w}$ p.u.
26.1	23.4	0.01	0.016	0.0063	0.00038
149.4	23.4	0.004	0.004	0.01	0.00057
31	70.8	0.0034	0.02	0.01	0.00058
154.9	70.8	0.02	0.0032	0.01	0.00047

note: data taken from experimental results

Equation C3 may now be used to calculate the error in efficiency for the above pump operating points.

Table C2: Total errors in pump efficiency

Pump Δp bar	Pump inlet temperature °C	$\delta\eta$ p.u.
26.1	23.4	± 0.0199
149.4	23.4	± 0.0115
31	70.8	± 0.0226
154.9	70.8	± 0.0226

Table C3: Pump experimental data used in the calculation of errors

Pump inlet Temperature °C	Viscosity Cpoise	Pump Δp bar	Drive Torque Nm	Pump Speed RPM	Delivery Flow rate $L.min^{-1}$
23.4	43.9	26.1	22.4	1481	45.2
23.4	43.9	149.4	82.8	1432	40.9
70.8	12.4	31	16.5	1484	42.7
70.8	12.4	154.9	79.1	1425	30.7

The error in pump temperature difference may now be established at the previously defined operating points (Table C3).

Table C4: Constituent errors in pump temperature difference

Pump inlet Temp DegC	Pump Δp bar	$\delta\Delta T_{\upsilon}$ °C	$\delta\Delta T_{\beta}$ °C	$\delta\Delta T_{Cp}$ °C	$\delta\Delta T_{p}$ °C	$\delta\Delta T_{T}$ °C	$\delta\Delta T_{\eta}$ °C
23.4	26.1	7.78E-3	1.69E-3	7.77E-2	4.32E-2	5.69E-4	9.86E-2
23.4	149.4	1.96E-2	9.64E-3	1.96E-1	1.93E-2	3.25E-3	1.55E-1
70.8	31	3.67E-3	2.24E-3	3.67E-2	1.74E-2	6.51E-4	5.37E-2
70.8	154.9	3.28E-2	1.12E-2	1.83E-1	3.12E-2	3.25E-3	4.42E-1

The total error in the predicted model pump temperature difference may now be calculated using equation C2 for the above operating points given in Table C3 and the information in Table C4.

Table C5: total error in pump temperature difference model prediction (equation C1) for four operating points (Table C3)

Pump inlet temperature °C	Pump Δp bar	Error in pump temperature difference δΔT °C
23.4	26.1	± 0.133
23.4	149.4	± 0.252
70.8	31	± 0.067
70.8	154.9	± 0.48

It is interesting to note in all cases that the model prediction would be more accurate than measuring the temperature difference with the instrumented 'T' type thermocouples. If using an identical procedure to determine the error in purely measuring the temperature difference then this would lead to a possible maximum measurement error of $\pm \sqrt{(0.5^2 + 0.5^2)}$ (based on the errors of the inlet and outlet thermocouples), or ± 0.707 °C. For the pump operating at 100 bar, 20 °C and an efficiency of 80%, would amount to a theoretical temperature rise of 2.66 °C. Therefore the error in measurement only at these conditions could be as much as ± 26.5% in the worst case. This has important implications. If for example an energy balance for the pump is required so that heat transfer may be calculated. Clearly if the deduction is based on temperature measurement only, then the accuracy of the thermocouples would ideally need to be an order of magnitude better.

It is evident that the predicted pump outlet temperature from the simulations in some instances was up to 1.5 °C different from the measured values. The differences can be attributed to both measurement and model inaccuracy. From the previous analysis it has been shown that the model is capable of producing a maximum error of approximately ± 0.5 °C at the pump outlet. If the error in the measured value is of a similar magnitude but opposes the predicted value, then

this amounts to 1 °C difference between measured and predicted value. In this respect, differences of the order of 1 °C should be regarded as possible under certain operating conditions.

In conclusion the results from the simulations undertaken in chapter 6 should be considered as representative. The example of the pump temperature difference has shown that the calculation of errors is not a trivial exercise, but necessary to provide quantitative information regarding the model prediction under varying operating conditions.

APPENDIX C REFERENCES

Davenport, T.C., 1973

The Rheology of Lubricants, pg 129, Applied Science Publishers Ltd.

Cameron, A., 1966

The Principles of Lubrication, pg 517, Longman.